UCLA/PPG--1274

DE90 004377

THE ARIES
TOKAMAK REACTOR STUDY

**The Collection of Papers presented at
IEEE 13th Symposium on Fusion Engineering
Knoxville, Tennessee, October 2-6, 1989**

UCLA-PPG-1274 **Oct. 1989**

THE ARIES TEAM

University of California, Los Angeles
Farrokh Najmabadi, Robert W. Conn

Nasr M. Ghoniem — Steven P. Grotz — Mohammad Z. Hasan
Erfan Ibrahim — *Tomoaki Kungi*[1] — Tak-Kuen Mau
Rodger C. Martin — Shahram Sharafat — Erik Vold

Argonne National Laboratory
David A. Ehst — Kenneth Evans, Jr. — Dai-Kai Sze

General Atomics
Kenneth R. Schultz, Clement P. C. Wong

Edward T. Cheng — Richard L. Creedon — Alan W. Hyatt
James A. Leuer — Michael J. Schaffer

Idaho National Engineering Laboratory
J. Stephen Herring

Los Alamos National Laboratory
Robert A. Krakowski

John R. Bartlit[2] — Charles G. Bathke — Ronald L. Miller

Massachusetts Institute of Technology
Daniel R. Cohn, Leslie Bromberg

Justin Schwartz — Joel Schultz — John E. C. Williams

Oak Ridge National Laboratory
Y-K. Martin Peng

William R. Beecraft — John T. Hogan — R. Lowell Reid
Dennis J. Strickler — J. C. Whitson

Princeton Plasma Physics Laboratory

Stephen A. Jardin — D. J. Ward

Rensselaer Polytechnic Institute
Don Steiner

Marc Klasky — Lance Snead — Mark Valenti

University Of Wisconsin, Madison
John Santarius, Gilbert A. Emmert

James P. Blanchard — Igor N. Sviatoslavsky — Layton J. Wittenberg

University of Illinois

George H. Miley — Cliff E. Singer — Winferd Kerbichler[3]

Georgia Institute of Technology
John Mandrekas

[1] Permanent Address: Japan Atomic Energy Research Institute.
[2] TSTA program.
[3] Permanent Address: Technische Universtat Graz, Austria.

PREFACE

The ARIES study is a community effort to develop several visions of tokamaks as fusion power reactors. The aims are to determine the potential economics, safety, and environmental features of a range of possible tokamak reactors, and to identify physics and technology areas with the highest leverage for achieving the best tokamak reactor.

Three ARIES visions are planned, each having a different degree of extrapolation from the present data base in physics and technology. The ARIES-I design assumes a minimum extrapolation from current tokamak physics (*e.g.*, 1st stability) and incorporates technological advances that can be available in the next 20 to 30 years. ARIES-II is a DT-burning tokamak which would operate at a higher beta in the 2nd MHD stability regime. It employs both potential advances in the physics and expected advances in technology and engineering. ARIES-III will examine the potential of the tokamak and the D^3He fuel cycle.

Following is a collection of 14 papers on the results of the ARIES study which were presented at the IEEE 13th Symposium on Fusion Engineering (October 2-6, 1989, Knoxville, TN). This collection describes the ARIES research effort, with emphasis on the ARIES-I design, summarizing the major results, the key technical issues, and the central conclusions.

The ARIES-I reactor is a 1000 MWe (net) reactor with a plasma major radius of 6.5 m, a minor radius of 1.4 m, a neutron wall loading of about 2.8 MW/m^2, and a mass power density of about 90 kWe/tonne of fusion power core. Parametric systems studies show that the optimum 1st stability tokamak has relatively low plasma current ($\sim$ 12 MA), high plasma aspect ratio ($\sim 4-6$), and high magnetic field ($\sim$ 24 T) at the coil. The ARIES-I reactor operates at steady state using ICRF fast waves to drive current in the plasma core and lower-hybrid waves for edge-plasma current drive and start-up. The current-drive system supplements a significant ($\sim$ 57%) bootstrap current contribution that is consistent with theoretical predictions and recent experimental observations. The impurity control system is based on high-recycling poloidal divertors. Because of the high field and large Lorentz forces in the toroidal-field magnets, innovative approaches with high-strength materials and support structures are used. The ARIES-I blanket is cooled by He and consists of SiC-composite structural material, Li_4SiO_4 solid breeder, and Be neutron multiplier, all chosen for their low activation and low decay after-heat in order to enhance the safety and environmental features of the design. The ARIES-I design has a competitive cost of electricity and potentially superior safety and environmental features relative to advanced fossil or fission power plants.

The ARIES Study

Papers Presented at
IEEE 13th Symposium on Fusion Engineering
Knoxville, TN, October 2-6, 1989

1. The ARIES Tokamak Fusion Reactor Study.
2. The ARIES-I High-Field Tokamak Reactor: Design Point Determination and Parametric Studies.
3. Design Integration of the ARIES-I Tokamak Reactor.
4. MHD Equilibrium and Stability Considerations for High-Aspect-Ratio ARIES-I Tokamak Reactor.
5. Vertical Stability Requirements for ARIES-I Reactor.
6. Current Drive Analysis and System Design for the ARIES-I Tokamak Reactor.
7. High-Field Magnet Design for the ARIES-I Reactor.
8. Blanket Design for the ARIES-I Reactor.
9. SiC Composites as Structural Material for the ARIES-I Reactor.
10. Neutronics Studies for the ARIES-I Reactor.
11. Safety in the ARIES Tokamak Design Study.
12. Thermal Cycle Power Conversion for the ARIES-I Tokamak Reactor.
13. Energy Conversion Options for ARIES-III – A Conceptual D^3He Tokamak Reactor.
14. Numerical Simulation of Turbulent Gas-Particle Fluid Flow and Heat Transfer.

THE ARIES TOKAMAK FUSION REACTOR STUDY[†]

F. Najmabadi,[‡] R. W. Conn,[‡] and

THE ARIES TEAM

J. R. Bartlit[5,*], C. G. Bathke[5], W. R. Beecraft[7], J. P. Blanchard[10], L. Bromberg[6], J. Brooks[2]
E. T. Cheng[3], D. R. Cohn[6], P. I. H. Cooke[13], R. L. Creedon[3], D. A. Ehst[2], G. A. Emmert[10]
K. Evans, Jr.[2], N. M. Ghoniem[1], S. P. Grotz[1], E. Greenspan[14], M. Z. Hasan[1], J. T. Hogan[7]
J. S. Herring[4], A. W. Hyatt[3], E. Ibrahim[1], S. A. Jardin[8], W. Kernbichler[11,**], M. Klasky[9]
A. C. Klein[15], R. A. Krakowski[5], T. Kungi[1,‡], J. A. Leuer[3], J. Mandrekas[12], R. C. Martin[1]
T-K. Mau[1], G. H. Miley[11], R. L. Miller[5], Y-K. M. Peng[7], R. L. Reid[7], J. F. Santarius[10]
M. J. Schaffer[3], J. Schultz[6], K. R. Schultz[3], J. Schwartz[6], S. Sharafat[1], C.E. Singer[11]
L. Snead[9], D. Steiner[9], D. J. Strickler[7], L. N. Sviatoslavsky[10], D-K. Sze[2], M. Valenti[9]
D. J. Ward[8], J. C. Whitson[7], J. E. C. Williams[6], L. J. Wittenberg[10], C. P. C. Wong[3]

Department of Mechanical, Aerospace and Nuclear Engineering
and Institute of Plasma and Fusion Research,
University of California, Los Angeles
Los Angeles, CA 90024-1597.

Abstract: The ARIES study is a community effort to develop several visions of the tokamak as fusion power reactors. The aims are to determine their potential economics, safety, and environmental features and to identify physics and technology areas with the highest leverage for achieving the best tokamak reactor. Three ARIES visions are planned, each having a different degree of extrapolation from the present data base in physics and technology. The ARIES-I design assumes a minimum extrapolation from current tokamak physics (*e.g.*, 1st stability) and incorporates technological advances that can be available in the next 20 to 30 years. ARIES-II is a DT-burning tokamak in 2nd stability regime and employs both potential advances in the physics and expected advances in technology and engineering; and ARIES-III is a conceptual D^3He reactor. This paper focuses on the ARIES-I design. Parametric systems studies show that the optimum 1st stability tokamak has relatively low plasma current ($\sim 12\,MA$), high plasma aspect ratio ($\sim 4-6$), and high magnetic field ($\sim 24\,T$ at the coil). ARIES-I is 1000 MWe (net) reactor with a plasma major radius of 6.5 m, a minor radius of 1.4 m, a neutron wall loading of about $2.8\,MW/m^2$, and a mass power density of about 90 kWe/tonne. The ARIES-I reactor operates at steady state using ICRF fast waves to drive current in the plasma core and lower-hybrid waves for edge-plasma current drive. The current-drive system supplements a significant ($\sim 57\%$) bootstrap current contribution. The impurity control system is based on high-recycling poloidal divertors. Because of the high field and large Lorentz forces in the toroidal-field magnets, innovative approaches with high-strength materials and support structures are used. The ARIES-I blanket is cooled by He and consists of SiC-composite structural material, Li_4SiO_4 solid breeder, and Be neutron multiplier, all chosen for their low activation and low decay after-heat in order to enhance the safety and environmental features of the design. The ARIES-I design has a competitive cost of electricity and superior safety and environmental features.

INTRODUCTION

The ARIES study is a community effort [1] to investigate the potential of tokamaks as fusion electric-power systems. The ARIES study is developing three visions for tokamak reactors, each with a different degree of extrapolation in physics and technology. The aim is to determine the potential economics, safety, and environmental features of a range of possible tokamak reactors. Furthermore, a comparison of the ARIES designs will provide a host of physics and technology areas with the highest leverage for achieving the best tokamak reactor.

All three ARIES designs are 1000 MWe (net) power reactors. The ARIES-I design assumes a minimum extrapolation in physics and, hence, is close to present tokamak data base (*e.g.*, ARIES-I operates in the first MHD stability regime). The ARIES-I reactor incorporates technologies that would be available over the next 20 to 30 years given the existing trends and gradients for these technologies within and outside the fusion program. The ARIES-II design assumes potential advances in plasma physics, such as second stability operation, which are predicted by theory but are not yet well established experimentally. Because of the improved plasma performance in ARIES-II,

[1] University of California, Los Angeles
[2] Argonne National Laboratory
[3] General Atomics
[4] Idaho National Engineering Laboratory
[5] Los Alamos National Laboratory
[6] Massachusetts Institute of Technology
[7] Oak Ridge National Laboratory
[8] Princeton Plasma Physics Laboratory
[9] Rensselaer Polytechnic Institute
[10] University of Wisconsin, Madison
[11] University of Illinois
[12] Georgia Institute of Technology
[13] Culham Laboratory, United Kingdom
[14] UC Berkeley & Nuclear Research Center-Negev, Israel
[15] Oregon State University
[*] TSTA program
[**] Permanent address: Technische Universitat Graz, Austria
[‡] Permanent address: Japan Atomic Energy Research Inst.

[†] Work supported by the U.S. Department Energy

the technology needs may be less demanding than those of ARIES-I. The ARIES-III vision will study the potential of tokamaks to operate with fuel systems such as D^3He as alternatives to deuterium and tritium. Such systems may have the potential for even greater environmental and safety advantages and for highly efficient conversion of fusion power to electricity [2].

In this paper, a description of the ARIES-I research effort is presented. The general features of the ARIES-I reactor are described and the plasma engineering and fusion power core design are summarized, including the major results, the key technical issues, and the central conclusions.

GENERAL FEATURES OF THE ARIES-I REACTOR

Extensive parametric system studies have been performed to select and optimize the design point and then to determine the overall sensitivity of the design to the physics and engineering assumptions and extrapolations. Specific parameters of the design, appropriate to the overall configurational options, were optimized to result in reactors with minimum cost-of-electricity (COE) [3]. These design points were then subjected to detailed engineering analyses and subsystem design, with the conceptual design results fed back to the systems code for further optimization and refinement.

The ARIES-I plasma operates in the first stability regime and the plasma beta is consistent with the predictions of MHD stability theory, which has proven to be in remarkable agreement with experimental findings. The parametric studies pointed to optimum first-stability tokamaks which have relatively low plasma current ($I_p \sim 12$ MA), high plasma aspect ratio ($A \sim 4-6$), and high magnetic field ($B_{coil} \sim 24$ T at the coil). Low-current, high-aspect-ratio, ARIES-I class reactors have the following distinctive features: (1) plasma beta is low and is compensated by a high toroidal field. (2) Because of low current, the poloidal beta is high which, together with relatively high safety factors, results in a high bootstrap current fraction, $f_{BS} = I_{BS}/I_p$. (3) Because of low current and high f_{BS}, the cost of the current-drive system and the recirculating power fraction is reduced which compensates the higher cost of the toroidal-field coils. (4) Because of lower plasma current, the disruption forces are much smaller and the poloidal-field system is cheaper.

The trade-offs among the plasma current, aspect ratio, and toroidal field for first stability tokamaks are shown in Figure 1. This figure compares the cost of electricity (COE) of 1000-MWe tokamak power plants for different aspect ratios and maximum fields at the coil. For a given A, a drastic reduction in COE is evident for higher peak fields, mainly because the fusion power density is increasing and the device is becoming smaller. For a given peak field, the increase in COE at low A reflects the larger plasma current, higher cost of the current-drive system, and higher recirculating power. At larger A, the plasma current is not decreasing much with A, and the cost of toroidal-field magnets become dominant. The minimum-COE design occurs at $A \sim 4-5$. The exact location depends on the unit cost of the toroidal-field magnets and current-drive system and the efficiency of the current drive.

A reference design point, corresponding to a plasma aspect ratio of 4.5 and the peak field of 24 T, was chosen for the ARIES-I reactor. Details of the ARIES-I trade-off studies leading to this design point are given in Reference [3]. The major parameters of the ARIES-I reactor are summarized in Table 1. Figure 2 shows an elevation view of the ARIES-I fusion power core (FPC).

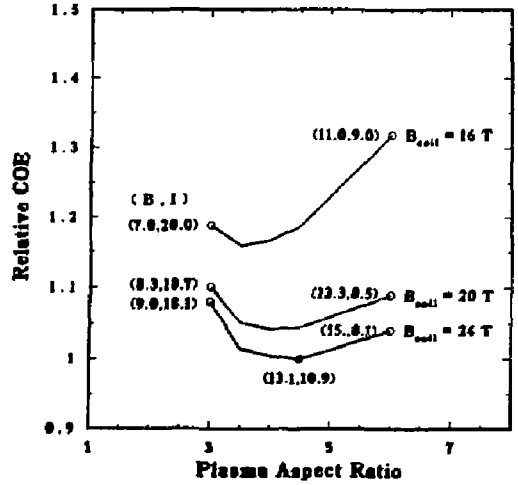

Figure 1. Relative COE of first-stability, 1000-MWe tokamak reactors with different aspect ratios and peak field at the coils (B_{coil}). The peak stress in the coil is set at 1000 MPa. Values given in parenthesis are those of the toroidal field on axis and plasma current.

Table 1: ARIES-I Major Parameters

Major plasma radius	6.52 m
Minor plasma radius	1.45 m
Plasma aspect ratio	4.5
Plasma elongation, κ_{95}	1.6
Plasma current	12 MA
Toroidal field (on axis)	13 T
Toroidal field (on coil)	24 T
Plasma beta	2%
Average electron density	1.6×10^{20} m^{-3}
Average electron temperature	20 keV
Neutron wall loading	2.8 MW/m^2
Fusion power	1991 MW
Net electric output	1000 MW
Gross thermal efficiency	0.48
Net plant efficiency	0.35

In addition to economic competitiveness, the ARIES-I study has placed a great emphasis on safety and environmental features aiming for Level 1 (inherent safety) or Level 2 (large-scale passive safety) of safety assurance [4]. This safety goal has been achieved by using low-activation, very-low decay-afterheat material in the

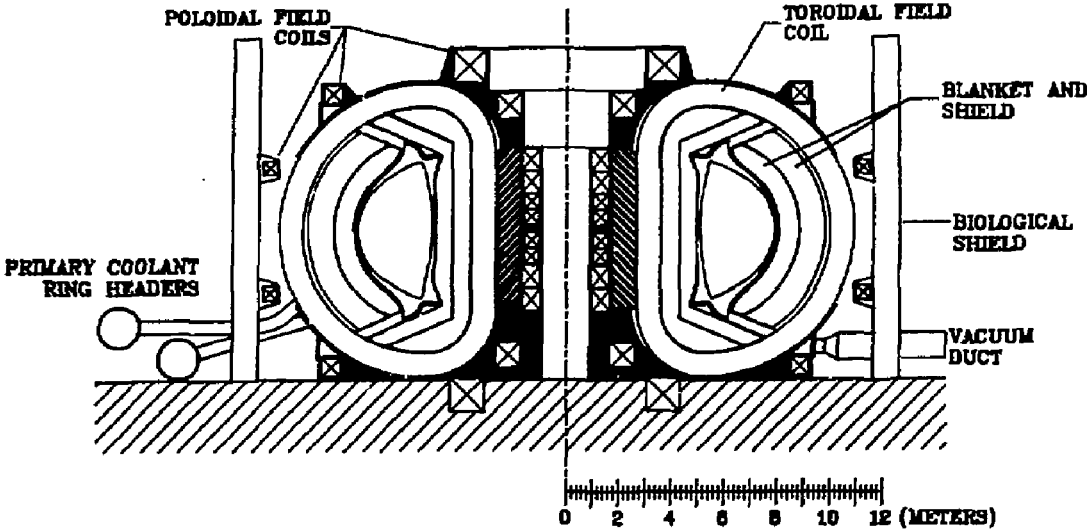

Figure 2. Elevation view of the ARIES-I FPC design.

FPC so that the inventory of radioactive material is low and the decay afterheat in the FPC is not sufficient to release hazardous material [5]. The ARIES-I FPC components also qualify as Class-C waste for shallow land burial [6].

ARIES-I PLASMA ENGINEERING

Self-consistent plasma profiles have been used for equilibrium and stability, current-drive, transport, and edge-plasma analyses. A standard radial pressure profile, $p(r) = p_o[1 - (r/a)^2]^{\alpha_p}$, is used with $\alpha_p = \alpha_n + \alpha_T$ where α_n and α_T are the respective profile exponent factors for density and temperature. For ARIES-I design, $\alpha_n = 0.3$ and $\alpha_T = 1.1$ are used, based on the results of the transport calculations; similar values have been used for ITER. One should note that a more peaked density profile (*i.e.*, larger α_n) would result in higher fusion power density and larger bootstrap current fraction leading to a lower COE (COE decreases by $\sim 10\%$ for $\alpha_n = 0.6$). The more peaked density profiles, however, require a central fueling scheme and/or an anomalous inward-pinch process and were ruled out for ARIES-I design.

The ARIES-I plasma equilibrium is constrained by several physics and engineering constraints, the most important being the vertical stability requirements. The growth rate of an externally excited vertical instability is on the order of the Alfven time scale ($10\,\mu s$). Usually a conducting shell is required to retard the growth rate to a more manageable value set by the electric time constant of the shell. An active feedback system then provides the necessary stabilization for longer times.

The ARIES-I blanket is made of SiC structural material which has a low electrical conductivity and, thus, cannot provide any passive stabilization. In order to maintain the excellent safety features of the ARIES-I blanket system, the passive stabilization shell is located behind the blanket, 0.9 m from the separatrix. Several models have been used to estimate the location and size of the conducting shell for passive stabilization [7]. Time-dependent simulations with TSC code [8] are used to determine the current, voltage, location, and size of the active feedback coils [7]. For ARIES-I plasma with an aspect ratio of 4.5 and a separatrix elongation, $\kappa_x = 1.8$ ($\kappa_{95} = 1.6$), a growth rate of $5.7\,s^{-1}$ is predicted for a 1-cm-thick, toroidally continuous, aluminium vacuum vessel positioned behind the blanket. The active feedback coils are located outside the toroidal-field coils (3 m behind the separatrix) and require ~ 2 MVA to correct a 50-mm vertical displacement of the magnetic axis.

The MHD equilibrium and stability of the ARIES-I design are summarized in Reference [9]. The reference MHD equilibria for ARIES-I are computed using the HEQ code [10] which calculates free-boundary solutions for a given plasma position, shape, and linked poloidal flux while minimizing the stored energy. The on-axis safety factor for the reference equilibrium is $q_o = 1.45$, $q_{95} = 4.85$, and the plasma triangularity at the x-point is 0.70 . High-n ballooning modes and the $n = 1$ kink mode were examined to determine the stability β limit for a conducting wall at infinity. The intermediate-n ballooning modes are avoided by retaining small gradients in the q-profile near the plasma axis. Stable equilibrium has been found with

$\beta = 1.9\%$, corresponding to a Troyon coefficient, $C_T = 3.2$ [9]. The bootstrap current fraction, $f_{BS} = I_{BS}/I_p$ for the ARIES-I reference equilibria is estimated at 0.57 [11].

The ARIES-I reactor operates at steady state using ICRF fast waves to drive the current at the core plasma, lower-hybrid waves for edge-plasma current drive, and bootstrap current. An alternate current-drive system based on high-energy neutral beam injection is also analyzed [11].

Substantial experience has been accumulated in recent years with high-power ICRF fast-wave heating in large tokamaks. Fast-wave current drive has been observed in smaller machines [12] and more definitive experiments are planned on DIII-D and JET. Details of ARIES-I current-drive system is given in Reference [11]. Self-consistent current-drive calculations have been performed to ensure that the total driven current density (including bootstrap) match the target equilibrium current-density profile.

The ICRF frequency is set at 158 MHz and the wave spectrum is centered at $N_{\parallel} = 1.6$ to avoid wave absorbtion by energetic alpha particles and minimize the power absorbed by the fuel ions. The fast-wave launcher is located above the equatorial plane on the outboard side to generate the desired broad current profile. The current-drive power is estimated at 160 MW. Recent calculations suggest that by further optimization, the current-drive power can be reduced to ~ 130 MW [11].

The fast-wave launcher is the folded wave guide [11] with a high-power handling capability of $\sim 40\,\mathrm{MW/m^2}$ [11,13]. The ARIES-I launching system consists of four modules with a total coverage of 1.6% of the first-wall area. Each module is 3.6-m wide, 0.6-m high, and includes an array of 12 folded wave guides. The four launcher modules are located in two special blanket segments, each having two poloidally stacked modules (at 25° and 46° in the poloidal direction, above the equatorial plane) to generate the desired target equilibrium current profile [11].

The impurity-control/particle-exhaust system for the ARIES design consists of a double-null divertor configuration with a toroidally continuous target plate. Because $\sim 50\%$ of core-plasma energy is radiated (mainly by synchrotron radiation) and because of the high upstream separatrix density of $\sim 10^{20}\,\mathrm{m^{-3}}$, a high-recycling divertor mode is expected. The peak heat flux on the divertor target is estimated at about 5 to $7\,\mathrm{MW/m^2}$ with a divertor plasma temperature of ~ 25 eV. The divertor target is coated with a high-Z, tungsten-rhenium alloy to reduce the sputtering erosion to negligible levels.

Extensive transport calculations have been performed, using BAULDER code [14], to gain confidence that the ARIES-I plasma would ignite and achieve the predicted steady-state burn condition [15]. These calculations show that the confinement needs of ARIES-I are consistent with present data base; only enhancement factors between 1 to 2 over L-mode, depending on the scaling relation used, are needed.

THE ARIES-I FPC DESIGN

The ARIES-I design uses advanced superconductor toroidal-field coils with a peak field of 24 T. Details of the ARIES-I magnet design are given in Reference [16]. Currently available Nb_3Sn-based superconductors are capable of producing fields up to ~ 20 T [17]. For higher fields, only NbN, Nb_3Al, and $Nb_3(Al,Ge)$ have demonstrated the capability of sufficient current density, J_c. In particular, the $Nb_3(Al,Ge)$-tape superconductor is capable of $J_c \simeq 300\,\mathrm{MA/m^2}$ at $B = 31$ T [18]. This level of performance, however, is only obtained in a superconductor tape and not in a multifilamentary wire. Therefore, the ARIES-I magnet uses $Nb_3(Al,Ge)$ tape superconductor in the high-field region of the coil ($B > 18$,T), while multifilamentary Nb_3Sn and NbTi superconductor wires are utilized in the low-field region. The ARIES-I magnet system consists of 16 coils with a total stored energy of 105 GJ and an overall current density of $30\,\mathrm{MA/m^2}$.

One of the features of the ARIES-I magnet is the CuNb stabilizer, a high-strength, high-modulus, low-resistivity composite, which carries some of the structural load [16]. This stabilizer offers superior mechanical properties when compared with the metalic stabilizers such as Al or Cu.

A large number of fibrous materials exist that have longitudinal ultimate tensile strength in the range of 2100 to 7900 MPa and longitudinal tensile modulus in the range of 150 to 700 GPa. The primary fibrous materials today are polymers, C, and SiC. As fibers tend to have poor transverse compressive strength, magnet applications require the incorporation of the fibers into a matrix that can support the compressive loads in the inner leg. For this reason, the ARIES-I magnet uses a C-fiber/Cr-Ni steel composite structural material. The composite consists of a 40% C-fiber fraction (fiber strength of 6 GPa and fiber modulus of 485 GPa) in a Cr-Ni matrix (50% volume fraction) and 10% interface (assumed to support negligible loads). The composite modulus is estimated at ~ 300 GPa and the allowable stress is estimated to be ~ 1.7 Gpa, much higher than the allowable stress used in the ARIES-I magnets [16].

A superstructure is used to support the out-of-plane loads and consists of a bucking cylinder and two structural caps [16,19]. The bucking cylinder is 5.6-m high and the out-of-plane loads are transferred by the use of keys and key-ways that are cut in the bucking cylinder. The break points between the center post and the top and bottom caps are located at the zero shear-stress points. The caps, therefore, are in near equilibrium, with the loads in the inner part of the coil balanced by the loads in the outer part. Some small keys and key-ways are provided to carry the small unbalanced forces that may occur during start-up or disruptions.

The ARIES-I blanket is made of SiC/SiC composite structural material, is cooled by He at 5 MPa and includes Be neutron multiplier and Li_4SiO_4 solid breeder [20]. The SiC/SiC composite allows a high operating temperature operation and features very low activation and very low decay-afterheat characterisitics. The breeder and multiplier material are also chosen to meet the low-activation, low-afterheat requirements. The first wall and blanket are constructed as a single unit. The internals of a blanket module is shown in Figure 3. Each blanket module is 0.35-m wide in the toroidal direction and 0.8-m long in the radial direction. The first-wall tubes are oval shaped and form one side of the blanket module. The blanket is divided into three zones.

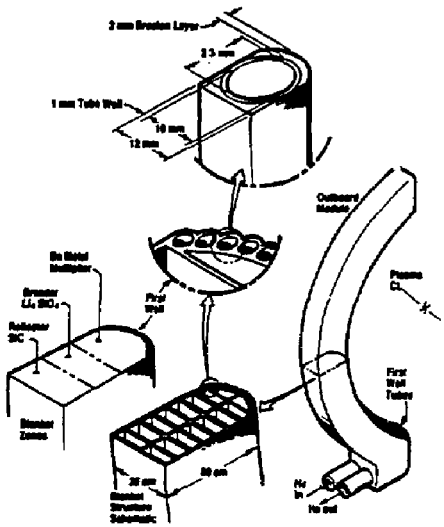

Figure 3 The ARIES-I blanket module.

The multiplier zone is 0.25-m thick and consists of ~ 21% SiC and ~ 51% Be in average volume fraction. The tritium-breeding zone is 0.20-m thick and consists of 19% SiC and 54% Li_4SiO_4 solid breeder. The reflector zone is 0.33-m thick and consists of 95% SiC. The shield is located behind the blanket and is 0.5-m thick on the inboard side and 1-m thick on the outboard side. There is a 1-cm thick, aluminum vacuum vessel between the blanket and shield component which also provide passive stabilization for vertical stability of the plasma. At a ^{6}Li enrichment level of 20%, the tritium breeding ratio for this design is 1.12 and the blanket energy multiplication is 1.37 [6].

The He coolant enters a blanket module at the bottom, flows upward through the first wall, breeder, and reflector zones and then downward through the multiplier zone. The coolant inlet temperature is 350° C and the the outlet temperature is 650° C.

The ARIES-I reference power cycle is a supercritical steam Rankine power cycle [21] which is similar to that proposed by a recent EPRI study [22] for present or near-term coal-fired plants. For a maximum steam temperature of 600 C, the estimated gross thermal efficiency of the ARIES-I power cycle is 48%, similar to that of Reference [22].

The ARIES-I blanket uses SiC/SiC composites as the structural material. Monolithic ceramic materials have been considered for fusion applications in the past. However, the brittle fracture response of bulk ceramic material causes the fracture tensile strength to have a wide statistical distribution, making the failure points unpredictable. Furthermore, failure of monolithic ceramic material is generally catastrophic. These concerns can be alleviated by using a ceramic composite with fibers dispersed in a ceramic matrix. High strength can be achieved by transferring the load from the matrix to the fibers, taking advantage of the superior tensile strength of the fibers. Fracture-toughness values for ceramic-matrix composites are very high because energy is absorbed as fibers are pulled away from the matrix causing crack deflection or arrest and reducing the probability of catastrophic failure significantly.

Recent advances in developing high-performance composites, especially by the areospace industry both as light-wight, high-strength air-foil material and for high-temperature heat-engine application have been phenomenal. In particular the development of SiC-fiber-reinforced SiC matrix composites has shown great improvements in failure-mode behavior, strain tolerances, and fracture toughness.

For the ARIES-I design, micromechanical design equations were used to estimate the thermomechanical properties of the SiC composite material. A conservative maximum allowable design stress of 180 MPa was estimated for a matrix with 60% fiber volume fraction and 10% porosity, operating at 1000° C [22]. Preliminary finite-element analyses of the thermal and pressure stresses indicate that these stresses are well below the estimated design limits [22].

A modular maintenance approach is envisioned for scheduled maintenance of the ARIES-I FPC [19]. The reactor is divided toroidally into 16 modules, each containing one toroidal-field coil and cryostat, nine outboard and six inboard blanket modules, a section of the shield, upper and lower divertor modules, and part of the vacuum vessel. The mass of one modules is estimated at 440 tonnes. Access to the FPC requires that the upper toroidal-field-coil superstructure to be lifted. Each FPC module can then be removed by vertical movement as one complete unit. This type of maintenance approach is expected to provide a more rapid turn-around time for scheduled repairs by eliminating a majority of the interfaces that will need to be removed with remote maintenance equipement [19]. Another key feature of this approach is that all hydraulic, vacuum, and electrical connections are made and broken with few, dedicated, single-function actuators that require a minimal amount of operator interaction.

SUMMARY AND CONCLUSIONS

The ARIES study is pursuing three visions of tokamaks as fusion power reactors, each with a different degree of extrapolation in physics and technology data base. The ARIES-I design assumes minimum extrapolation in tokamak physics and utilizes advanced technologies that would be available in the next 30 years, given the present trends.

The ARIES-I reactor has superior safety and environmental features. All FPC material qualify as Class-C shallow-land burial waste. Because of the use of low-activation, low-decay-afterheat material through the ARIES-I FPC, the temperature rise during an accident would be so small that no materials would be released from the blanket. Therefore, more of the plant can be constructed from industrial-grade components rather than from those of nuclear-safety grade. It has been estimated that a cost reduction of up to 25% can be achieved by avoiding nuclear-safety-grade equipement [23]. The projected cost of electricity for ARIES-I reactor is 69 mill/kWh (55 mill/kWh with safety credits) and is competitive with fission PWRs which range from

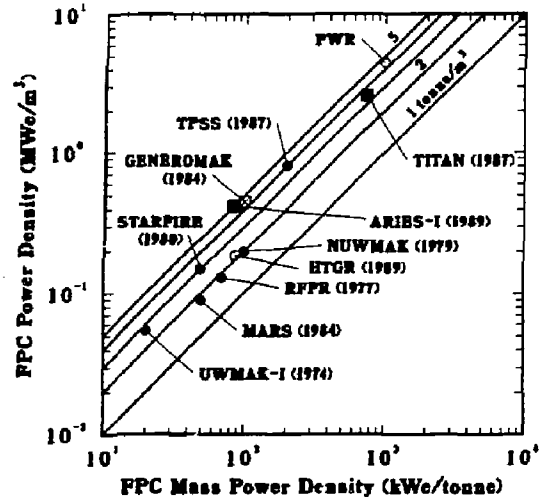

Figure 4. The mass power density and the FPC power density of several conceptual fusion reactor designs, including ARIES-I, a fission PWR, and a fission HTGR.

46 to 78 mill/kWh (using the same cost methodology) and GENEROMAK [24] with 57 mill/kWh. The economic competitiveness of ARIES-I, as characterized by the mass-power-density figure of merit, is also illustrated in Figure 4.

Technological requirements for ARIES-I are many; the most important are the development of high-field superconductor coils and SiC composite material. But, noting the recent development in these areas in recent years, and assuming that these historical trends will continue, these technologies would be available in the next 30 years.

The ARIES-I reactor is a low-current, high-aspect-ratio, high-field tokamak operating in the first MHD stability regime. The ARIES-I reactor operates at steady state using ICRF fast wave current drive and bootstrap current. The confinement needs for ARIES-I plasma are consistent with present projection; only enhancement factors of 1 to 2 over L-mode, depending on the scaling relationship used, are needed Given the relative conservatism in ARIES-I plasma performance projections, the successful outcome of CIT and ITER programs will provide the necessary data base for ARIES-I-class reactors.

REFERENCES

[1] R. W. Conn and F. Najmabadi, "A Program in Tokamak Reactor Studies," University of California - Los Angeles report UCLA-PPG-1201, Dec. 1987.

[2] J. F. Santarius *et al.*, "Energy Conversion Options for ARIES-III - A Conceptual D^3He Tokamak Reactor," in these Proceedings.

[3] R. L. Miller *et al.*, "The ARIES-I High-Field Tokamak Reactor: Design Point Determination and Parametric Studies," in these Proceedings.

[4] S. J. Piet, "Approaches to Achieving Inherently Safe Fusion Power Plants," *Fusion Technol.* **10** (1986) 7.

[5] J. S. Herring *et al.*, "Safety in the ARIES Tokamak Design Study," in these Proceedings.

[6] E. T. Cheng *et al.*, "Neutronics Studies for the ARIES-I Reactor," in these Proceedings.

[7] C. G. Bathke *et al.*, "Vertical Stability Requirements for ARIES-I Reactor," in these Proceedings.

[8] S. C. Jardin *et al.*, *J. Comp. Phys.* **66** (1986) 481.

[9] Y-K M. Peng *et al.*, "MHD Equilibrium and Stability Considerations for High-Aspect-Ratio ARIES-I Tokamak Reactor," in these Proceedings.

[10] D. J. Strickler *et al.*, "MHD Equilibrium Methods for ITER PF Coil design and System Analysis," Oak Ridge National Laboratory report ORNL/FEDC-88/7 (1989).

[11] T-K. Mau *et al.*, "Current Drive Analysis and System Design for the ARIES-I Tokamak Reactor," in these Proceedings.

[12] D. A. Ehst *et al.*, "Fast Wave Heating/Current Drive Scenarios for ITER," ITER Internal report ITER-IL-Ph-6-9-U19 (1989).

[13] T. L. Owens *et al.*, "A Folded Waveguide Coupler for Plasma Heating in the Ion Cyclotron Range of Frequencies," *IEEE Trans. Plasma Sci.* **PS-15** (1987) 273.

[14] C. E. Singer *et al.*, "Baulder: A One-Dimensional Plasma Transport Code," *Comp. Phys. Comm.* **48** (1988) 124.

[15] E. Ibrahim *et al.*, "Plasma Transport and Confinement Simulations for the ARIES-I Tokamak Reactor," in these Proceedings.

[16] L. Bromberg *et al.*, "High-Field Toroidal-Field Magnets Designs for ARIES-I," in these Proceedings.

[17] S. Pourrahimi *et al.*, in *Proc. App. Superconductivity Conf.*, baltimore, MD (October 1986).

[18] K. Togano and K. Tachikawa, *Adv. Cryo. Engr.* **34** (1988) 451.

[19] S. P. Grotz *et al.*, "Design Integration of the ARIES-I Tokamak Reactor," in these Proceedings.

[20] C. P. C. Wong *et al.* "Blanket Design for the ARIES-I Tokamak Reactor," in these Proceedings.

[21] M. Z. Hasan, *et al.*, "Thermal Cycle Power Conversion for ARIES-I Tokamak Reactor," in these Proceedings.

[22] S. Sharafat *et al.*, "SiC Composites as Structural Material for the ARIES-I Reactor," in these Proceedings.

[23] J. P. Holdren *et al.*, "Exploring the Competitive Potential of Magnetic Fusion Energy," *Fusion Technol.* **13** (1988) 55.

[24] J. Sheffield *et al.*, "Cost Assessment of a Generic Magnetic Fusion Reactor," *Fusion Technol.* **9** (1986) 199.

THE ARIES-I HIGH-FIELD-TOKAMAK REACTOR: DESIGN-POINT DETERMINATION AND PARAMETRIC STUDIES†

R. L. Miller and the ARIES Team, Los Alamos National Laboratory, Los Alamos, NM 87545

ABSTRACT: The multi-institutional ARIES study has examined the physics, technology, safety, and economic issues associated with the conceptual design of a tokamak magnetic-fusion reactor. The ARIES-I variant envisions a DT-fueled device based on advanced superconducting coil, blanket, and power-conversion technologies and a modest extrapolation of existing tokamak physics. A comprehensive systems and trade study has been conducted as an integral and ongoing part of the reactor assessment in order to identify an acceptable design point to be subjected to detailed analysis and integration as well as to characterize the ARIES-I operating space. Results of parametric studies leading to the identification of such a design point are presented.

I. INTRODUCTION

The Advanced Reactor Innovation and Evaluation Study (ARIES)[1] is a multi-year, multi-institutional effort to develop several visions of the tokamak as an attractive magnetic-fusion reactor with enhanced economic, safety, and environmental features. One approach, ARIES-I, combines advanced superconducting coil, blanket, and power-conversion technologies with a modest extrapolation of existing first-stability-regime tokamak physics (i.e., equilibrium, stability, and transport). This approach,[2] which contrasts with possible extrapolations[3] of *both* near-term physics and engineering, attacks the current-drive problem by reducing the plasma current, with increased on-axis field being used to compensate for the otherwise low-beta plasma that results. As a part of this study, the reactor operating space, key tradeoffs, and crucial sensitivities are examined using a comprehensive systems model to identify an acceptable ARIES-I design point to be subjected to detailed engineering-design analysis and integration. Additionally, the parametric variations characterize the robustness of the ARIES-I "design window" and establish the context of any specific design point, given unresolved uncertainties and future developments in both physics and engineering. The ARIES study provides an opportunity in the decade since the STARFIRE study[4] to integrate in a fairly detailed model the key tokamak features and subsystems that have been examined in recent years using simpler models.[5,6] Results of plasma engineering, blanket and shield, impurity-control, magnet, power-conversion, maintenance, tritium-handling, safety, and other analyses are integrated, sometimes in approximate form, into a systems optimization model, which typically uses cost of electricity (COE) as an object function. Key aspects of the ARIES-I physics model are summarized in Sec. II, and the engineering and costing models are discussed in Sec. III. Representative parametric results leading to the reference ARIES-I design point are presented in Sec. IV. Conclusions of the work to date are summarized in Sec. V.

II. PHYSICS MODELS

The axisymmetric tokamak plasma equilibrium is described by the major toroidal radius, R_T, minor plasma radius, a, vertical elongation $\kappa = b/a$, triangularity, δ, and standard radial profiles of density $\{n(r) = n_o[1-(r/a)^2]^{n_n}\}$, temperature $\{T(r) = T_o[1-(r/a)^2]^{n_T}\}$, pressure $\{p(r) = p_o[1-(r/a^2)]^{n_p}$, $\alpha_p = \alpha_n + \alpha_T\}$, and current density. The ratio $A \equiv R_T/a = 1/\epsilon$ is the plasma aspect ratio, with A = 3-6 being the range of parametric interest. The ratio of plasma pressure to magnetic-field pressure (i.e., $\beta = <p> / (B_{\phi o}^2/2\mu_o)$ is taken to be limited by the Troyon relation: $\beta = C_T I_\phi/(aB_{\phi o})$, where $I_\phi(MA)$ is the toroidal plasma current, $B_{\phi o}(T)$ is the vacuum toroidal magnetic-field strength on axis ($R \simeq R_T$), and $C_T \simeq 0.032$ is a nearly constant coefficient [$C_T = f(A, \kappa, \delta,$ etc.)] set by kink and ballooning stability considerations.[7]

†Work supported by US DOE, Office of Fusion Energy.

Combining the definitions of the edge safety factor, q, and C_T, the plasma beta, as monitored by separate equilibrium and stability studies,[7] scales approximately as

$$\beta \equiv 5 C_q \frac{C_T}{q} \frac{\epsilon}{(1-\epsilon^2)} S^2 \quad , \qquad (1)$$

where $C_q \simeq (1.17 - 0.65\epsilon)$, $S \simeq [(1+\kappa^2)/2]^{1/2}$; the on-axis safety factor q_o is ~ 1.3. Values of κ approaching 2, desirable from the viewpoint of increasing β, are considered inaccessible for reasons of vertical stability (e.g. passive-shell placement behind the blanket).[8] Higher values of A result in lower beta and current for fixed q and κ. A DT thermonuclear burn model that includes fusion-product contribution to p ($Z_{eff} \equiv 1.6$) calculates the fusion power and satisfies the Lawson criterion [$n\tau_E = 1.75(10)^{20} s/m^3$ at $T_i \simeq T_e \simeq 20$ *keV*] for a driven (heating power *includes alpha power, P_α, and absorbed CD power, P_{CD}, plus ohmic heating power, P_Ω*) system with radiation (*synchrotron power, P_{SY}, and* bremsstrahlung, P_{BR}) and transport losses. The operating temperature is obtained by balancing considerations of fusion power density and CD coupling efficiency. Transport is calibrated against a number of tokamak confinement scaling relations[9] [e.g., $H_G \equiv \tau_E/\tau_E(GOLDSTON) \simeq 1.3$]. Impurity control is provided by two poloidal-field divertors. Steady-state operation is achieved by noninductive CD provided by ICRF fast waves [*with neutral-beam injection (NBI) as a backup option*]. The efficiency of the CD process is characterized by the coupling efficiency $\gamma(10^{20} A/m^2 W) \equiv n_i R_T I_\phi / P_{CD} \propto T_e^{0.77}$ and the hardware efficiency, η_{CD}, appropriate for either CD option. The ratio of fusion power, P_F, to absorbed current-drive power, P_{CD}, is denoted by the gain, Q_p. A significant fraction ($f_{BC} \simeq 0.57$ for $A = 4.5$ and the assumed values of α_n and α_T) of the plasma toroidal current, I_ϕ, is provided by the pressure-gradient-driven bootstrap effect, calculated self-consistently.[10]

III. ENGINEERING AND COSTING MODELS

The ARIES-I fusion power core [FPC, ie., first-wall (FW), blanket, shield, coil set, and divertor system] is characterized in the systems model in order to estimate the cost-of-electricity [COE, (mill/kWeh)] figure of merit, which is a strong and counteracting function of the FPC mass power density [MPD (kWe/tonne)], and the engineering Q-value, $Q_E = P_{ET}/P_C$, where P_{ET} is the gross electric power and P_C is the total recirculating power. The SiC composite ceramic first wall is a relatively poor reflector of synchrotron radiation, but the high radiation fraction [$f_{RAD} \equiv (P_{BR} + P_{SY})/(P_\alpha + P_{CD} + P_\Omega) \simeq 0.5$] serves to spread the heating power over the entire first-wall surface and limit the W divertor-plate peak heat load ($q_{PL} \simeq 5.5\ MW/m^2$) and the edge temperature ($T_{PL} \simeq 27\ eV$) to reduce sputter erosion. The gas-cooled blanket consists of a SiC composite ceramic structure, a Be (metal) neutron multiplier, and Li_2SiO_4 tritium breeder. The shield is composed of bulk SiC and B_4C. The inboard blanket/shield stand-off is 1.4 m and the outboard (top/bottom) standoff is 1.8 m. The blanket neutron-energy multiplication is $M_N \simeq 1.4$, and thermal-conversion efficiency (supercritical-steam Rankine cycle) is 48%. The toroidal-field (TF) coil model assumes a D-coil (N = 16) incorporating an advanced superconductor [(e.g., $Nb_3(Al,Ge)$ with 46-T critical field] to allow peak field strengths on the inboard TF-coil legs, $B_{\phi c} \simeq 24\ T$. The stabilizer current density is $j_{ST} = 200\ MA/m^2$, and stress is $\sigma_{ST} = 800\ GPa$ and the TF-coil structural allowable stress is $\sigma_{all} = 1000\ MPa$. TF-coil centering forces are reacted by a bucking cylinder constrained by elastic buckling and peak hoop stress ($\sigma_\theta \simeq 1000\ MPa$) limits. The TF-coil thickness is determined by a current-density/field-strength scaling.[11] The coil conductor technology and structural requirements are taken to be appropriate extrapolations from existing technology.[12]

The ARIES-I reactor power-balance equations are solved subject to a specified net output power (e.g., P_E = 1000 MWe). The nominal ICRF fast-wave system efficiency is η_{CD} =68%. The recirculating power is dominated by the CD requirement, with 5% of the gross electric power, P_{ET}, used for primary-coolant circulation and other site-power uses. The reciprocal of the recirculating power fraction is denoted by the engineering Q-value, Q_E. Appropriate unit costs, summarized in TABLE I, are used to determine the total direct cost, TDC. Standard assumptions[13,14] regarding construction time (τ_c = 6 yr), plant availability (p_f = 0.76), economies of scale, and operation and maintenance (O & M) charges are used to estimate the constant-dollar (1988) COE. In the cost estimates presented herein, no safety-assurance cost credits,[15] which may be expected to result from the use of low activation materials, have been taken. Calculated on a consistent basis, the projected[16] COEs for "median-experience" and "better experience" fusion PWR (P_E = 1100 MWe) are 78 and 46 $mill/kWeh$, respectively, with a coal (P_E = 2 x 550 MWe) cost projected[16] at 50 $mill/kWeh$.

TABLE I. ARIES-I UNIT COSTS(a)

Li_2SiO_4	($/kg)	70
SiC (composite ceramic FW/blanket)	($/kg)	106
SiC (bulk shield)	$/kg)	25
Be neutron multiplier	($/kg)	530
PF coils (Nb_3Sn)	($/kg)	70-80
TF coils [$Nb_3(Al, Ge)$]	($/kg)	90
ICRF fast wave CD power (η_{CD} = 0.68)	($/W)	1.6
NBI CD power (η_{CD} = 0.75)	($/W)	3.0
LH CD power	($/W)	1.25

(a) Including 10th-of-a-kind learning-curve credits.

The systems code incorporates a series of computational search loops (e.g., fixed A and variable a) which solve for the FPC physics and engineering characteristics. Subject to certain constraints (e.g., $B_{\phi c} < B_{MAX}$, radial build, etc.), cost dependencies are identified and the key interactions between system variables are determined. Design points identified by this procedure are subjected to more detailed analysis and subsystem design, with conceptual-design results being fed back to the systems-design code throughout the project for further optimization and refinement. Ongoing calibrations with separate subsystem models are made. The system code, therefore, is used as an actual tool in the iterative conceptual-engineering-design process.

IV. RESULTS

A. DESIGN SPACE

A typical result of the systems model is summarized in Fig. 1, leading to the choice of the reference P_E = 1000 − MWe minimum-COE design point at A = 4.5. The cost of the tokamak reactor (for any A) increases as its size increases (i.e. larger a or R_T with fixed A). Small values of a are associated with higher values of $B_{\phi c}$ and $B_{\phi c}$, resulting in a thicker build of the TF-coil inboard leg and a thicker bucking cylinder. The ARIES-I operating space is summarized as in Fig. 2 to emphasize the interaction between plasma current, I_ϕ, and peak TF-coil field, $B_{\phi c}$, in setting the cost minimum. The locus of minimum-COE points tracks from 75 mill/kWeh ($A \simeq 3.5$, $B_{\phi c} \simeq 16T$) to 69 mill/kWeh ($A \simeq 4.5$, $B_{\phi c} \simeq 24T$), as I_ϕ decreases from 13 to 11 MA.

The underlying factors leading to the COE dependence on A are illustrated in Fig. 3. Low values of A yield higher values of β and reduced B_ϕ. The correspondingly higher values of I_ϕ result in higher P_{CD} and, together with a lower bootstrap-current fraction, $f_{BC} = I_{BC}/I_\phi$, yield lower values of Q_E. Higher values of $B_{\phi c}$ at higher A are associated with a more massive coil set and lower MPD values. The costs of massive coils at higher A trade with the dominant costs of current drive at low A to minimize the COE near $A \simeq 4.5$. The tradeoff between FPC cost reflected in MPD and recirculating power costs associated with CD reflected in Q_E is a recurrent theme in optimizing the tokamak reactor, which, for the unit costs assumed, generally favors high MPD at the expense of reduced Q_E for a given A; this balance is illustrated in Fig. 4. Low values of Q_E also result in increased thermal-cycle and electric-power-generation costs, not in the FPC itself, but in the balance of plant (BOP).

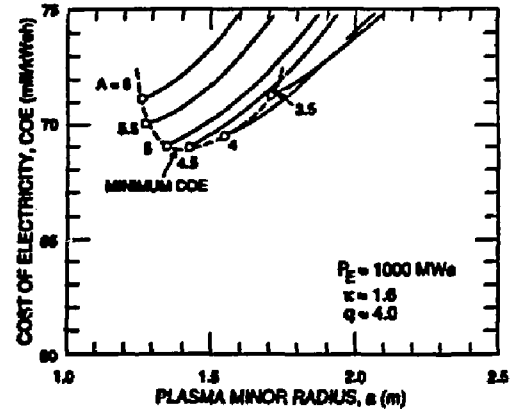

Fig. 1. Dependence of COE (1988 dollars) on ARIES-I minor radius, a(m), for fixed net electrical power, P_E = 1000 MWe, plasma vertical elongation, κ = 1.6, and edge safety factor, q = 4.0. The minimum-COE point (~69 mill/kWeh) occurs near plasma aspect ratio $A \equiv R_T/a \simeq 4.5$.

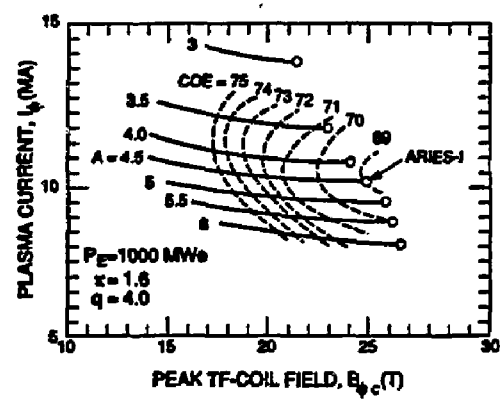

Fig. 2. ARIES-I operating space expressed in terms of plasma current, I_ϕ, and peak TF-coil field, $B_{\phi c}$, for the indicated fixed parameters. Shown are contours of constant plasma aspect ratio, $A \equiv R_T/a$, and constant COE (mill/kWeh). The reference ARIES -I design point at A= 4.5 is indicated.

B. DESIGN POINT

Key operating parameters of the ARIES-I design point as determined by the systems tradeoffs described in Figs. 1-4 are summarized on TABLE II. This design point provides a basis for more detailed conceptual engineering design leading to a "reference" design as well as serving as a point of departure for sensitivity studies of important physics (e.g. plasma profiles, Troyon coefficient, bootstrap-current fraction, etc.), engineering (e.g. blanket/shield thickness, coil stress, conductor field limits, thermal-conversion efficiency, etc.), and cost (unit costs, plant availability, etc.) variables.

As an example of a physics sensitivity study, Fig. 5 displays variations in ARIES-I performance as a function of the plasma density profile exponent, α_n. An increased value of α_n results in higher Q_E as the bootstrap-current fraction, f_{BC}, increases. A more efficient system requires lower B_ϕ values (i.e. thinner coils and increased MPD). The value of α_n appropriate for ARIES-I is calculated separately by plasma transport models. Other "hidden" tradeoffs include the increase in f_{RAD} as A increases and the favorable dependence of γ on β and T_e.

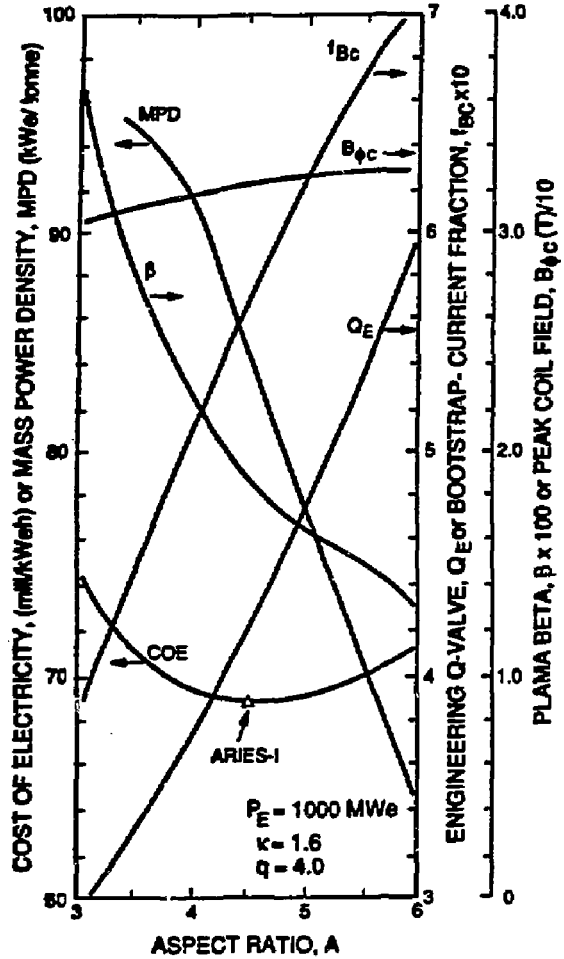

Fig. 3. Dependence of key ARIES-I cost drivers on plasma aspect ratio, $A \equiv R_T/a$.

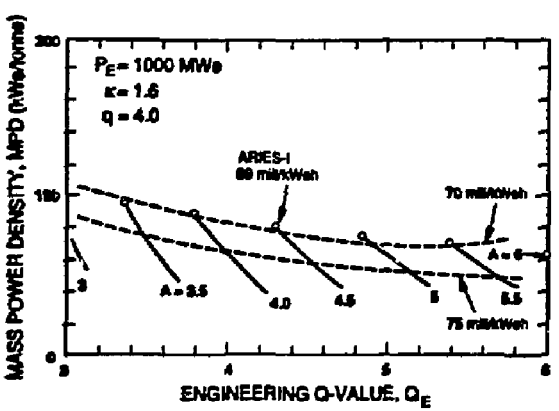

Fig. 4. Mass power density (MPD, kWe/tonne) as a function of engineering Q-value, $Q_E \equiv P_{ET}/P_C$, for fixed values of plasma aspect ratio, $A = R_T/a$. Curves of constant COE (70 and 75 mill/kWeh) are included for the indicated fixed parameters.

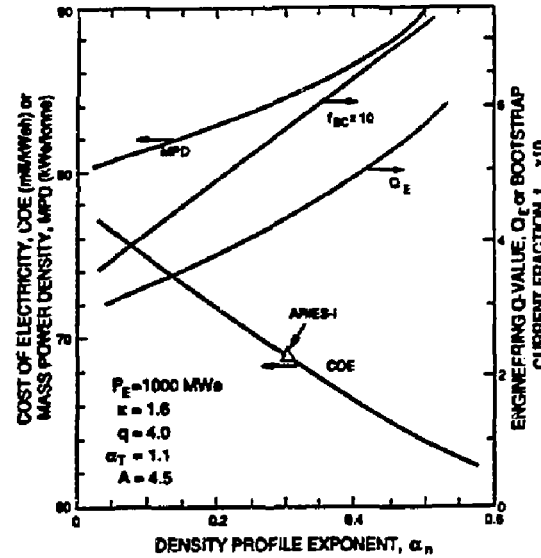

Fig. 5. Dependence of ARIES-I performance on the plasma radial density profile exponent, α_n.

The advantage of access to the regime of high-field operation relative to an extrapolation of nearer-term (NT) Nb_3Sn coil technology is illustrated in Fig. 6. Using ICRH fast-wave CD, the NT values of COE are $\geq$ 80 *mill/kWeh* in large systems. The advanced-coil feature of ARIES-I opens the parameter space to allow smaller systems with COE $\simeq$ 70 *mill/kWeh*. It may be noted that systems based on NT technology optimize at $A \simeq 3.5$, consistent with present experimental experience. It may be noted that the ratio $B_{\phi c}/B_{\phi o}$ decreases with increasing A. Also, the TF stored magnetic energy, $W_B(GJ)$, increases with increasing A, providing a safety disincentive for higher-A operation.

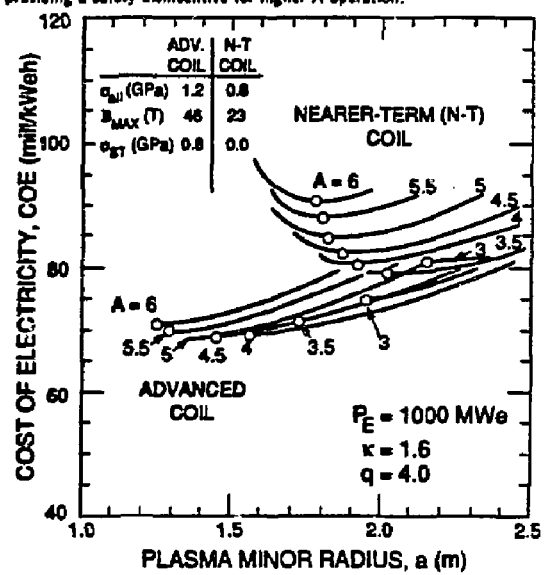

Fig. 6. Cost of electricity, COE, as a function of tokamak plasma minor radius, a(m), for the indicated fixed parameters and various values of plasma aspect ratio, $A \equiv R_T/a$, for nearer-term (NT) coil technology and the advanced ARIES-I coil extrapolation.

TABLE II. ARIES-I DT-FUELED TOKAMAK REACTOR

Stability Regime	First
Aspect ratio, $A = R_T/a$	4.5
Major toroidal radius, $R_T(m)$	6.525
Minor plasma radius, $a(m)$	1.45
Plasma vertical elongation, $\kappa = b/a$	1.6
Plasma safety factor, q	4.0
Troyon coefficient, $C_T[\beta = C_T I_\phi/aB_{\phi o}]$	0.032
Plasma toroidal beta, β	0.0194
Plasma temperature, $T_o \simeq T_i(keV)$	20
Plasma ion density, $n_i(10^{20}/m^3)$	1.42
Plasma electron density, $n_e(10^{20}/m^3)$	1.62
Lawson parameter, $n_i\tau_E(s/m^3)$	1.8
Plasma Q-value, $Q_p = P_F/P_{CD}$	12.7
On-axis toroidal magnetic field, $B_{\phi o}(T)$	13.0
Peak TF-Coil magnetic field, $B_{mc}(T)$	23.75
Stored magnetic energy, $W_B(GJ)$	160.0
Plasma toroidal current, $I_\phi(MA)$	30.9
Bootstrap current fraction, f_{BC}	0.57
Current-drive efficiency, γ $(10^{20}\ A/m^2W)$[A/W]	0.314[0.03]
Absorbed current-drive power, $P_{CD}(MWe)$	157
14.1-MeV neutron wall loading, $I_w(MW/m^2)$	2.74
Thermal power, $P_{TH}(MWt)$	2812
Gross electric power, $P_{ET}(MWe)$	1306
Net electric power output, $P_E(MWe)$	1000
Recirculating power fraction, $1/Q_E$	0.23
Magnet costs (M$)	500
CD costs (M$)	252
Current drive FW/Blanket/Shield costs (M$)	157
Total direct cost TDC (M$)	2271
Unit direct cost UDC ($/kWe)	2271
Total cost (M$)	3837
Cost of electricity, COE (mill/kWeh)	68.9
Mass power density, MPD (kWe/tonne)	84

V. CONCLUSIONS

ARIES-I explores one of several possible approaches to improving eventual DT tokamak reactor performance by exploiting high-field operation in order to reduce the current-drive power requirements of steady-state operation. The bootstrap current fraction, f_{BC}, increases and the plasma current, I_ϕ, itself drops as aspect ratio, A, increases. The increasing field offsets the lower beta values at higher A to maintain an adequate fusion power density. At higher values of A, the increasing coil mass results in higher costs and determines an A-value that minimizes COE. A definite cost advantage of the advanced-coil ARIES-I approach relative to reactors based on nearer-term technology is seen, given that both approaches share the existing set of tokamak physics performance assumptions. The specific reference design point and the associated parametric studies that establish the ARIES-I design window suggest the possible benefit of developing this overview of future tokamak reactor improvements. The attractiveness of the ARIES-I design point is dependent on the future availability of advanced, high-field-coil technology. The high-radiation plasma operating regime is critical to effective divertor performance. The high bootstrap-current contribution depends on appropriate plasma profile shaping. These concerns and possible improvements continue to be addressed in the course of the ongoing ARIES study.

REFERENCES

1. F. Najmabadi, R. W. Conn, and the ARIES Team, "The ARIES Tokamak Reactor Study," these Proceedings.
2. J. Schwartz, L. Bromberg, D. R. Cohn, and J. E. C. Williams, "Performance Limits of High Field Tokamak Reactors," *Nucl. Fus.*, **29**, 983 (1989).
3. R. S. Devoto, et al., "Projections for a Steady-state Tokamak Reactor Based on ITER," Lawrence Livermore National Laboratory document UCID-21519 Rev. 1 (July 1989).
4. C. C. Baker, (ed.), "STARFIRE - A Commercial Tokamak Fusion Power Plant Study," Argonne National Laboratory report ANL/FPP-80-1 (September 1980).
5. J. Sheffield, et al., "Cost Assessment of a Generic Magnetic Fusion Reactor, *Fus. Tech.* **9**, 199 (March 1986).
6. R. A. Krakowski and J. G. Delene, "Connections Between Physics and Economics for Tokamak Fusion Power Plants," *J. Fus. En.* **7**, 49 (1988).
7. Y-K. M. Peng et al., "*MHD Equilibrium and Stability Considerations* for High-Aspect-Ratio ARIES-I Tokamak Reactor," these Proceedings.
8. C. G. Bathke, S. C. Jardin, J. A. Lauer, D. J. Ward, and the ARIES Team, "Vertical Stability Requirements for ARIES-I Reactor," *ibid.*
9. N. A. Uckan and the ITER Physics Group," ITER Physics Design Guidelines," International Thermonuclear Experimental Reactor report ITER-TN-PH-8-6 (November 1988).
10. M.-Y. Hsiao, D. A. Ehst, and K. Evans, Jr., "Bootstrap Currents in Radiofrequency Driven Tokamak Equilibria," *Nucl. Fus.* **29**, 49 (1989).
11. J. Schwartz, J. R. Miller, and J. E. C. Williams, "TF Overall Current Density Scaling," personal communication (November 1988).
12. L. Bromberg, et al., and the ARIES Team, "High Field Magnet Designs for the ARIES-I Reactor," these Proceedings.
13. J. G. Delene, et al., "GENEROMAK Fusion Physics, Engineering, and Costing Model," Oak Ridge National Laboratory report ORNL/TM-10728 (June 1988).
14. J. G. Delene, K. A. Williams, and B. H. Shapiro, "Nuclear Energy Cost Data Base," US DOE report DOE/NE-0095 (September 1988).
15. J. P. Holdren, et al., "Report of the Senior Committee on Environmental, Safety, and Economic Aspects of Magnetic Fusion Energy," Lawrence Livermore National Laboratory report UCRL-53766 (June 1989).
16. J. G. Delene, H. J. Bowers, and B. H. Shapiro, "Economic Potential for Future Water Reactors," *Trans. Am. Nucl. Soc.*, **57**, 205 (November 1988).

DESIGN INTEGRATION OF THE ARIES-I TOKAMAK REACTOR

S.P. Grotz, F. Najmabadi, and the ARIES Team
Institute of Plasma and Fusion Research
University of California, Los Angeles
Los Angeles, CA 90024-1597

D.K. Sze
Argonne National Laboratory
Argonne, Illinois 60439

Y-K.M. Peng
Fusion Engineering Design Center
Oak Ridge National Laboratory, P.O. Box Y
Oak Ridge, TN 37831

R.L. Creedon[1], C.P.C. Wong
General Atomics, P.O. Box 85608
San Diego, CA 92138-5608

R.L. Miller
Los Alamos National Laboratory
P.O. Box 1663
Los Alamos, NM 87545

L. Bromberg
Massachusetts Institute of Technology
Plasma Fusion Center
Cambridge, MA 02139

Abstract: ARIES-I is a 1000 MWe commercial tokamak reactor design based on minimal extrapolation of present-day physics and expected technological development in the next 30 years, such as high-field, superconducting magnets and low-activation silicon carbide composite materials. This paper summarizes the design integration of the fusion-power core and the reactor subsystems. Consideration has been given to such details as support of the toroidal field coils, divertor module access, blanket access, design and support of the RF antennas, location of the primary vacuum and cryostat vacuum boundaries. The maintenance procedure being considered for ARIES-I is a modular approach. With this type of maintenance, a module consisting of the first-wall, blanket, shield, divertor module, and toroidal field coil is replaced as a single unit at the end-of-life of the module. Rapid replacement of the irradiated FPC components is expected. Should the first-wall or blanket fail before the end of its design lifetime, *in-situ* repair and replacement schemes are proposed for blanket sub-modules. Replacement of the divertor plate assemblies is simplified by providing a direct access path through which damaged plates can be removed and new plates installed without interfering with the other FPC components.

I. INTRODUCTION

The ARIES-I research program is a multi-institutional effort to develop several versions of the tokamak as an attractive magnetic-fusion reactor with enhanced economic, safety, and environmental features [1]. The ARIES-I design is a D-T burning, first stability 1000 MW_e (net) reactor based on modest extrapolation from the present physics database and features advanced technology such as utilization of very high-field superconducting magnets and a low-activation blanket. As part of this study, the reactor operating space, key tradeoffs, and crucial sensitivities are examined using a comprehensive systems model [2] to identify an acceptable ARIES-I design point which is subjected to detailed engineering-design analysis and integration. The design integration task provides feedback to the other systems designers (*e.g.*, blankets, magnets and supports, current drive launching structures, etc.) to maintain self-consistency throughout the detailed design stage of the study. During the detailed design process, attention is focused on areas which are perceived to be key feasibility and credibility issues. Several technical areas have been identified for which the existing database is insufficient to predict performance with certain accuracy. Since these items have the potential for increasing the attractiveness of the tokamak reactor, the ARIES team will outline possible research and development pathways such that these advanced technologies will be available in the timeframe necessary for commercial fusion reactor construction and operation.

The general configuration of the ARIES-I fusion power core (FPC) is presented in Section II. The options for maintenance of the FPC and divertor are presented in Section III. A summary of outstanding issues and ongoing activities is covered in Section IV.

II. MACHINE CONFIGURATION

Major operating parameters of the ARIES-I reactor are listed in Table I. The plasma major and minor radii are 6.525 m and 1.45 m, respectively, with an aspect ratio of 4.5 design point corresponding to a minimum cost-of-electricity (COE) [2]. An elevation view of ARIES-I is shown in Figure 1. The primary structural material in the blanket is a silicon carbide/silicon carbide composite allowing high temperature operation while meeting requirements for low levels of activation and afterheat [3]. The first-wall and blanket are constructed as a single unit with the first-wall tube-sheet forming the front side of the blanket submodule. The internals of the blanket submodule form three zones; a neutron multiplier zone, a tritium breeding zone, and a reflector zone. Overall radial depth of the blanket is 80 cm on the outboard and 70 cm on the inboard. The multiplier material is beryllium and the breeder is Li_4SiO_4. All three blanket zones and the first-wall are cooled by helium with moderate operating pressure of 5 MPa. A detailed description of the blanket design and analysis can be found in Reference [4]. Only 2% of the neutron power is recovered in the shield, located behind the blanket, so lower-temperature operation is expected. A peak operating temperature in the shield which is less than the design limit will assure that reactor operation can continue in the event that some of the shield channels become plugged.

Between the high-temperature blanket-zone and the shield is the plasma chamber vacuum boundary. The vacuum vessel is an aluminum shell with appropriate stand-offs for support of the blanket modules. The peak nuclear heating rate in the vacuum vessel is less than 1 W/cc, and helium cooling should be adequate. The blanket is not electrically conducting, therefore

[1] Present address: Advanced Cryomagnetics, P.O. Box 210132, San Diego, CA 92121.

no appreciable forces will be transferred to the vacuum vessel during a plasma disruption. Forces produced by eddy currents in the vacuum vessel will need to be calculated and restrained appropriately. The vacuum vessel is toroidally continuous and provides passive vertical stabilization of the plasma. Active vertical control coils are located outside the boundary of the toroidal field coils envelope.

ARIES-I utilizes a double-null divertor configuration with toroidally continuous divertor targets. The high-recycle divertor has a high-Z surface made of a tungsten-rhenium (W-Re) alloy. The present design has a SiC-composite substrate with a thin plasma-side layer of the W-Re. This type of duplex structure minimizes the amount of W-Re, which is not low activation. The low-activation SiC also acts as a heat sink in the event of a loss-of-flow or loss-of-coolant accident. An alternate design being considered has a vanadium alloy substrate with a W-Re coating. The peak heat flux is about $5\,MW/m^2$ and the feasibility of a gas-cooled design is being studied. High volume flow rates and pumping power of the helium may offset the benefit of energy recovery from the target, however, plant design and operation is simplified by eliminating a water-cooling system. The concerns about tritium-contaminated water are also eliminated.

Neutronics calculations, using a 1-dimensional model, predict a tritium breeding ratio of 1.12 for full first-wall coverage [5]. However, approximately 20% of the first-wall area is covered with the divertor target and assembly. It was therefore considered necessary to install tritium breeding zones behind the divertor target assembly to help recover the lost neutrons. Another blanket penetration which affects the tritium breeding is the RF current drive launcher. ARIES-I uses a folded wave guide launcher, as shown in Figure 2. This type of wave guide is capable of delivering power at high power densities ($\sim 10\,MW/m^2$) [6], thus only a small fraction of the blanket is affected, about 2%. The location of the launcher structure has a more pronounced affect on the overall FPC configuration. The launcher is installed at the first-wall, slightly above the reactor midplane. This position requires that the blanket and shield must be split poloidally into two separate modules. The RF launching structures are installed in only two of the FPC modules.

The superstructure used to support the out-of-plane loads and the poloidal field coils is divided in three sections. The middle section is the centerpost, a bucking cylinder, which reacts both the centering force of the toroidal field coils and the out-of-plane loads generated in the throat of the toroidal field coils. Both the toroidal field coils and the structure cryostats are flush against each other, eliminating hot-to-cold interfaces and simplifying the transfer of loads. The out-of-plane loads are transferred by the use of keys and keyways, the keyways being cut in the centerpost. The centerpost is 5.6 m high. Above and below the centerpost the out-of-plane loads are carried by structural caps (partial shells with toroidal continuity). The breakpoint between the centerpost and the top and bottom caps is determined by location of zero shear stresses (from the out-of-plane loads). It has been determined that the location of the null is not very sensitive to the plasma/poloidal field operating scenarios that have been considered. The caps are then in near equilibrium, with the loads in the inner part of the coil balanced by the loads in the outer part of the coils. There will be some small keys and keyways to carry the small unbalances that occur during the startup scenario or the disruptions.

The caps thickness is determined by out-of-plane loads. It has been determined that a thick shell with a varying thickness of 0.05 m to 0.20 m, subjected to a maximum 400 MPa stress, can carry the loads [7]. This is the case even when there are 1×1 m^2 ports (windows) cut into the caps (both top and bottom) in order to obtain access to the top/bottom divertor plates.

III. MAINTENANCE

The baseline approach to the scheduled maintenance of the FPC is with modular component design. The reactor is divided toroidally into 16 modules, each containing one TFC and cryostat, 9 outboard and 6 inboard first-wall/blanket submodules, a section of the shield, upper and lower divertor modules, and 1/16 of the vacuum vessel. The mass of one module is about 440 tonnes, within the capacity of present crane technology. Typical dimensions of the FPC-module are listed in Table II. Access to the FPC-modules requires that the upper TFC superstructure be removed and temporarily stored in a hot cell. After the upper superstructure is removed, the FPC-modules can be removed with either vertical or horizontal movement. If horizontal motion is selected, then the outboard poloidal field coils will need to be either raised or lowered to provide radial access to the module. Figure 3 illustrates the two major component lifts required for ARIES-I FPC scheduled maintenance.

Modular maintenance approaches are expected to provide a more rapid turn-around for scheduled repairs by eliminating a majority of the interfaces that will need to be removed with remote maintenance equipment. A key feature of the modular maintenance approach is that all hydraulic, vacuum, and electrical connections are made and broken with few, dedicated, single function actuators that require a minimal amount of operator interaction.

The cryosystems in the FPC include the toroidal field coils, poloidal field and plasma-shaping coils, bucking cylinder, and the TFC superstructure. The modular maintenance procedures of ARIES-I require that each TFC has its own cryostat. The cryostat for the TFC's are removed with the FPC-module during scheduled maintenance and no cutting and re-welding is required. Vertical recesses are made in the outer wall of the bucking cylinder cryostat in which the straight leg of each of the TFC cryostats rest.

One disadvantage of this type of cryo-configuration is that it is necessary to warm the coils and the superstructure to room temperature in order to separate the cryostats (frozen water/air between the cold surfaces plugs the gap). One advantage is that the absence of shear panel between the toroidal field coils minimizes the time required for assembly/disassembly.

The time required for cooling of the coil/structure is determined by the size of the refrigerator/storage of liquid helium. The process is limited in speed by the need of uniform cool-down. This time is on the order of 1-2 weeks. If the refrigerator is sized for the steady state cooling requirements [7], then the time for cool-down is 2 weeks. A larger refrigerator would allow faster cooldown, but the limit on the isothermal cool-down would be approached.

The time required for warming the coils and structure prior to removal is determined by the need of nearly isothermal warming in order to minimize the thermal stresses. Typical numbers for the sizes being considered is 1-2 weeks, depending on how many heating elements are placed in the cold structure.

The superstructure is attached to the toroidal field coil through keys and mechanical actuators, to add rigidity to the system. No bolts are used to minimize the hands-on, or remote maintenance operations. This would greatly simplify

the remote handling equipment which must be in the vicinity of the reactor. This equipment will be in the nature of automatic devices which are built to perform a specific function with minimal human monitoring, instead of manipulators which require human operators.

During normal operation, it is expected that an average of three or four modules will need to be replaced annually throughout the lifetime of the plant. In the event of an unplanned outage due to failure of a single blanket module, then large, outboard ports in the vacuum vessel are available to access the failed blanket module. Access to the vacuum vessel ports requires temporary removal of a portion of the outboard shield. It is anticipated that removal of a single blanket submodule will be quicker than replacement of the entire FPC-module. However, during scheduled, annual maintenance, when as many as 60 blanket submodules will need to be replaced, it is expected that the baseline FPC-module removal approach will result in the shortest reactor downtime. Small leaks in the first-wall tubes may be fixed *in-situ* by applying either plasma-sprayed or chemical-vapor-deposited silicon carbide directly to the failed region. Access to the first-wall for the *in-situ* repair equipment can be made via the divertor maintenance port. Specific details of the scheduled and un-scheduled maintenance procedures are undergoing further study and analysis.

It is expected that the divertor target will require more frequent maintenance and replacement than the FPC-modules. To provide rapid access and removal of the divertor targets, a separate port is provided in the TFC superstructure, between TFC's, for direct access to the divertor assembly. The divertor plates are segmented toroidally into 32 "pie-slices." Each FPC-module contains four segments (two for the upper divertor and two for the lower). The first divertor segment is withdrawn through the port with a single, radial translation. The second segment is first moved toroidally into the position occupied by the previous segment and then withdrawn radially. None of the other components of the FPC-module are affected by the *divertor maintenance procedure*. Each divertor segment has an attached shield-plug which fills the access pathway when installed in the FPC. The lower divertor access ports also serve as the vacuum pumping ducts for the plasma exhaust and primary vacuum pumps.

IV. ONGOING ACTIVITIES

Detailed design analysis of the ARIES-I FPC and subsystems is on-going and several design integration activities are continuing. Some of the areas receiving further attention and more detailed analysis are the following:

1. Design of the fusion power core module;
   a. Detailed blanket/vacuum vessel interfaces including support of the blanket on the vessel, removal and installation of single blanket modules, and effects of disruption loads on the blanket and vessel,
   b. Design of the hot-to-cold interfaces including heat loss and transfer of magnetic and static loads.
   c. Design and location of intermodule welds for the primary vacuum seal.
   d. Design and analysis of the interfaces between separate cryostats for the bucking cylinder and each toroidal field coil.
2. Disruption analysis of the thermal loads (first-wall and divertor) and electromagnetic loads (divertor target, RF launching structure, and vacuum vessel).
3. Evaluation of other critical interfaces;
   a. High-temperature, high-pressure joints between the ceramic pipes in the FPC and the metal pipes in the remainder of the primary loop.
   b. Design of remotely activated connect/disconnects for the hydraulic, vacuum, and electrical connections associated with each FPC module.
   c. Evaluate the integrity of thin metal coatings on SiC-substrate for use in the divertor and RF antenna.
4. Outline of the procedures for scheduled FPC-module maintenance as well as procedures for un-scheduled maintenance (*e.g.*, replacement of individual blanket modules and divertor plates). Evaluation of potential benefits and drawbacks to alternate maintenance schemes.

In summary, the ARIES-I fusion power core has reached a state of development that exhibits attactive features for use as a commercial tokamak reactor power plant. A simple, three-piece toroidal field coil support structure allows for rapid access to the irradiated fusion power core components during annual, scheduled maintenance. Modular maintenance of the reactor is expected to reduce down time during scheduled repairs, particularly if dedicated, remote connect/disconnects are installed on all or most of the module interfaces. The divertor, which may be subject to a shorter lifetime than the blanket, is accessed through ports which require a minimal amount of machine disassembly and downtime. The position of the RF launching structure, a folded wave guide, requires that two of the sixteen FPC modules have modified outboard blankets and shields to accommodate the antenna. Non-electrically-conducting materials used in the first-wall and blanket should result in little or no disruption forces on the blanket. Detailed engineering analysis is continuing in the areas deemed to be critical, however, only minor changes to the overall configuration are expected during the final stages of the ARIES-I design phase.

ACKNOWLEDGMENT

This work is supported by the U.S. Department of Energy.

REFERENCES

[1] F. Najmabadi, *et al.*, "The ARIES-I Tokamak Reactor Study," these proceedings.

[2] R.L. Miller, "The ARIES-I High-Field Tokamak Reactor: Design-Point Determination and Parametric Studies," these proceedings.

[3] S. Sharafat, *et al.*, "Silicon Carbide-Composites as Structural Material for the ARIES-I Reactor," these proceedings.

[4] C.P.C. Wong, *et al.*, "Blanket Design for the ARIES-I Tokamak Reactor," these proceedings.

[5] E.T. Cheng, "Neutronics Studies for the ARIES-I Reactor," these proceedings.

[6] T.K. Mau, *et al.*, "Current Drive Analysis and System Design for the ARIES-I Tokamak Reactor," these proceedings.

[7] L. Bromberg, *et al.*, "High Field Magnet Designs for the ARIES-I Reactor," these proceedings.

Table I: OPERATING PARAMETERS OF ARIES-I

Parameter	Units	Value
Aspect ratio	(-)	4.5
Major toroidal radius	m	6.525
Minor plasma radius	m	1.45
Plasma volume	m^3	441.
First-wall area	m^2	580.
Peak toroidal field	T	13.0
Thermal power	MW_{tA}	2812
Gross electric power	MW_e	1306
Net electric power	MW_e	1000
Average neutron wall load	MW/m^2	2.74
Average first-wall heat load	MW/m^2	0.48
Primary coolant	(-)	Helium
Inlet pressure	MPa	5.0
Inlet temperature	°C	350
Outlet temperature	°C	650
Tritium breeding ratio	(-)	1.12
Energy multiplication	(-)	1.37

Table II: ARIES-I FPC MODULE DESIGN

Parameter	Units	Value
Height	m	11.2
Width, inboard	m	1.06
Width, outboard	m	4.31
Radial depth	m	8.28
Weight	tonne	440.
Lift for vertical maintenance	m	~14
Lift for horizontal maintenance	m	~3

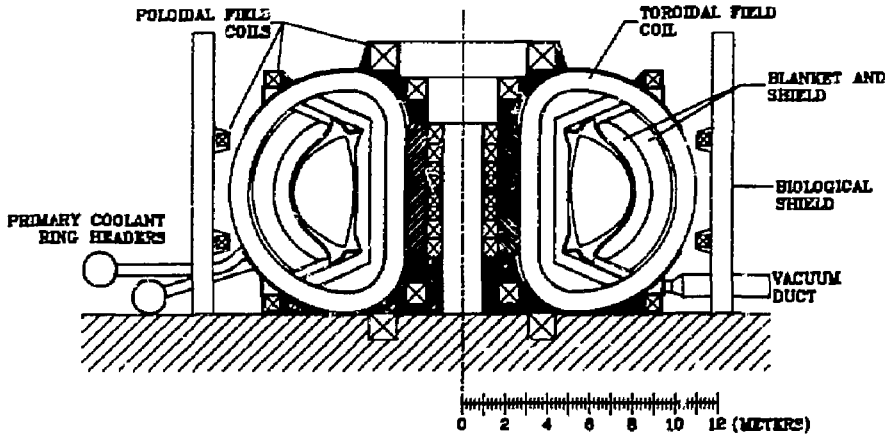

Figure 1. Elevation view of the ARIES-I reactor illustrating the major components of the fusion power core.

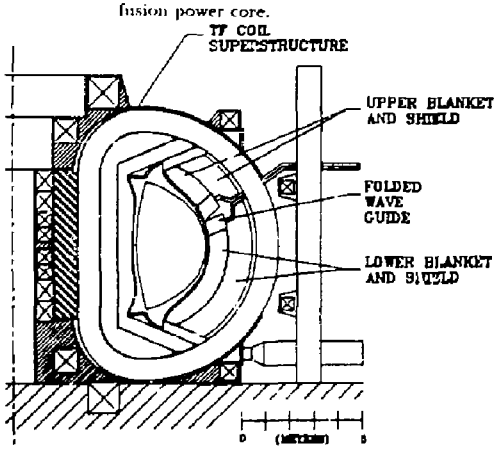

Figure 2. Poloidal cross section of ARIES-I, illustrating the location of the folded wave guide RF launcher and the modified outboard blanket and shield.

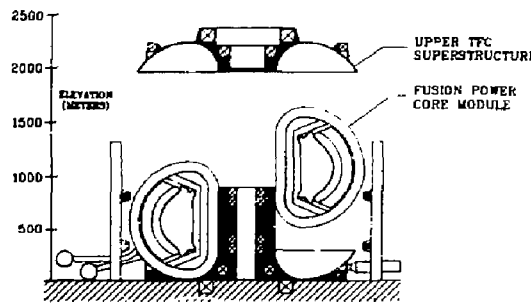

Figure 3. Two major component lifts for scheduled maintenance of the ARIES-I FPC.

MHD EQUILIBRIUM AND STABILITY CONSIDERATIONS FOR HIGH-ASPECT-RATIO ARIES-I TOKAMAK REACTORS*

Y-K. M. Peng, D. J. Strickler, J. T. Hogan, J. C. Whitson
Oak Ridge National Laboratory,† Oak Ridge, Tennessee 37831

C. G. Bathke
Los Alamos National Laboratory, Los Alamos, New Mexico 87545

K. Evans, Jr.
Argonne National Laboratory, Argonne, Illinois 60439

S. C. Jardin
Princeton Plasma Physics Laboratory, Princeton, New Jersey 08544

M. Klasky
Rensselaer Polytechnic Institute, Troy, New York 12180

J. A. Leuer
General Atomics, San Diego, California 92138

and the ARIES Team

ABSTRACT

The requirements of an (1) external poloidal field coil (PFC) system with minimum stored energy, (2) double-null divertor plasmas with elongated D shape, (3) adequate passive stabilization of plasma vertical displacement by a vacuum vessel located behind the blanket zone, and (4) an enhanced plasma beta limit in the first stability regime are incorporated in the ARIES-I concept for a high-field tokamak reactor with high aspect ratio ($A = 4.5$). The plasma current and pressure profiles are also made consistent with enhanced bootstrap current I_{bs} and reduced current drive power by means of ion cyclotron wave (ICW) or neutral beam (NB) injection. These lead to plasmas characterized by an elongation κ_x of 1.8 to the divertor X-point, a triangularity δ_x of 0.7, a safety factor q on axis of $q_0 \approx 1.5$, a safety factor at the edge $q_{95} > 4$, a plasma beta $\beta \approx 2\%$, and a poloidal beta given by $\varepsilon\beta_p = 0.5$ ($\varepsilon = 1/A$). With a plasma current I_p of 11 MA, a toroidal field B_t of 13 T at the major radius R_0 of 6.5 m, and over 3.5 m of clearance between the PFCs and the plasma edge, the stored energy in the PFC system ranges from 20 GJ during plasma operation at low beta to 12 GJ during plasma operation at high beta.

INTRODUCTION

ARIES-I [1] is a tokamak reactor concept based on modest extrapolation from the near-term physics data base characterized by present ITER design assumptions [2], advanced technologies [3], attractive safety and environmental properties [4], and optimized reactor economy using costing assumptions projected for future tenth-of-a-kind reactors [5]. These latter characteristics engender requirements on the plasma design that lead to variations from ITER, which is a first-of-a-kind experimental device.

In the area of MHD equilibrium and stability, these different requirements include:

1. placing the PFCs at a distance of ≈2.5 times the plasma minor radius a away from the plasma edge, leading to large increases in the PFC stored energy,
2. placing passive conductor (such as the vacuum vessel) between the blanket and the shield at a distance of at least $0.6a$, leading to a reduced κ_x (= 1.8) and an increased δ_x (= 0.7) to ensure plasma vertical stability [6], which in turn lead to further increases in the PFC stored energy,
3. reducing the steady-state current drive power by limiting I_p to ≈10 MA while maintaining adequate H-mode plasma confinement [7],
4. raising the plasma $\varepsilon\beta_p$ to ≈0.5 to increase the bootstrap current fraction I_{bs}/I_p to ≈0.5 [8], and
5. enhancing the plasma beta in the first stability regime for plasma current profiles characterized by $q_0 \approx 1.5$ and $q_{95} > 4$, which are consistent with those producible by ICW or NB current drive [8]. Here q_{95} refers to the flux surface at 95% of the poloidal flux toward the divertor X-point.

Iterations with the current drive analysis, tokamak integration, and systems code calculations have led to the design parameters discussed here. This paper presents the results in the areas of PFC distribution, free-boundary MHD equilibria, PFC current and energy requirements, and MHD stability beta limit. Details of plasma vertical stability

*Research sponsored by the Office of Fusion Energy, U.S. Department of Energy.

†Oak Ridge National Laboratory is operated by Martin Marietta Energy Systems, Inc., under contract DE-AC05-84OR21400 with the U.S. Department of Energy.

analysis for the ARIES-I plasma are presented in an accompanying paper [6].

PFC DISTRIBUTION

A recent study [9] of free-boundary divertor D-shaped plasmas showed that the PFC stored energy increases when κ_x is decreased for constant δ_x and constant distance between the PFC and the plasma edge. Since the plasma vertical stability is improved by lowering κ_x [10], it is important to minimize the increase in PFC stored energy as κ_x is reduced.

To this end, we study the dependence of the externally applied poloidal field on κ_x and δ_x. The analysis can be simplified by examining the lower-order multipole components of the poloidal field (nullapole, dipole, quadrupole, and hexapole), since these represent roughly the field properties of minimum stored energy. A set of free-boundary equilibria is calculated from fields composed of only these components, and a key result is shown in Fig. 1. It is seen that the desired δ_x depends strongly on κ_x when these multipole field components are used alone. When κ_x decreases from 2.2 to 1.8, δ_x must be increased by 0.3. It is also clear that, as δ_x increases under this restriction, the magnitude of the hexapole component increases relative to the quadrupole component. As a result, the divertor and D-shaping coils, located in the direction of the X-point of the plasma, are expected to carry relatively large currents.

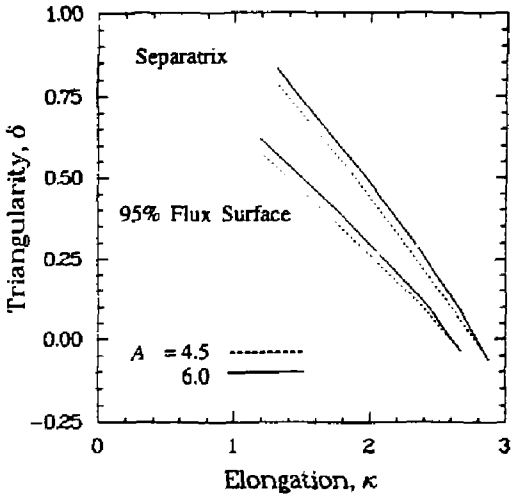

Fig. 1. The relationship between δ and κ for free-boundary plasmas calculated using only the dipole, the quadrupole, and the hexapole field components, for $\beta_p = 2.5$ and $A = 4.5$ and 6.

The overall distribution of the PFCs is then roughly determined, as shown in Fig. 2, which assumes six coil groups. This number is considered the minimum required because of the need for controlling the plasma position and shape (R_0, a, κ_x and δ_x), minimizing the stored energy, and providing some induction capability during plasma operation through varying plasma conditions [9]. It is clear that coil groups 1 and 2 contribute dominantly to the induction field (the nullapole), groups 1 and 6 to the vertical field (the dipole), groups 3 and 5 to the elongating field (the quadrupole), and groups 4 and 6 to the triangulating field (the hexapole). Higher-order multipoles exist in any PFC system with discrete coils. The PFCs are distributed so as to minimize the higher-order multipoles and thus the stored energy.

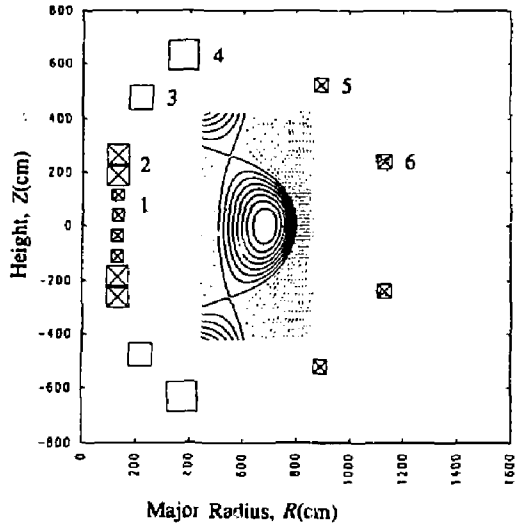

Fig. 2. Plasma equilibrium flux configuration and PFC placement.

FREE-BOUNDARY MHD EQUILIBRIA

Given the coil distribution, reference MHD equilibria for ARIES-I are computed using the VEQ code [9], which calculates free-boundary solutions for a given plasma position, shape, and linked poloidal flux while minimizing the stored energy. The plasma shape is chosen to have $\kappa_x = 1.8$ and $\delta_x = 0.7$ to allow for adequate vertical stabilization [6]. The plasma pressure and current profiles are consistent with an enhanced first stability beta and I_{bs}. The current profile should be maintainable solely by ICW or NB current drive [8]. Trade-offs among these requirements lead to a choice of profiles, that are close to the following pressure (p) and poloidal current profile (ff') functions:

$$p'(x) = p_0(e^{-\alpha x} - e^{-\alpha})/(e^{-\alpha} - 1),$$

$$ff'(x) = \mu_0 R_0^2 p_0(1/\beta_J - 1)(e^{-\gamma x} - e^{-\gamma})/(e^{-\gamma} - 1),$$

where x is the poloidal flux normalized to 1 within the plasma. The toroidal plasma current density is

$$J_t = Rp' + ff'/\mu_0 R,$$

where R is the major-radius variable. A reference equilibrium assuming $\alpha = -3$, $\gamma = -3$, and $\beta_J = 2.75$ is provided in Fig. 2 (the poloidal flux distribution), Fig. 3 [the $p(R)$ and $J_t(R)$ profiles], and Fig. 4 [the $q(x)$ profile]. Parameters of this reference equilibrium that are relevant to stability and current drive analyses are given in Table I.

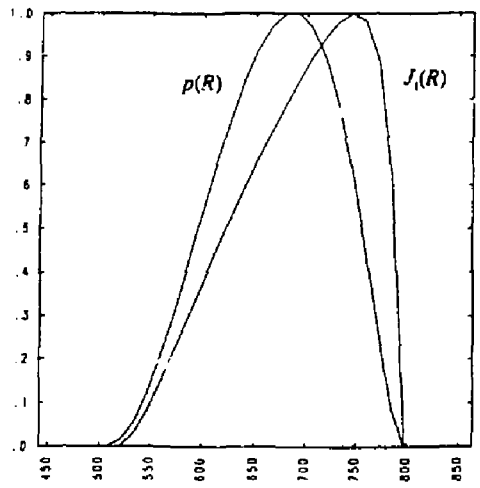

Fig. 3. Pressure and toroidal current density profiles along the major radius R for the plasma shown in Fig. 2.

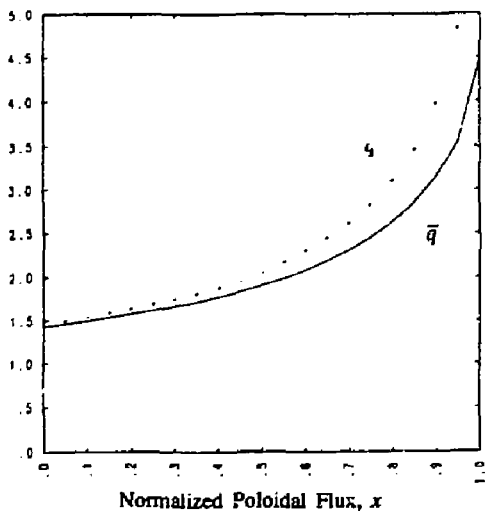

Fig. 4. The profiles of q and $\bar{q}$ (the average-field safety factor) along x, the normalized poloidal flux within the plasma edge.

This reference case provides an adjustment to the conditions that relate I_p to q, a, B_t, and the plasma shape parameters:

$$I_p\bar{q} = 5aB_t[\varepsilon(1.15 - 0.65\varepsilon)/(1 - \varepsilon^2)^2](1 + \kappa_x^2)/2,$$

where $\tilde{q}$ is the average-field safety factor using the averaged poloidal field at the plasma edge. For the reference equilibrium, we also have

Table I. Plasma Parameters of a Reference Divertor MHD Equilibrium for the ARIES-I Concept

Parameter	Symbol (unit)	Value
Major radius	R_0 (m)	6.53
Minor radius	a (m)	1.45
External toroidal field at R_0	B_t (T)	13.0
Plasma current	I_p (MA)	11.1
Safety factor on axis	q_0	1.45
Average-field safety factor	$\bar{q}$	4.47
Safety factor at 95% flux	q_{95}	4.85
Average beta	β (%)	1.90
Poloidal beta	β_p	2.18
Elongation at x-point	κ_x	1.80
Elongation at 95% flux	κ_{95}	1.62
Triangularity at x-point	δ_x	0.70
Triangularity at 95% flux	δ_{95}	0.44
X-point location	R_x (m)	5.51
	Z_x (m)	2.61
Internal inductance	l_i	0.74

$$\delta_x/\delta_{95} = 1.59, \quad \kappa_x/\kappa_{95} = (1.13 - 0.08\varepsilon), \quad q_{95}/\bar{q} = 1.09$$

to relate the edge and 95% flux surface quantities.

Different forms of the profile functions can be used to produce equilibria nearly identical to this case in all its global parameters as given in Table I. The results of the free-boundary equilibrium and the PFC currents do not change significantly when these different profile functions are used as long as the global parameters remain unchanged.

PFC CURRENT AND ENERGY REQUIREMENT

The PFC cross sections shown in Fig. 2 assume an overall current density of 20 MA/m^2 for each coil. The maximum values of the PFC currents during plasma operation, together with the required distance from the toroidal field coils and their structure [11], contribute to determining the locations of the PFCs. It is therefore necessary to calculate the PFC current variations through typical conditions of the plasma during operation.

Since the ARIES-I tokamak assumes noninductive methods to assist startup of the plasma current [8], the amount of poloidal flux linkage between the plasma and the PFCs can be chosen to reduce the PFC stored energy. Some flexibility exists near the condition of minimum stored energy to vary the PFC currents and provide some degree of induction for plasma operation. The range of plasma parameters can

therefore be characterized by three separate conditions, all at full plasma current with a fixed X-point location: low beta and low linked flux, high beta and low linked flux, and high beta and high linked flux. The PFC currents are listed in Table II for these cases. The maximum current for each coil is then estimated and used in sizing its cross sections and locating the coil as plotted in Fig. 2. These data are also used as input to the PFC design concept [12].

Table II. PFC currents and the maximum currents for each coil group shown in Fig. 2 at three typical operation conditions. (Coil groups 1 and 2 have 2 coils each.)

Operation conditions	I	II	III	Maximum
β (%)	0.62	1.90	1.90	
Linked flux (Wb)	39.2	50.5	90.1	
Stored energy (GJ)	19.8	13.2	12.2	
Coil group current (MA-turn)				
I_1	−14.8	−0.0	−7.5	15.0
I_2	−20.9	−12.0	−26.0	26.0
I_3	20.0	20.0	15.0	20.0
I_4	33.7	26.4	24.1	34.0
I_5	−10.7	−4.8	−5.2	11.0
I_6	−0.9	−5.3	−5.3	6.0

It is seen from Table II that an induction flux of about 40 Wb is available by varying the nullapole component of the PFC currents, leading only to a small (<10%) change in the stored energy from its minimum of about 12 GJ. However, the stored energy is significantly larger (about 20 GJ) at low beta and full I_p if the X-point is to be fixed during plasma heating to burn at high beta (*e.g.*, to satisfy the divertor operation requirements). This difference in the stored energy leads to a reactive power supply requirement of hundreds of megavoltamperes during a plasma heating time of 10–20 s. However, this requirement may not be necessary if the plasma can be heated to high beta during current ramp-up.

MHD STABILITY BETA LIMIT

The first stability regime requires that all ideal MHD modes be at least marginally stable in the absence of a conducting shell beyond the plasma edge [13]. While this requirement is broad in scope, it is usually adequate to examine only the high-n ballooning modes and the low-n (n = 1) kink modes to determine the stability beta limit. The intermediate-n ballooning modes (the "infernal" modes) are easily avoided by retaining small gradients in the q-profile near the plasma axis.

As an input to design trade-offs involving plasma shaping, profiles, A, and the beta limit, our study emphasizes clarifying the dependences of beta on A, κ_{95}, q_0, and q_{95}. We use only the traditionally successful profile functions for the analysis. This study is therefore limited in its scope, since several other parameters, such as δ, the q-profile, and the pressure profile, also affect the plasma beta limit. However, the study benefits from an extensive study of the beta limit recently carried out for ITER [14] and from reviews of the large body of information in the literature. Calculations are carried out for high A (4.5 and 6.0) ARIES-I plasmas using the PEST equilibrium and stability codes [15] to "fill in" data where needed. The combined data base of the stability analysis covers a range of A = 2.6–6.0, κ_{95} = 1.6–3.2, q_0 = 1.05–2.0, and $q_{95} \le 5$.

The p and q profile functions used include those optimized for JET plasmas [13] and those used in the ITER studies [14]:

$$p = p_0[(1 - y^{\alpha})^{\gamma} + p_1 y^{\zeta}(1 - p_2 y^{\eta})],$$

$$q = q_0 + q_1 y^{\lambda} + q_2 y^{\nu} \text{ or } q = q_0/(1 - \xi y^{\rho})^{\sigma}.$$

Here, y is the poloidal flux normalized to 95% of the X-point flux, p_0 determines beta, p_1 determines the profile, α = 1.5, γ = 2.5, ζ = 3, η = 1.2, and p_2 = 0 or 1. The first q-profile gives q_{95} (= $q_0 + q_1 + q_2$) = 3.1, where q_1 and q_2 are independent variables; λ = 6; and ν = 2. The second function for q has $\sigma = \ln(q_0/q_{95})/\ln(1 - \xi)$, ξ = 0.7, and ρ = 2, and is used for the case with A = 6.

The shape of the 95% flux surface is given by

$$R = R_0 + a\cos(\theta + \delta' \sin\theta), \quad Z = \kappa_{95} a \sin\theta,$$

where $\delta' = \delta_{95}$. The 95% flux surface is used in the stability analysis to avoid the numerical difficulties near the X-point, which are a subject of present investigations [16].

The results are summarized in Figs. 5 and 6, which indicate the dependence of beta-limit on κ_{95} (for A = 6) and the dependence of Troyon factor limit ($C_T = \beta a B_t/I_p$, in % m T/MA) [13] on A. From these, one obtains

$$C_T = 2.8[1 - 0.4(\kappa_{95} - 1)^2]/(1 - \varepsilon)^{1.5},$$

which gives C_T = 3.5 and β = 2.06% for the reference plasma parameters in Table I. It is important to note that this approximate scaling has a limited basis; its use should be limited to the profiles given here and to the range of parameters indicated above. For A ≈3, it has also been shown that this beta limit remains relatively unchanged as long as l_i remains below 0.75.

Additional studies of the beta limit have also been carried out for plasmas using polynomial profiles and with parameters encompassing the reference case: I_p ranging from 16 to 8 MA, q_{95} from 3 to 6, and β_p from 1.4 to 3. The value of C_T is 3.1 to 3.2 as long as q_{95} is above 3.7. This result is considered conservative relative to the preceding indications. Design values of C_T = 3.2 (corresponding to β = 1.9%) and l_i = 0.74 are therefore adopted for ARIES-I (see Table I).

DISCUSSION

The results summarized in this paper, together with those of Ref. [6], provide a relatively sound basis for the plasma equilibrium and stability of the ARIES-I reactor concept. They also provide approximate scaling relationships of the beta limit that are useful in the systems trade-off studies [5] needed to choose the ARIES-I parameters. The key parameters produced by our study are given in Tables I and II. They are made consistent with the current drive requirements [8] after reducing C_T from the nearly stability-optimized value of about 3.5 to a more conservative limit of 3.2, which assumes relatively "mild" pressure and current profiles. It is felt that a value of $C_T = 3.5$ can also be made consistent with steady-state current drive, but may lead to more stringent requirements on current drive, given more detailed analysis.

Iterations with the ARIES-I design integration have led to the reference PFC configuration of minimum stored energy as shown in Fig. 2. This configuration provides adequate flexibility for maintaining proper plasma position, shape, and flux linkage during heating and burn operation. Our results suggest the study of various scenarios of plasma heating and current ramp-up to reduce the stored poloidal field energy required at low beta.

The authors acknowledge useful comments and discussion from their colleagues at ORNL, PPPL, GA, and LLNL.

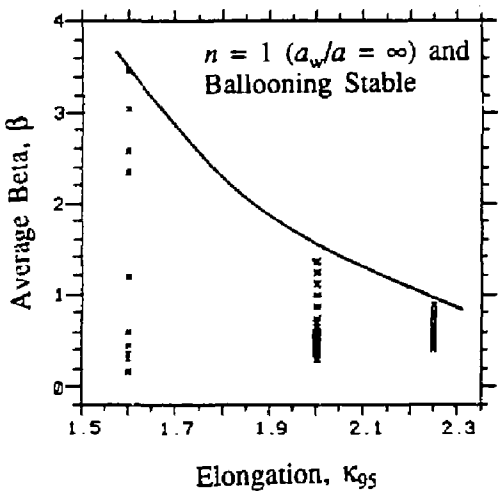

Fig. 5 Plasma beta values (×) of stable equilibria for κ_{95} = 1.6, 2.0, and 2.25 with A = 6 using the profile functions given.

REFERENCES

[1] Farrokh Najmabadi et al., "The ARIES Tokamak Reactor Study," these proceedings.

[2] N. A. Uckan et al., "Physics Design Guidelines for ITER," these proceedings.

[3] See the papers on ARIES-I magnets, blanket design, composite materials, and power conversion concept in these proceedings.

[4] J. S. Herring et al., "Safety Engineering for the ARIES-I Tokamak Reactor," these proceedings.

[5] R. L. Miller et al., "The ARIES-I High-Field-Tokamak Reactor: Design Point Determination and Parametric Studies," these proceedings.

[6] C. G. Bathke et al., "Vertical Stability Requirements for ARIES-I Reactor," these proceedings.

[7] M. Keilhacker et al., "Confinement and Beta-Limit Studies in ASDEX H-mode Discharges," in *Plasma Physics and Controlled Nuclear Fusion Research*, London, 1984, Vol. I, pp. 71–85, 1985.

[8] T. K. Mau et al., "Current Drive Analysis and System Design for the ARIES-I Tokamak Reactor," these proceedings.

[9] D. J. Strickler et al., "MHD Equilibrium Methods for ITER PF Coil Design and Systems Analysis, ORNL/FEDC-88/7, March 1989; D. J. Strickler et al., "Equilibrium Shape Control in CIT PF Design," these proceedings.

[10] G. Laval et al., *Phys. Fluids*, Vol. 17, p. 835, 1974.

[11] S. P. Grotz et al., "Design Integration of the ARIES-I Tokamak Reactor," these proceedings.

[12] L. Bromberg et al., "High Field Magnet Designs for the ARIES-I Reactor," these proceedings.

[13] F. Troyon et al., *Plasma Physics and Controlled Fusion*, Vol. 26, p. 209, 1984.

[14] T. Tsunematsu et al., "Operational Limits and Disruptions in Tokamaks—Status and Application to ITER," JAERI-M-89-056, May 1989.

[15] R. C. Grimm et al., *Methods Comput. Phys.*, Vol. 16, p. 769, 1977; R. C. Grimm et al., *J. Comput. Phys.*, Vol. 49, p. 94, 1983.

[16] Y-K. M. Peng et al., "Access to Second Ballooning Stability in Divertor Plasmas," to be presented at the Annual Meeting of the American Physical Society Division of Plasma Physics, Anaheim, California, November 13–17, 1989.

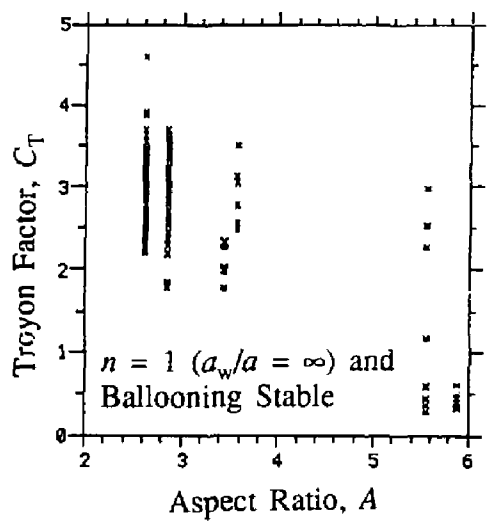

Fig. 6. Troyon factor (C_T) values (×) of stable equilibria for A = 2.6–6 with κ_{95} = 1.6–3.2, q_0 = 1.05–2.0, and $q_{95} \leq 5$ using the profile functions given.

VERTICAL STABILITY REQUIREMENTS FOR ARIES-I REACTOR†

C. G. Bathke, S. C. Jardin,* J. A. Leuer,** D. J. Ward,*
and the ARIES Team

Los Alamos National Laboratory, Los Alamos, NM 87545.

ABSTRACT: The vertical stability of the ARIES-I reactor design is analyzed with the NOVA-W, PSTAB, and TSC codes. A growth rate of $\sim 5.7\ s^{-1}$ is predicted for a vacuum vessel positioned behind the scrapeoff, first wall, and blanket (0.7-m inboard and 0.9-m outboard thickness) and acting as a passive stabilizer. A reactive power of $\sim 2\ MVA$ would be required for active feedback coils located outside of the TF coils (~ 3 m beyond the plasma in the equational plane) to correct a 50-mm vertical displacement of the magnetic axis. A multipole-expansion technique used in the TSC analysis is also used to examine options that minimize stored energy.

I. INTRODUCTION

The ARIES-I tokamak reactor design[1] minimizes the cost of electricity (COE) by minimizing the plasma current and the associated current-drive cost. The resulting low beta ($\beta \sim 0.02$) device[2] is characterized by a large safety factor ($q_{95} \sim 4$), moderate-to-high aspect ratio ($A \geq 4.5$), high field [24 T at the toroidal-field (TF) coils], and high separatrix elongation ($\kappa_x = 1.8$). The large A and κ make vertical stability an important issue for ARIES-I; related issues that must be addressed by the ARIES-I conceptual design are outlined below. A toroidally continuous conducting shell is required to retard the growth of an externally excited vertical instability that ranges from an Alfvén time scale ($\tau_A \sim 10\ \mu s$) without a shell to a time scale on the order of the electrical L/R time constant of the shell, $\tau_{L/R}$. The passive stabilization provided by this shell must be augmented by an active-feedback system that provides vertical stability for times $\gtrsim \tau_{L/R}$. A rigid-plasma model (PSTAB)[3] and linear (NOVA-W)[4] and non-linear (TSC)[5] deformable-plasma models are used to estimate the conductor location and size required for passive stabilization. Time-dependent TSC simulations are used to determine the current, voltage, location and size of the feedback coils.

The placement of the ARIES-I poloidal-field (PF) coils external to the TF coils permits the use of a multipole-expansion technique[6,7] to describe accurately the PF-coil fields used in TSC computations. Limiting the multipole expansion to hexapole and lower moments minimizes the number of dependent variables required to describe the plasma shape. Using the multipole-expansion technique to examine plasma equilibria parametrically for a range of κ and triangularity, δ, values resulted in a prescription for minimizing the PF-coil stored energy, W_{PF}, that is used in the ARIES-I systems code.[2]

II. MULTIPOLAR APPROACH

The TSC code[5] was modified so that the poloidal flux produced by a PF-coil set could be determined either by specifying the PF-coil locations and currents or by specifying the amplitudes of the even and odd moments in the multipole-expansion series[6] that is truncated beyond the even decapole. In addition, TSC was modified to perform the inverse operation of decomposing the poloidal flux produced by a PF-coil set into the multipole components of the same truncated series. The TSC code was then used to analyze parametrically the equilibrium of an $A = 4.5$ and $\kappa_x = 2.13$ interim design point. Because the PF-coils are relatively far from the plasma, the multipole expansion could be limited to hexapole and lower moments, thereby reducing the number of variables. The plasma current, toroidal field, profile form factors, major and minor radii, and the nullapole and dipole moments were held fixed at the interim design values, which differ somewhat from those reported in Ref. 2. The ratio of the hexapole to quadrupole amplitudes was selected as the dependent variable. The absolute magnitudes of these amplitudes were determined as the minimum amplitudes that produced a separatrix with the specified minor radius. This algorithm, subsequently, generates a set of plasma equilibria that are produced with a minimum PF-coil current, $\sum |I_{PF}|$, and a minimum W_{PF}. Because plasma elongation and triangularity are produced primarily by the quadrupole and hexapole moments, respectively, this algorithm yields the δ that minimizes W_{PF} for a given κ, as is shown in Fig. 1. Plasmas below the δ-κ correlation of Fig. 1 would not have a separatrix, and those above the correlation would either have a smaller minor radius (larger A) or require higher multipole moments and larger W_{PF} to maintain the same minor radius. This analysis also produced a correlation between W_{PF} and κ that indicates W_{PF} increases as κ is decreased (δ increased). This W_{PF}-κ correlation did not have a significant impact on determining the final design values[2] of κ and δ, however.

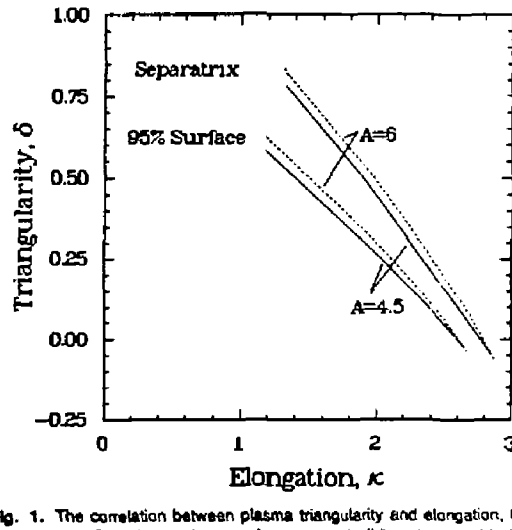

Fig. 1. The correlation between plasma triangularity and elongation, that minimizes the PF-coil stored energy for $A = 4.5$ (solid) and $A = 6$ (dash).

To pursue further the issue of minimizing W_{PF}, a code FLXCON was developed to determine the locations and currents of a PF-coil set that would reproduce the flux pattern of a given set of multipole moments. The FLXCON code moves the coils along a specified surface while minimizing an object function defined as the sum of a term measuring the relative error with which the coils reproduce the flux of the given set of multipole moments on a test surface representative of the plasma surface and a term measuring W_{PF}. To illustrate the use of FLXCON, an HEQ-generated equilibrium[8] for $A = 4.5$ and $\kappa_x = 1.74$ was modeled with TSC using the same set of 12 PF coils with 6 current groups; the HEQ and TSC results are given for comparison in Table I. The small differences in R_T, a, and κ_x between the HEQ and TSC results are directly attributable to numerical inaccuracies in both codes. The multipole decomposition of the PF-coil flux was used to generate three sets of six PF coils and six current groups labeled DEC, OCT, and HEX in Table I to denote the maximum multipole moment used. As the higher moments are eliminated $\sum |I_{PF}|$ decreases as expected, but W_{PF} is lower only for the HEX case. The plasma shape, however, drifts from the base

†Work supported by US DOE, Office of Fusion Energy.
*Princeton Plasma Physics Laboratory, Princeton, NJ 08543.
**General Atomics, San Diego, CA 92138.

shape because the higher moments were used inefficiently to suppress κ and provide additional triangularity. A more efficient method to generate the same plasma shape would require less quadrupole and more hexapole, and will be used in the future.

TABLE I

Equilibria Comparison with Different Multipole Moments

	HEQ[a]	BASE[b]	DEC[b]	OCT[b]	HEX[b]
Major Radius, $R_T(m)$	6.12	6.12	6.12	6.13	6.13
Minor Radius, $a(m)$	1.36	1.35	1.35	1.34	1.34
Magnetic Axis, $R_M(m)$	6.33	6.35	6.35	6.35	6.34
Elongation					
κ_x	1.75	1.73	1.68	1.70	1.84
κ_{95}	1.58	1.59	1.55	1.56	1.67
Triangularity					
δ_x	0.74	0.77	0.75	0.68	0.46
δ_{95}	0.48	0.50	0.49	0.47	0.36
Separatrix Coordinates (m)					
R_x	5.11	5.12	5.14	5.25	5.51
z_x	2.38	2.39	2.31	2.32	2.53
Beta					
Total, β (%)	1.84	1.86	1.94	1.98	1.86
Poloidal, β_θ	1.85	1.77	1.78	1.78	1.74
Plasma Volume (m^3)	347	348	337	329	343
Safety Factor					
$q(0)$	1.59	1.59	1.54	1.50	1.58
$q(a)$	7.84	7.02	6.46	6.19	6.52
Current, $\sum\|I_{PF}\|(MA)$	142	142	114	111	82
Stored Energy, $W_{PF}(GJ)$	7.57	7.57	7.78	8.10	6.80

(a) PF-coil flux determined by PF-coil currents and locations.

(b) PF-coil flux determined by truncated multipole-expansion series.

III. PASSIVE STABILIZATION

Without passive stabilization the plasma will move vertically on an Alfvén time scale ($\sim 10\ \mu s$). The placement of passive conductors around the plasma will slow this vertical motion sufficiently to allow an active feedback system to operate on a longer time scale ($\gtrsim 100\ ms$) to control the vertical position of the plasma with a reasonable expenditure of reactive power ($\lesssim 10\ MVA$). To simplify the ARIES-I design the only passive conductor is the vacuum vessel. The radial location of the vacuum vessel is then determined from compliance with a passive stability constraint in conjunction with other assembly and maintenance requirements.[9] Passive-stability performance is measured by the stability parameter $f \equiv 1+\tau_v/\tau_{L/R}$, where $\tau_v = \gamma^{-1}$ is the vertical-instability time constant and γ is the growth rate. A design constraint of $f \geq 1.3$ is adopted to ensure that a sufficient stability margin exists above the $\gamma = \infty$ limit under all plasma conditions.

A preliminary analysis of the maximum allowable distance permitted between the plasma and the vacuum vessel for passive stability was performed with the PSTAB[3] code. The PSTAB formulation assumes the plasma is a massless, rigid body simulated by an array of filamentary current elements. The equations describing a small vertical displacement in the presence of an array of resistive filamentary conductors simulating the passive stabilizer are linearized and solved as an eigenvalue problem.[3]

The notation used to describe the location of the passive stabilizer relative to the plasma is shown in Fig. 2. The plasma surface is assumed to be given by $x = a\ \kappa\ sin\theta$ and $R = R_T + a\ cos(\theta + \delta\ sin\theta)$, where $R_T = 6\ m$ is the major radius, $a = 1\ m$ is the minor radius, $\kappa = 2$, $\delta = 0.5$, and the angle θ varies from 0 to 2π. The passive stabilizer is placed on a surface parallel to the plasma surface. The poloidal coverage, p/a, and the normalized radial location, c/a, of a passive outboard stabilizer were varied for $A = 6$; results are shown in Fig. 3. Relatively small passive stabilizers ($p/a \sim 0.2$) meet the stability constraint, but these conductors must be located close to the plasma ($c/a \lesssim 1.1$). Such small values of c/a would have an adverse effect on tritium breeding and problems related to neutron damage and activation are expected. Placement of the passive stabilizer behind the 0.9-m-thick outboard blanket, first wall, and scrapeoff with full

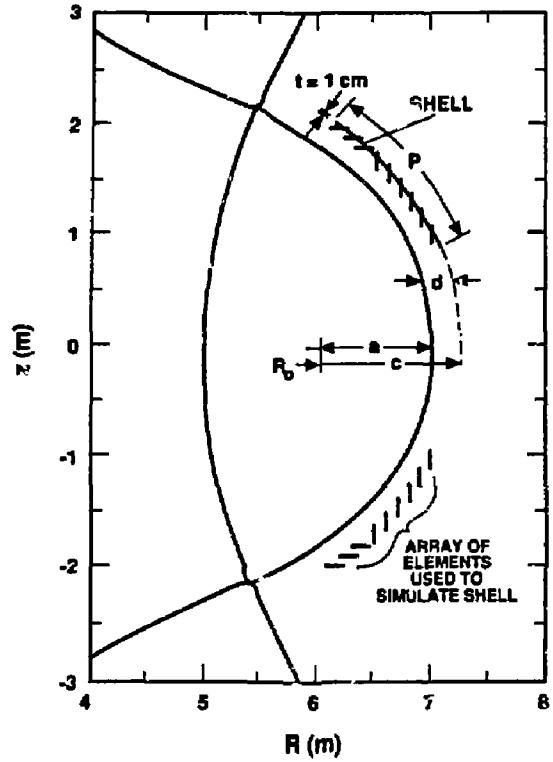

Fig. 2. The geometry of the plasma and the passive stabilizer (shell).

coverage on the outboard side does not provide sufficient stabilization (i.e., $f > 1.3$). Vertical-stability and physics considerations drove the design to A = 4.5, which turns out to be the minimum cost design,[2] with a passive stabilizer positioned behind both 0.7-m-thick inboard and the 0.9-m-thick outboard blanket, first wall, and scrapeoff. In order to find a vertically-stable design at $A = 4.5$, the elongation was varied with the passive-stabilizer geometry shown in Fig. 4, results are shown in Fig. 5. This analysis indicates that $\kappa_x \lesssim 1.83$ is required for a stabilizer located behind the inboard and outboard blankets.

The accuracy of the PSTAB results was then checked by benchmarking the $\kappa_x = 1.74$ case against the TSC and NOVA-W codes. The TSC code[5] performs time-dependent simulations of free-boundary, axisymmetric plasmas and the associated external circuits and, consequently, is more costly to use than either PSTAB or NOVA-W. A two-dimensional transport model is used in TSC to describe a plasma interacting with external conductors that obey circuit equations with active-feedback amplifiers included. The plasma force balance in TSC is modified by scaling up the plasma mass and viscosity to maintain the plasma in force balance, while alleviating the time-scale disparity between wave and diffusion phenomena. This parameter scaling does not affect plasma bulk motion that is stable on the ideal MHD time scale (μs), but does affect the growth rate of a vertical instability. To calculate τ_v, TSC is set up with the plasma and passive-stabilizer geometry shown in Fig. 4. The PF coils are represented with a multipole series truncated with the even decapole. The simulations begin with a radial magnetic field applied for 1 μs to produce an initial $\sim$ 3-mm vertical displacement of the plasma. The plasma simulation is then continued until the equilibrium effects of the initial perturbation are damped out and the vertical instability asymptotically relaxes to a linear growth rate, as reported by inboard and outboard pickup coils. Corroboration of the value of τ_v predicted from the pickup coils was obtained by fitting the vertical displacement of the magnetic axis, z_M, with the functional form $z_M(t) = z_0 e^{t/\tau_v}$. This τ_v calculation was then made for four values of plasma mass and denoted as squares in Fig. 6. A quadratic polynomial was fit to the three results with the largest mass enhancement

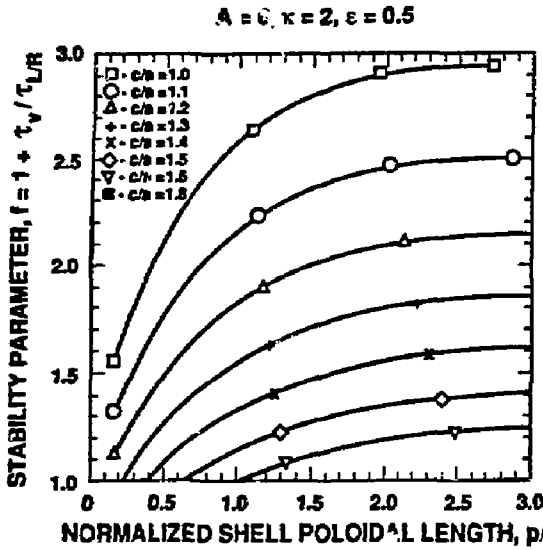

Fig. 3. The stability parameter f versus poloidal coverage (p/a) of an outboard stabilizer for various radial locations (c/a) (Fig. 2).

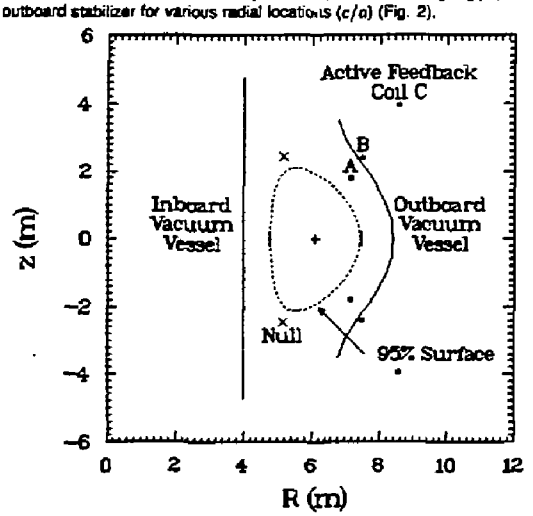

Fig. 4. The geometry of the plasma and the passive stabilizer (vacuum vessel) for $A = 4.5$ and $\kappa_x = 1.74$. A similar geometry was used for the other cases in the κ parametric study. The coil locations used in the active-feedback analysis are also indicated.

factor and then extrapolated to a unity mass enhancement factor to determine the mass independent value of τ_v reported in Table II. This extrapolation is accurate as is demonstrated by the passage of the polynomial fit through the smallest mass-enhancement-factor result displayed in Fig. 6.

This calculation was repeated with the NOVA-W code,[4] which is an extension of the non-variational ideal MHD code NOVA[10] that allows for resistive walls and feedback circuits in the vacuum region. A Green's function formulation is used to express the perturbed poloidal flux in the vacuum region in terms of the perturbation amplitude on the plasma boundary. A thin-wall approximation is used to calculate the time derivative of the poloidal-flux perturbation at the resistive wall where a discontinuity exists in the flux gradient. The NOVA-W result is given in Table II. Agreement between NOVA-W and TSC is good at 1% for τ_v and <1 % for f, but agreement between PSTAB and TSC is 24 % for τ_v and 21 % for f. The differences between PSTAB and TSC result in part from rigid-versus-deformable plasma effects

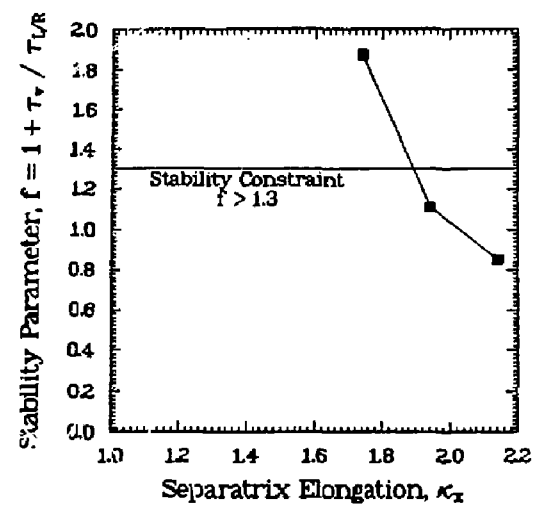

Fig. 5. Dependence of the stability parameter on elongation for $A = 4.5$ and stabilizer geometry shown in Fig. 4.

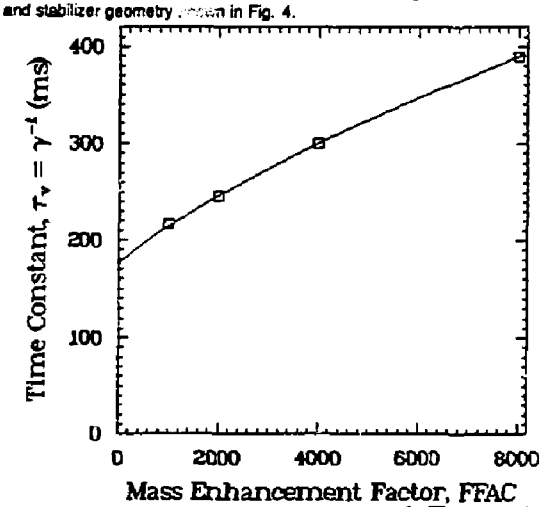

Fig. 6. Dependence of the vertical-stability time constant, τ_v, on plasma mass enhancement factor as calculated with TSC for $A = 4.5$, $\kappa_x = 1.74$, and the stabilizer geometry shown in Fig. 4.

and from differences in the calculation of the stabilizer inductances. Also, a 20 % difference was obtained in the PSTAB and TSC calculations of $\tau_{L/R}$ with a vertically asymmetric current distribution in the stabilizer.

TABLE II. Benchmark of the vertical-stability time constant, τ_v, and stability parameter, f, as calculated by PSTAB[3], NOVA-W[4], and TSC[5] for the configuration shown in Fig. 4.

Code	τ_v(ms)	f
PSTAB	217	1.88
TSC	175	1.56
NOVA-W	173	1.55

IV. ACTIVE FEEDBACK

The active-feedback power requirements were determined from TSC simulations of the A = 4.5 and $\kappa_x = 1.74$ case used in the passive-stability benchmark described in the previous section. A simulation begins with the vertical coordinates of the plasma magnetic axis, z_M, maintained in the equatorial plane for 0.1 s. The feedback coils are preprogrammed to initiate

a 50-mm vertical displacement of z_M at 0.1 s into the simulation and to maintain that position once attained. As the plasma mass does not affect the voltage or current of the feedback coils, a large mass enhancement factor (FFAC = 8,000) was used for computational expediency. Simulation results for Feedback Coil A (Fig. 4) are given in Fig. 7. A gain for driving the feedback-coil current was selected to yield a common value of $G \sim -2.6$ for the dimensionless gain defined as the ratio of the response flux difference produced by the feedback coils to the flux difference produced by the plasma in the pickup coils. The dimensionless gain must be in the range of -1 to -10 to ensure stability and practicality of the feedback system (yet to be designed). A value of $G \sim -2.6$ rapidly moves the plasma to a 50-mm displacement with only an $\sim$ 10-mm overshoot. The gain for driving the feedback-coil voltage is set at a low value of 1 mVA to ensure a smooth voltage response. A pickup-coil location approximately equal to the location of Feedback Coil B in Fig. 4 was used for Feedback Coils A and C. For Feedback Coil B a pickup-coil location corresponding approximately to the location of Feedback Coil A was used to obtain a clear resolution of the flux difference produced by the plasma.

The maximum reactive power occurs at the maximum vertical displacement of z_M and scales with $z_M{}^2$. The reactive-power requirements for the three feedback-coil locations of Fig. 4 are shown in Fig. 8 for a common 50-mm displacement of z_M. The feedback coils were simulated with a 0.1×0.1-m cross section of room-temperature, copper alloy with a conductor filling fraction of 0.7. Feedback Coil C is preferable over the other two coil locations. This coil is positioned just outside of the TF coil and is the easiest coil to maintain. The $\sim 2\ MVA$ reactive power required to drive this coil is well within the 26 MW of recirculating power set aside for miscellaneous plant needs.[2] Furthermore a 50-mm displacement could not be tolerated by the divertor and represents a maximum design constraint.

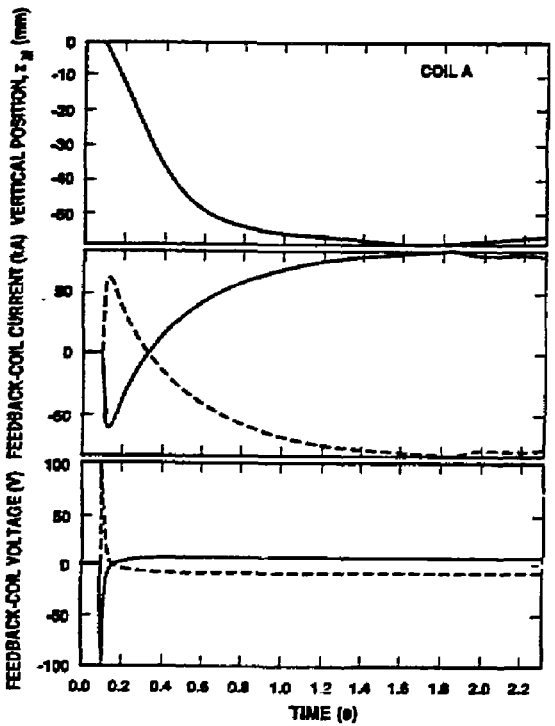

Fig. 7. The vertical position of the magnetic axis, z_M, and the feedback-coil current and voltage versus time as calculated with TSC for $A = 4.5$, $\kappa_x = 1.74$, the stabilizer geometry shown in Fig. 4, and Feedback Coil A in Fig. 4.

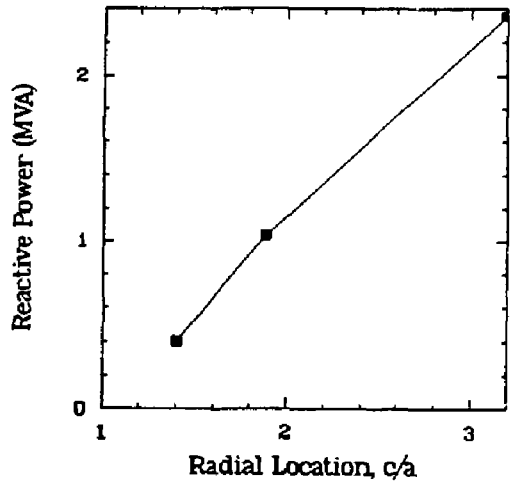

Fig. 8. The dependence of reactive power on normalized radial location, c/a, calculated with TSC for $A = 4.5$, $\kappa_x = 1.74$, and the geometry shown in Fig. 4. Simulation results were scaled to a common 50-mm displacement of z_m.

V. CONCLUSIONS

A prescription for choosing a plasma shape that minimizes the stored energy in the PF coils has been developed. A benchmark of the PSTAB, NOVA-W, and TSC codes indicated that a passive-stability analysis produced by the less-expensive NOVA-W is comparable in accuracy to TSC. The vacuum vessel was found to provide suitable passive stabilization (i.e., $f > 1.3$) if positioned between the blanket (0.7-m inboard and 0.9-m outboard thickness of scapeoff, first wall, and blanket) and shield. The final ARIES-I equilibrium configuration[8] has the same A as, but larger a (= 1.45 m) and κ_x (= 1.8) than the case reported here. The larger a for constant blanket, first-wall, and scrapeoff thickness will improve passive stability (i.e., raise f). However, the larger κ will exacerbate the passive-stability problem. Further analysis of the new design point is required to resolve fully the passive stability of ARIES-I. An active-feedback power of $\sim 2\ MVA$ was required to suppress a 50-mm displacement of the magnetic axis with coils positioned outside of the TF coils.

REFERENCES

1. F. Najmabadi, R. W. Conn, and the ARIES Team, "The ARIES Tokamak Fusion Reactor Study," these Proceedings.
2. R. L. Miller and the ARIES Team, "The ARIES High-Field Tokamak Reactor: Design-Point Determination and Parametric Studies," *ibid.*
3. J.A. Lauer, *Fusion Tech.* 15, 489 (1989).
4. D. Ward and S. C. Jardin, to be published in *Bull. Am. Phys. Soc.*, (1989).
5. S.C. Jardin, N. Pomphrey, and J. DeLucia, *J. Comput. Phys.* 66, 481 (1986).
6. M. F. Reusch and G. H. Neilson, *J. Comput. Phys.* 64, 416 (1986).
7. C. E. Kessel, Jr. and M. A. Firestone, *Trans. Am. Nucl. Soc.* 52, 185 (1986).
8. Y-K. M. Peng, et al., "MHD Equilibrium and Stability Considerations for High-Aspect-Ratio ARIES-I Tokamak Reactor," these Proceedings.
9. S. P. Grotz, F. Najmabadi, L. Bromberg, R. L. Creedon, C. Wong, R. L. Miller, and the ARIES Team, "Design Integration of the ARIES-I Tokamak Reactor," ibid.
10. C. Z. Cheng and M. S. Chance, *J. Comput. Phys.* 7, 71 (1987).

CURRENT DRIVE ANALYSIS AND SYSTEM DESIGN FOR THE ARIES-I TOKAMAK REACTOR[1]

T. K. Mau,[1] D. A. Ehst,[2] J. Mandrekas,[3] M. J. Schaffer,[4] and
THE ARIES DESIGN TEAM
Department of Mechanical, Aerospace and Nuclear Engineering
and Institute of Plasma and Fusion Research
University of California, Los Angeles
Los Angeles, CA 90024-1597.

Abstract: Fast wave current drive is selected as the primary scenario for steady-state operation of the ARIES-I tokamak reactor. With the projected efficiency of $\gamma \approx 0.3 - 0.4$, the current drive method employs low-cost, off-the-shelf technology, making it attractive compared to neutral beam current drive. At a frequency of 158 MHz and a wave spectrum centered at $N_{\parallel} = 1.6$, it is found that as much as 160 MW of power may be required to drive the 4.7 MA seed current on ARIES-I. To generate the desired current profile, the wave power is launched from above the equatorial plane on the outboard edge of the plasma. A toroidal array of 12 folded waveguides forms the basic launcher module which transmits the desired spectrum with a 95% directivity. Efficiency of coupling to the high density scrape-off layer is expected to be high (>90%). The overall launcher system consists of 4 modules delivering 192 MW through 1.6% of the first wall area. Each waveguide is envisaged to be a closed rectangular box made of SiC/SiC fiber composites, with the conducting surfaces formed by a copper coating on the inside of the structure. With the klystrode as the transmitter, the overall RF system efficiency can be as high as 72%. A viable alternative system based on neutral beam current drive and RFQ technology has also been designed.

INTRODUCTION

ARIES-I is a conceptual design of a commercial tokamak reactor which will be operational in 20-30 years [1]. The design philosophy is based on conservative physics extrapolation from the present database and projection of technological advances in the intervening years. The main goal of the ARIES-I study is to incorporate a high level of safety assurance and attractive environmental features into an economically competitive reactor design, as compared to fission reactors. As such, the major characteristics of this device include steady-state operation, first regime MHD stability, high magnetic field, low plasma current, high recycling divertors, and ceramic fiber composites as the structural material.

Table 1 lists the key parameters for the ARIES-I tokamak reactor and those relevant to current drive [2]. Note that because of the high on-axis magnetic field (13 T) and the relatively high aspect ratio (A=4.5), the resulting plasma current is modest (I_p=11 MA). With a projected bootstrap current fraction of 0.57, it is necessary only to drive a 4.7 MA seed current. The high magnetic field also provides a unique environment for fast wave current drive in a frequency range where the attractive features of a folded waveguide antenna can be utilized. The ARIES-I high recycling divertor region has a separatrix density of $1.0 \times 10^{20}\ m^{-3}$, which is consistent with the average density of $1.62 \times 10^{20}\ m^{-3}$ at a peaking factor of 0.3. The resultant high-density scrape-off layer (SOL) facilitates coupling of RF power to the plasma. SiC/SiC fiber composites are proposed as the structural material for the ARIES-I blanket, which has favorable safety and environmental features. For similar reasons, this material is used to construct the waveguides.

In this paper, a current drive scenario is first determined for ARIES-I. Secondly, the primary current drive scenario using fast waves is examined in some detail. Thirdly, the design of the launcher is described, with the folded waveguide as a basic unit. The unique features of the launchers related to the copper-coated SiC composite structural material are also pointed out. Fourth, the electrical efficiency of the RF system is assessed. Fifth, a current drive scenario based on high energy neutral beams and RFQ accelerators is highlighted. Finally conclusions are drawn on the viability of the fast wave current drive system within the ARIES-I reactor.

Table I: Key Parameters of ARIES-I

Major Radius R	6.52 m
Minor Radius a	1.40 m
Aspect Ratio A	4.5
Elongation κ_{95}	1.6
Triangularity δ_{95}	0.47
Field at Coil B_c	23.75 T
Field on Axis B_0	12.95 T
Plasma Current I_p	10.92 MA
On-axis Safety Factor q_0	1.30
Edge Safety Factor q^*	3.29
Peak Density n_{e0}	1.82×10^{20} m^{-3}
Average Density $<n_e>$	1.62×10^{20} m^{-3}
Separatrix Density n_s	1.0×10^{20} m^{-3}
Peak Temperature T_{e0}	37.7 keV
Average Temperature $<T_e>$	18.9 keV
Toroidal Beta β	0.019
Effective Charge Z_{eff}	1.62
Bootstrap Fraction I_{BS}/I_p	0.57

CURRENT DRIVER SELECTION

Many factors are taken into consideration in selecting a suitable current driver for ARIES-I. Among them, the efficiency of the current driver, measured by the figure of merit γ ($=n[10^{20}/m^3]I[MA]R[m]/P[MW]$), is a crucial parameter to maximize, in order to minimize the cost of electricity (COE) of the reactor. Equally important is the wall-plug to first-wall electrical efficiency of the power delivery system associated with the current driver. Furthermore, the system unit cost ($/W) should also be minimized, which depends on the method of power generation and the maturity of the technology involved within the time frame of application. Other less quantifiable factors such as system compatibility in a neutron environment, required space for system components, first wall intrusion and system versatility are also important. In the context of conservative physics assumptions for ARIES-I, the current driver (CD) candidates are narrowed down to neutral beams (NB), fast waves (FW) and lower hybrid waves (LHW). Of these, LHW is particularly suited to current generation in the plasma periphery at steady-state. The advantages of multi-MeV NBCD in efficiency ($\gamma \sim 0.6$) is offset by its relatively high power cost (~$3/W) whereas for FWCD, efficiency is marginal ($\gamma \sim 0.3$-0.4) but the cost is comparatively low (~$1.50/W). As a result, the impact of the choice of current driver between NB and FW on the reactor COE appears to be insignificant. For the ARIES-I design, FWCD is chosen as the primary steady-state scenario on which most of the design work is focused, with NBCD as a viable alternative.

FAST WAVE CURRENT DRIVE SCENARIO

Substantial experience has accumulated in recent years with high power ICRF fast wave heating experiments in large toroidal machines, notably JET where 18 MW of power has been launched and H-mode discharges have been achieved. Fast wave

[1] Work supported in part by the U.S. Department of Energy.
[1] University of California, Los Angeles
[2] Argonne National Laboratory
[3] Georgia Institute of Technology
[4] General Atomics

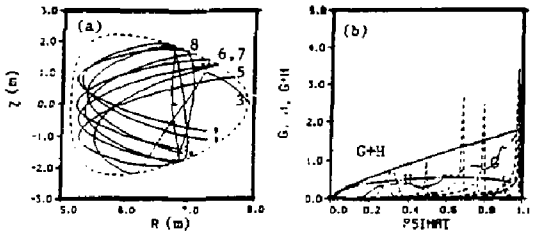

Figure 1. (a) Ray trajectories for LHW (#3) and FW (#5,6,7,8). See Table II for details. (b) Contributions to the flux-surface averaged current density from bootstrap effect (H) and RF waves (G). Solid curve indicates target equilibrium current while dashed curves show contributions from individual rays.

Table II: Wave Parameters of Rays for Fig. 1

Ray #	f(GHz)	$N_\parallel$	N_θ	θ_o	P(MW)
3	8.0	1.4	0.0	0.0	18.0
5	8.16	2.1	8.0	36.	31.6
6	8.16	2.1	8.0	27.	44.1
7	8.16	2.1	4.0	27.	28.8
8	8.16	2.1	4.0	18.	4.5

current drive has been observed and identified on JIPPTII-U, JFT-2M and other smaller machines [3] in the higher harmonic regime, and more definitive experiments are now planned on DIII-D and JET. Most recently, JET [4] reported measurements of direct electron heating by fast waves in the ICRF. Based on these latest results, it is anticipated that a sizable database on FWCD will be developed in the coming years.

The fundamental current drive process involves pushing electrons via a combination of the wave electric field (Landau damping) and the $\mu\nabla B$ force (TTMP) along the static magnetic field. In this scenario, the frequency is set at 158 MHz so as to locate the $2f_{ce}$ resonance surface on the outboard edge of the plasma and the $2f_{cT}$ surface inside the plasma near the inboard edge. As a result, wave absorption by the energetic alphas is completely avoided and only a few percent of the power is deposited in the fuel ions. For a single-pass absorption scenario, there exists a broad maximum of the CD efficiency in the spectral region of $N_\parallel$=1.5-2.2. Generation of a broad seed current profile requires the wave launchers to be located above the equatorial plane on the low field edge of the plasma [5].

To calculate the CD efficiency, γ, a series of FW and LHW ray tracing and equilibrium calculations using the RIP code [6] are performed to obtain an empirical scaling of γ as :

$$\gamma(A/m^2W) \;=\; 0.72\times < T_e >^{0.77} [0.041 + 0.235\beta]$$

where $< T_e >$ is in keV and 0.72 is an approximate correction factor accounting for degradation due to trapped electron effects [7]. For the ARIES-I parameters of Table I, γ=0.31 and, with I_{BS}/I_p=0.57, the required CD power $P_{CD} \approx$160 MW, including the LHW power.

Presently various methods are under consideration to improve the CD efficiency, an example of which is shown in Fig. 1. Here five rays are used to simulate the launching of 109 MW of FW power and 18 MW of LHW power into the ARIES-I plasma, with the wave parameters given in Table II, where N_θ and θ_o denote the poloidal refractive index and angle at the starting point of the rays, respectively. It is noted that very large N_θ components are launched, which may be provided by the fine structure of the poloidal power distribution of the launcher and by phasing the poloidally stacked antenna modules. In Fig. 1(a), the FW rays undergo 3-4 radial transits before the wave power is totally absorbed, 7% of which is deposited in tritium ions. Because of the large initial N_θ, the FW rays are only weakly focused towards

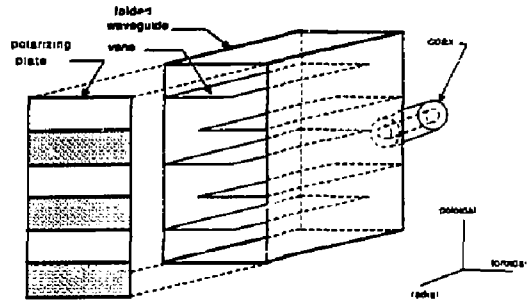

Figure 2. Isometric View of Folded Waveguide (w/o Diaphragm).

the magnetic axis which, together with their $N_\parallel$ evolution, results in relatively weak damping per radial pass. Improved CD efficiency is expected because the wave is damped on more energetic electrons with $v_\parallel/v_e > 1$ and more power is deposited in regions where trapped electron effects are weak. Turning of the rays near the plasma boundary are the results of either refraction through the density gradient or cutoff in the SOL, and not wall reflection. In this case, the current on axis is generated by the fast waves after the initial transit of the rays. Fig. 1(b) displays the contributions to the flux-surface averaged current density, defined as $< j_\parallel B > / < B^2 >$, from bootstrap effect and RF waves, denoted by $H(\bar{\psi})$ and $G(\bar{\psi})$ respectively. Reasonable agreement is obtained between the total driven current $H(\bar{\psi})+G(\bar{\psi})$ (dotted curve) and the target equilibrium current (solid curve), and the converged equilibrium attains parameters close to those listed in Table I. With a total current of 10.6 MA and CD power of 127 MW, γ_{total}=0.81 which, for a conservative estimate of $I_{BS}/I_p \approx$0.5, can lead to a much improved γ of 0.4.

FAST WAVE LAUNCHER DESIGN

The folded waveguide antenna [8] is proposed as the basic wave launching unit for the FWCD system. Each waveguide can be considered as a TE_{101} rectangular cavity folded in the long transverse dimension, with one end weakly coupled to the plasma via apertures in alternate folds. Attractive features of this innovative launcher concept include high power handling capability (~40 MW/m^2 ~ 4×loop), low impedance feedpoint at the backplate, compact and robust structure which make it particularly compatible to a reactor environment. Earlier low power bench tests [9] on scaled-down versions of the waveguide at the ORNL/RFTF facility produced results which agree with the theory. In recent high power tests, [10] at 1-sec, 80 MHz, 200 kW pulses, an E_{max}=43 kV/cm has been recorded and multipactor breakdown has been eliminated by careful conditioning of the device. So far, the experimental database appears to confirm the high power potential for this launcher.

A schematic of the folded waveguide unit designed for 158 MHz operation in ARIES-I is displayed in Fig. 2, with its dimensions and performance parameters listed in Table III. Each guide will have 6 folds, with a folded path length of 1.8 m which is far above the TE_{10} cutoff but slightly below the TE_{20} cutoff in order to minimize the radial thickness, which can be further shortened by introducing a diaphragm inside the structure. The toroidal width of the folded guide is set to a quarter wavelength of the dominant $N_\parallel$ wave component of the launched spectrum. To prevent destructive interference of the fields from adjacent folds, the front of the guide is covered with a polarizing plate as shown in Fig. 2. In the apertures, Faraday shields in the form of thin, horizontal rows of conductors are used to insure optimal coupling to the fast wave polarization. At the back plate, a tapered coax with a 10 cm diameter at the feedpoint (as in Fig. 2) is used to inductively couple the power into the guide.

Coupling of the wave power from the individual launcher to

Table III: Folded Waveguide Parameters (w/o Diaphragm)

Number of Folds	6
Unfolded Waveguide Height b	0.10 m
Toroidal Width	0.30 m
Toroidal Width of Vane	0.20 m
Poloidal Height	0.60 m
Unfolded Waveguide Width	1.80 m
Radial Thickness	1.12 m
Power Transmitted	4.0 MW
Coupling Efficiency	0.98
Peak Electric Field E_{max}	18.0 kV/cm

the plasma is investigated using the FWQ code [10]. For the high density SOL in ARIES-I, with $n_e=10^{20}$ m^{-3} at the separatrix and 10^{19} m^{-3} at the first wall, the coupling efficiency is found to be 98%. It should be mentioned that the coupling efficiency is sensitive to the plasma edge conditions and this dependence certainly deserves further investigation. For a transmitted power of 4 MW per guide, the peak electric field is found to be 18 kV/cm, well within the present achievable limit. Fig. 3 shows the poloidal and toroidal profile of the toroidal wave magnetic field from a single waveguide at the plasma surface. The discrete structure of the field due to the three radiating apertures is noted, lending support to the high N_θ used in the previous CD calculations.

It is proposed to build the folded waveguide launcher with SiC/SiC-fiber composite structural material to take advantage of its low activation, low decay afterheat, high strength and other favorable thermo-mechanical properties [11]. For non-irradiated SiC, the relative dielectric constant is 10 and the loss tangent is 10^{-3}. At 158 MHz, the power dissipation ratio through a 1.0 cm slab of SiC is 0.009% with a reflection coefficient of 0.016, implying that the thin SiC slab or the first wall coolant tubes are essentially transparent to the fast waves. With

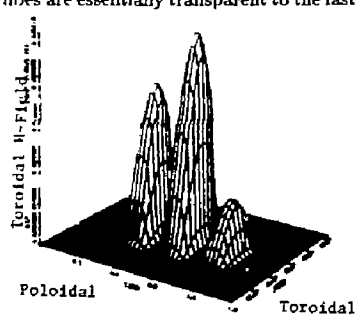

Figure 3. Poloidal and Toroidal Profile of Wave Magnetic Field due to a Single Folded Waveguide at the Plasma Surface.

adequate cooling, the waveguide structure can then be envisaged as a closed rectangular box made of thin (<1.9 cm) SiC walls. Through plasma spraying or CVD processes, a 0.02 mm thick copper coating is applied where a conducting surface is needed, such as the inside wall and vane surfaces, the front polarizing plate and the Faraday shield. A high quality vacuum ($< 10^{-7}$ torr) can easily be maintained inside the closed, well-conditioned waveguide structure, which is completely shielded from plasma particles, thus enhancing the possibility that ultra-high electric fields ($\sim$50 kV/cm) can be sustained without breakdown. An initial assessment indicates that if the copper plating is only several skin depth thick, the waveguide structure should be relatively transparent to a typical disruptive load. Further studies are being conducted to confirm this finding.

To fit the waveguide launchers inside the vacuum vessel, [12] the radial thickness of the waveguide must be reduced to 0.8 m. This reduction can be achieved by introducing a

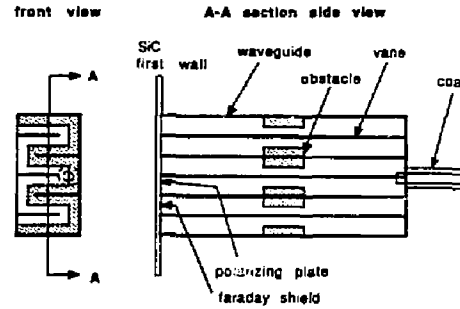

Figure 4. End and Side Views of Folded Waveguide with Diaphragm.

simple diaphragm structure of finite thickness [13] into each waveguide, as shown in Fig. 4. This diaphragm (or obstacle) is a transverse ridge placed midway along the axis, where the waveguide height is reduced from b to b', having an aspect ratio of b'/b. It essentially acts as a capacitor that effectively reduces the waveguide axial wavelength.

Approximate design curves of the waveguide thickness as a function of the diaphragm (or obstacle) thickness and aspect ratio have been obtained for the transverse dimensions given in Table III. For a waveguide thickness of 0.8 m, the design obstacle is 0.2 m thick and 0.055 m high. Even though the peak electric field is approximately doubled to 36 kV/cm for the same stored energy in the guide, this value is still well within the limit. The shape and edges of the obstacles (and vanes) can be contoured to substantially reduce the local electric fields. Joule dissipation in the walls may be increased but detailed wave calculations are needed for an accurate assessment. It is evident from the resonant wave structure that peak dissipation occurs at the front and back ends, and at the side walls midway along the waveguide axis. Horizontal coolant tubes can be placed near the ends without affecting the waveguide performance while the diaphragm can provide space for coolant flow and extra support for the vanes, if desired. Cooling of the SiC structure and its required thickness are outstanding issues which remain to be addressed in detail.

The overall launching system consists of 4 waveguide modules capable of delivering 192 MW of power through 1.6% of the first wall area. To launch the desired wave spectrum, each module is designed to be 3.6 m wide, 0.6 m high, and consists of a toroidal array of 12 waveguides with a 90° phase shift between adjacent guides. Simulations with a 2-D magnetostatic loop antenna code, CAV2D, [14] indicate that a maximum directivity of 0.95 is possible with such a module. The four launcher modules are located in two special blanket segments, each accommodating two poloidally stacked modules (at θ_0=25°, 46°), in order to generate the target equilibrium seed current profile [12].

RF SYSTEM DESIGN

Design of the RF support system for the fast wave current driver in ARIES-I is in its preliminary stage. For now, it is anticipated that this system will use primarily off-the-shelf technology and only a modest development program is required to upgrade the operating parameters of its key components. At 158 MHz, the most viable choice for the RF transmitter appears to be the klystrode, [15] a linear beam device having the desirable features of both a klystron and a tetrode. These tubes are commonly used as transmitters in UHF-TV stations and are available in sub-MW CW units having an efficiency of 70-75%. With a reasonable development program, a 90% efficiency should be within reach. Issues related to stable phasing of the waveguide array and high power coax transmission in a neutron environment are perceived to be solvable in the near future given the appropriate amount of R&D effort. As given in Table IV, the maximum projected system electrical efficiency, from wall plug to first wall, is 72%. Presently, the RF power cost is project to be \$1.50/W, but if 5 MW units of the klystrode are indeed

Table IV: Projected RF System Efficiency

DC Power Supply	0.95
RF Transmitter (Klystrode)	0.90
Transmission Line, Matching & Phase-Shift Circuits	0.90
Launcher Coupling Efficiency	0.98
Launcher Directivity	0.96
Overall Electrical Efficiency	0.72

available, the cost can be further lowered to \$1/W.

NEUTRAL BEAM CURRENT DRIVE SYSTEM

An alternative current drive scenario based on high energy neutral beams has also been considered for the ARIES-I reactor. In next-generation tokamaks, such as ITER, NBCD is the leading option for steady-state operation because of its developing database, attractive CD efficiency ($\gamma \approx 0.6$) and its projected capability for profile control. However, in reactor applications, neutral beams in excess of 2 MeV will be required for core current drive, implying major R&D efforts in new technologies beyond those of ITER.

NBCD calculations are performed to determine the required CD power for the set of ARIES-I parameters shown in Table 1. To produce the required seed current profile, two 2 MeV beamlines are used: (1) 35 MW with R_{tan}= 6.52 m (inboard) and (2) 50 MW with R_{tan}=7.13 m (outboard). Beam deposition is calculated with the 2-D Monte-Carlo code NFREYA, including multi-step ionization effects [16]. To ensure consistency with the ARIES-I stable equilibrium, the same 2-D flux surface geometry produced by the NEQ code is used in the calculations. Fig. 5 shows the bootstrap, seed, NB and equilibrium flux-surface averaged current density profiles, denoted respectively by j_{BS}, j_{seed}, j_{NB} and j_{tot}. As can be seen, the NB-driven current profile agrees well with that of the seed current. In this case, 85 MW of NB power is used to drive a seed current of 4.7 MA with 0.4% shine through, leading to γ=0.6.

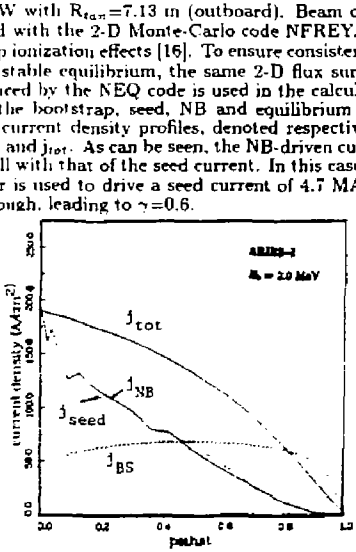

Figure 5. Flux-surface averaged current density profiles of bootstrap (BS), NB, seed and equilibrium components.

A high energy NB system based on the RFQ accelerator concept is appropriate for ARIES-I application. [17] For the desired profile control, a vertical column of beamlets at the first wall should be used. A 2 MeV, 20 A, 40 MW RFQ module that consists of 24 channels (1 A per channel) in a 2×12 matrix to provide 24 A of ions (20A of neutrals) can be envisaged as the basic building block. In particular, the divergence of this 23 MHz, 1 A per RFQ module is approximately 10 milliradians. According to calculations, two such beam modules should be adequate for ARIES-I. Provided an aggressive beam development program be in place in the next two decades, the efficiencies of the major components are estimated to be: 90% for the RF sources utilizing solid-state technology, 80% for the superconducting RFQ's and 95% for the photo-detachment neutralizers, giving an overall electrical efficiency of 68% for the NB system. The unit cost is estimated to be as high as \$3/W.

CONCLUSIONS

Fast wave current drive has been studied as a steady-state operating scenario in a commercial tokamak reactor such as ARIES-I. Provided that the database will be developed and the CD efficiency maintained at γ ~0.3-0.4, this technique employs relatively inexpensive, efficient, near-term technology which makes it attractive compared to neutral beam current drive. The high field in ARIES-I offers a unique environment to utilize the special features of the folded waveguide as a reactor-compatible launcher unit. Construction of the waveguide as a closed structure with copper-coated SiC composites walls further enhances its high power handling capability. As a result, a rather compact launcher system that devlivers 192 MW of power through 1.6% of the first wall area is realized. However, two major issues need to be studied: (1) cooling of the waveguide structure, and (2) dependence of wave coupling efficiency on plasma edge conditions.

ACKNOWLEDGEMENTS

The authors wish to thank W. Becraft, S. Grotz, M. Loring, Jr., L. Reid, D. Remsen, S. Sharafat and J. Yugo for providing valuable information for this paper.

REFERENCES

[1] F. Najmabadi, *et al.*, "The ARIES Tokamak Reactor Study," in *these proceedings.*

[2] R. L. Miller, *et al.*, "The ARIES-I High-Field-Tokamak Reactor: Design-Point Determination and Parametric Studies," in *these proceedings.*

[3] D. A. Ehst, "RF Power Applications to ITER," *Proc. 8th APS Topical Conf. on Radio-Frequency Power in Plasmas*, Irvine, CA, p. 393, 1989.

[4] L.-G. Eriksson, T. Hellsten, "Electron Heating During Ion Cyclotron Resonance Heating in JET," *Nucl. Fusion* vol. 29, p. 875, 1989.

[5] T. K. Mau, *et al.*, "Studies of ICRF Fast Wave Current Drive in Reactors," *Bull. Am. Phys. Soc.* vol. 33, p. 1900, 1988.

[6] D. A. Ehst, K. Evans, Jr., "Multiple Wave Radiofrequency Current Driven Tokamak Reactors in the First Stability Regime," *Nucl. Fusion* vol. 27, p. 1267, 1987.

[7] D. A. Ehst, et al., "Fast Wave Heating/Current Drive Scenarios for ITER," *ITER Internal Report ITER-IL-Ph-6-9-U19* June 1989.

[8] T. L. Owens, "A Folded Waveguide Coupler for Plasma Heating in the Ion cyclotron Range of Frequencies," *IEEE Trans. Plasma Science* vol. PS-14, p. 934, 1986.

[9] T. L. Owens, *et al.*, "Tests of a High-Power Folded Waveguide Coupler for ICRF Heating," *Proc. 7th APS Topical Conf. on Applications of Radio-Frequency Power to Plasmas*, Kissimmee, FL, p. 298, 1987.

[10] G. R. Haste, D. J. Hoffman, "High-Power Testing of the Folded Waveguide," *Proc. 8th APS Topical Conf. on Radio-Frequency Power in Plasmas*, Irvine, CA, p. 266, 1989; and subsequent communication.

[11] S. Sharafat, *et al.*, "SiC-Composites as Structural Material for the ARIES-I Reactor," in *these proceedings.*

[12] S. P. Grotz, *et al.*, "Design Integration of the ARIES-I Tokamak Reactor," in *these proceedings.*

[13] N. Marcuvitz, "Waveguide Handbook," McGraw-Hill, 1951.

[14] T. K. Mau, *et al.*, "Coupling Analysis for the ICRF Resonant Cavity Launcher on DIII-D," *IEEE Trans. Plasma Science* vol. PS-15, p. 273, 1987.

[15] D. H. Preist, M. B. Shrader, "The Klystrode-An Unusual Transmitting Tube with Potential for UHF-TV," *Proc. IEEE* vol. 70, p. 1318, 1982.

[16] J. W. Stearns, *et al.*, "Penetration of an Energetic D° Beam into an ETR Plasma," LBL 26505, University of California Lawrence Berkeley Laboratory, 1988.

[17] W. L. Stirling, *et al.*, "A Neutral Particle Beam System for ITER Employing RF Acceleration," in *these proceedings.*

13th Symposium on Fusion Engineering, Hyatt Regency Hotel, Knoxville, Tennessee, Oct. 2-6, 1989.

HIGH FIELD MAGNET DESIGNS FOR THE ARIES-I REACTOR[†]

Leslie Bromberg, D.R. Cohn, Joel Schultz, Justin Schwartz[‡], John E. C. Williams
MIT Plasma Fusion Center, Cambridge, MA, 02139

Steven P. Grotz
Institute of Plasma and Fusion Research
University of California, Los Angeles, CA 90024

Richard L. Creedon, Clement P. C. Wong
General Atomics, San Diego, CA 92138

and the ARIES Team

Abstract

The requirements for the development of large, very high field superconducting tokamaks are investigated. The superconducting material, the structure and the integration issues are investigated for both the toroidal field coils and the poloidal field coils. The interaction between the two system (out-of-plane and heating) are studied. Near term and longer term materials are compared. However, no materials or properties that have not been determined in the laboratory have been assumed.

Introduction

ARIES-I is a conceptual tokamak reactor design based on advanced technology and modest extrapolation from the present physics data base.[1] A major feature of the ARIES-I reactor is the use of high fields at the coil. The design and feasibility issues of the toroidal field magnet system are critical. This paper discusses the design approaches for superconducting magnet systems with $\geq$ 20T fields at the coil.

The HFCTR design incorporated the use of high field[2] and super high field concepts have recently been considered[3]. In this paper, we discuss magnet design for the very high fields used in ARIES-I[1].

Incorporating these concepts and materials into toroidal and poloidal field magnets suitable for a commercial tokamak reactor constitutes a difficult challenge. Due to the high field and large Lorentz loads, innovative uses of high strength materials and support structures are required. The choice of propeties of advanced magnet materials (both for the conductor and the structure) has been limited to those already attained in the laboratory although extrapolations to the sizes and lengths required for use in a tokamak fusion power reactor may be required.

Currently Nb_3Sn based superconductors are capable of producing fields up to about 20 T in short samples. Obtaining fields greater than this will require the development of a higher field superconductor. The choice of superconducting material are presented in §2.

Advanced structural materials with allowables beyond 900 MPa would be desirable, although not required. Both isotropic and composite materials are under consideration for structural application in the high field magnets. The choices for structural materials are discussed in §3.

Advanced structural design, such as using strong load-carrying stabilizer, grading the conductor and carefully matching the strains between the different magnet components are helpful. Details of this optimization are described in §4. Special attention is given to the system integration, to the structural conceptual design choices (out-of-plane structureis described in §5) and to the cryogenics (pulsed loads, thermal magnet insulation) for both toroidal and poloidal field magnets. The poloidal field system for ARIES-I is described in §6.

Finally, research areas critical to the successful development of high field magnets for fusion applications are identified.

2. Superconductors

High field operation requires advanced, high performance superconductors. Currently available Nb_3Sn alloys[4] are capable of producing fields up to about 20 Teslas. Obtaining fields greater than this requires the development of a higher field material. For fields greater than about 20 T, only three superconductors have demonstrated the capability of carrying sufficient current density. NbN is capable of $J_c \simeq 10^4 A/cm^2$ at $B_{\parallel} = 22T$, while Nb_3Al and $Nb_3(Al,Ge)$ are capable of $J_c \simeq 3x10^4 A/cm^2$ at $B = 24T$ and 31T, respectively.[5,6] The only advantage of NbN over Nb_3Al may be strain and irradiation insensitivity. However, as Nb_3Al and $Nb_3(Al,Ge)$ are less sensitive to strain and neutron irradiation than Nb_3Sn, severe limits are not expected.

Figure 1 shows the current density vs field for Nb_3Al and $Nb_3(Al,Ge)$. These levels of performance have only been obtained in a superconducting tape (after irradiation with electron beams), and there is yet no known method of obtaining similar performance in a multifilamentary wire. In order to stay within the developmental assumption that the material exist in the laboratory, we have assumed that the tape is used in the high field region.

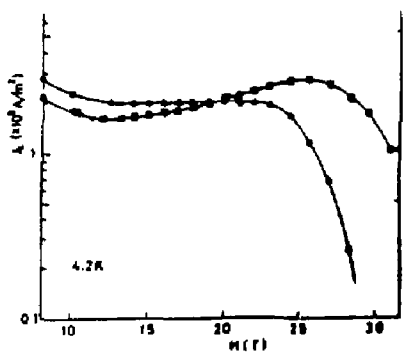

Fig 1 Critical current density for $Nb_3(Al,Ge)$ tape prepared by electron beam irradiation (from reference 5)

[†] Work supported by USDOE

[‡] This work performed under appointment to the Magnetic Fusion Energy Fellowship which is administered for the U. S Department of Energy by Oak Ridge Associated Universities.

The strain sensitivity of Nb_3Sn and Nb_3Al is shown in Figure 2 (from reference 7). The value of B^*_{c2} has been normalized to the maximum (nearly strain free) value B^*_{c2m}. Not only is the value of B^*_{c2m} larger for $Nb_3(Al,Ge)$ than for the ternary alloys but its sensitivity to strain is less.

In the toroidal field magnet, several grades of conductors are used. $Nb_3(Al,Ge)$ is used at high field ($\geq$ 18T), Nb_3Sn is used for intermediate field ($\geq$ 6T) and NbTi is used for low field.

3.0 Structural materials

Both isotropic and composite materials are under consideration for structural application in the magnets. The isotropic materials could be used by themselves or combined with fibers to obtain increases in both strength and moduli (to reduce strains). The consequences of using the isotropic and anisotropic materials are described in §4.

3.1 Isotropic materials

Commercially available structural steels currently have ultimate tensile stresses (UTS) in the neighborhood of 1.8 – 2GPa, (allowable equivalent stress 600 - 800 MPa) [8,9,10]. Also commercially available, but not necessarily optimized for low temperature applications, are the Ni-Co and Ni-Ti maraging steels. Depending on the particular composition and aging of the steel, the cryogenic UTS ranges from 2.2 - 3.7 GPa.[11] The largest UTS materials tend to have the lowest fracture toughness, so it is not clear what maximum allowable stress is acceptable. Detailed cryogenic characterization of these materials is currently being performed and will aid in determining the applicability of these materials.[12] It is not known whether alloying can improve the fracture toughness without simultaneously reducing the UTS.

The Fe-Mn and Fe-Cr alloys have been developed by the Japanese specifically for cryogenic applications[13]. They are distinguished by high strength and fracture toughness at LHe temperature ($\sigma_y \sim 1550$ MPA, $K_{Ic} \sim 200$ MPa$\sqrt{m}$). As shown in Figure 4 these materials show a tradeoff between strength and toughness. Thus, with minor variations in the amounts of alloying additions, it may be possible to develop an alloy with much higher strength and sufficient, although reduced, fracture toughness. For 25Cr-15Ni, this tradeoff can be expressed as[13]

$$K_{Ic} \sim 240 - 0.25(\sigma_y - 1390)$$

where K_{Ic} is in MPa$\sqrt{m}$ and σ_y is in MPa. This relation is shown in Figure 4. For $\sigma_y \sim 1800$ MPa, $K_{Ic} \sim 137$ MPa$\sqrt{m}$, providing an allowable equivalent tensile stress of 1200 MPa while maintaining sufficient toughness.

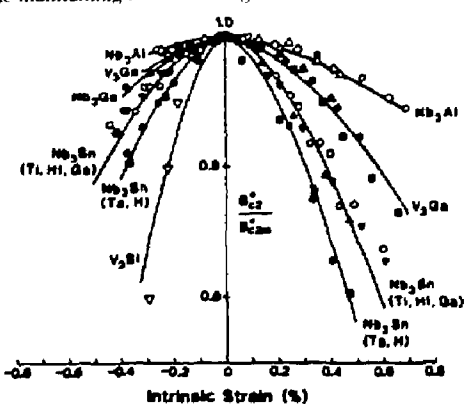

Fig 2 Effect of uniaxial strain on the upper-critical field of practical A15 superconductors (from reference 7)

Certain Ti alloys[14] may also be good materials for cryogenic applications. Yield stress as high as 1892 MPa has been reported at 4 K, although with low fracture toughness. The allowed strength would be in the range 1100 – 1300 MPa. It may be possible to improve the strength-toughness relationship by further optimization of alloying.

3.2 Anisotropic materials: fibers and composites

A large number of fibrous materials exist that have longitudinal UTS in the range of 2.1 – 7.0 GPa. These materials have longitudinal tensile modulus in the range of 150 GPa - 700 GPa. The primary fibrous materials under consideration are polymers, C and SiC.[15,16,17] Applications employing these materials depend not only on the properties of the fiber, but on the ability to fabricate the material in a composite with satisfactory properties in every direction. As fibers tend to have poor transverse compressive strength, magnet applications require the incorporation of the fibers into a matrix that can support the compressive loads in the inner leg. For this reason, only metal matrix composites (MMCs) are considered. The isotropic materials discussed previously are primary matrix candidates.

Of all the available fibers, the best combination of mechanical properties, availability, cost and applicability is found in carbon. Carbon fibers have been reported with $S_{f11,T} \geq 7$ GPa and with $E_{f11} \geq 700$ GPa (not simultaneously)[18]. These fibers are inherently anisotropic, with $E_{f22} < 0.1\ E_{f11}$, where E_{f22} is the transverse Young's modulus. This may prove advantageous for TF coil structural applications. By aligning the fibers with the vertical (tensile) load, the fibers provide very high vertical modulus and strength. Owing to the very low E_{f22}, however, the radial load is concentrated in the matrix. Thus, the loads are concentrated in the material best suited to support them.

In graphite, the carbon atoms are arranged in hexagonal layers, causing highly anisotropic bonding and mechanical behaviour[19]. In the layer planes (A and B), where high strength carbon bonding occurs, the Young's modulus is about 1000 GPa. Normal to those planes (along the c-axis), the layers are bonded together by weak van der Waals bonds, so the modulus is only 35 GPa. The quality of carbon fibers and the ability to control their properties depends on obtaining a high degree of preferred orientation of the hexagonal planes.

The sensitivity of mechanical properties to the degree of orientation of the layer planes leads to a broad range of obtainable C fiber properties. A strength/stiffness tradeoff exists. Thus, a fiber can be developed to provide optimized composite properties for a particular application.

Carbon fibers retain very good mechanical properties over a broad temperature range. For application in an MMC, however, one serious limitation must be overcome: high temperature reactions with nickel. The most probable mechanisms for the decline in strength observed in Ni coated graphite fibers are nickel-catalyzed graphitization and reduced fiber size due to C-Ni interdiffusion[20].

Recent results indicates that C/Ni reactions can be prevented by coating carbon fibers with a diffusion barrier that stabilizes the interface. The most promising coating materials are SiC and CoW. C/SiC fibers have been produced at MIT with very good results. Unfortunately, the only production method known is chemical vapor deposition (CVD), which is an inherently slow and expensive process. C/CoW fibers have been produced by NIST and American Cyanamid with very good results[21]. CoW, selected because it is carbide forming, is directly electrodeposited onto the fiber, forming a layer of Co_3W_3C and/or Co_6W_6C at the interface. As a result, no change in the size of the fibers occurred after annealing at 800 C for 24 hours in Ni. The protective barrier may be thinner than 0.1μm and still be effective. Electrodeposition is significantly faster than CVD (two orders of magnitude) and allows very good

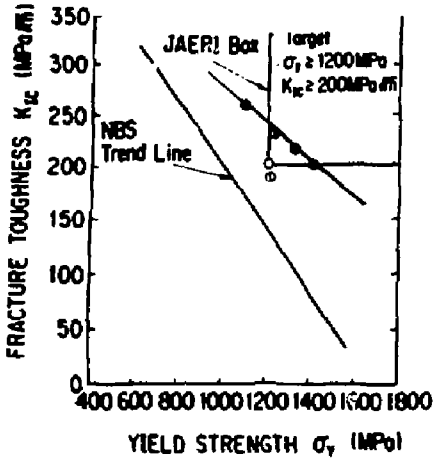

Fig 3 Tradeoff between strength and fracture toughness at 4.2 K. (from reference 13)

control of the W concentration gradient. By maintaining a concentration gradient in W, mobile dislocations in the composite experience an increasing resistance to motion when approaching the fiber/matrix interface. This provides increased strength and toughness.

Although there are a number of feasibilty issues to be evaluated, there are numerous potential solutions to the structural problem in the high field magnet, both with isotropic materials and MMCs.

4 TF Coil design and optimization

Each coil of the ARIES-I TF magnet consists of 14 plates, with the conductor wound into grooves. The coils were designed subject to the following constraints: superconductor stability, quench protection, superconductor strain (including thermal), stress and strain limits in the structure and fabricability. 5 grades of conductor winding pack are employed. For $B > 18$ T, $Nb_3(Al,Ge)$ tapes are deposited onto a CuNb substrate. The tapes are stacked and wound into the plate. An alternative to CuNb substrate is Al/SiC composite. For $B > 6$ T, multifilamentary Nb_3Sn superconductor is employed. For $B < 6$ T, NbTi is sufficient.

The toroidal dimension of each plate is fixed at 8.5 cm. The groove depth is determined such that sufficient thickness remains to support the vertical and radial loads. The vertical load is calculated assuming constant vertical strain across the inner leg. The radial loads builds up from the outer radius of the inner leg to the inside bore (where the coil meets the bucking cylinder). The rate of increment of radial load is the product of the local magnetic field and the winding pack current. The radial load is transmitted radially inward, so the required plate thickness is largest in the low field region of the coil. The conductor thickness in the radial dimension (the distance between grooves) is determined from the winding pack current, the conductor current density and the toroidal groove depth. The current and current density determine the required conductor area, so the groove depth determines the required spacing. Coolant requirements are based upon 2mW cm^3 uniform throughout the coil (a conservative assumption, since only the highest field turn would experience this level of heating).

Coil parameters are in Table I. Three cases are considered: a) low strength, low moduli, b) low strength, high moduli, and c) high strength, high moduli. There are 32 dump circuits (two per coil). The mechanical strain refers to the vertical strain thermal and primary mechanical (no bending). The mechanical stress then refers to the mechanical strain times the moduli.

The conductor properties for each grade for the case of low strength/low moduli are shown in Table 2. The coil inner leg cross section is in Figure 4.

5 Out-of-plane considerations

In ARIES, there are very large out-of-plane loads. Figure 5 shows the distribution of the loads along the coils, starting from the inner midplane. The poloidal field configuration of the baseline case was used (see Peng). The support of these loads is described in this section.

The coils are supported against the radial loads by a thick bucking cylinder. The thickness of this cylinder is determined by the radial loads. The out-of-plane loads generated in the inner leg of the magnet are also supported by the bucking cylinder.

Above and below the bucking cylinder there is a shell (cap). The inner part of this shell is a full continuation of the bucking cylinder. The poloidal field coils adjacent to this structure are supported by it. The outer part of the cap/poloidal field assembly is fully vacuum insulated. Removal of these poloidal field coils is accomplished by removing the entire cap. This simplifies the modular assembly and maintenance of the machine (see reference 23).

There is no insulation between the cap and the toroidal field magnets. For more details about the cryogenic aspects of the design, see Grotz[23].

A thick-shell code is used to calculate the out-of-plane stresses. The model used is based on the orthotropic toroidal shell model.[24] The model treats the superstructure assembly as a thick, continuous orthotropic shell. The thickness of the shell and the elastic moduli (allowed to be different in two directions) are allowed to vary along the lenght of the shell. The treatment is axisymmetric, but by appropriately changing the moduli along the shell it is possible to study the global effects of ports (stress concentrations would require a full 3-d analysis, beyond the scope of this work). It is assumed that the loads are transferred locally to the superstructure, i.e., the coils themselves do not react the out-of-plane loads.

The code is used in order to determine the thickness of the cap. The maximum shear stresses in the cap are limited to 300 MPa; however, the thickness of constrained to be at least 0.85 m thick, for structural integrity.

Table I
Global Characteristics of the TF magnet

Field at the case (T)	23.8		
Current pack (kA)	200		
Superconductor moduli (GPa)	175		
Stabilizer moduli (GPa)	185		
Plate moduli (GPA)	210	300	300
Allowable stress (MPa)	1000	1000	1200
toroidal thickness of plate (m)	0.085		
J_{magnet} (Ma/m^2)	21.4	21.6	25.1
Radial build (m)	1.03	1.02	0.85
Mechanical strain (%)	0.34	0.25	0.30
Mechanical stress (MPa)	676	682	807
Stored energy per dump circuit (GJ)	4.14	4.13	3.91

Table II
Grading of the TF magnet
Low-modulus and low-strength case

conductor	Grade 1 mf NbTi	Grade 2 mf Nb_3Sn	Grade 3 mf Nb_3Sn	Grade 4 tape $Nb_3(Al,$	Grade 5 tape $Nb_3(Al,$
Field of split (T)	4.0	11.0	18.0	20.5	24.1
Sc current (10^9 A/m^2)	4.65	3.14	0.498	0.251	0.194
Critical temperature (K)	6.58	11.06	6.45	10.57	8.88
Areas (10^{-4} m^2)					
Superconductor	0.432	0.639	4.03	8.01	10.3
Structure	7.75	7.75	7.75	14.8	18.2
Conductor	8.19	8.39	11.8	22.8	28.6
He	0.659	0.665	0.744	5.02	5.44
Cable space	8.85	9.06	12.5	27.8	34.0
Total area	71.3	93.9	65.2	65.8	65.0
Plate	59.1	81.0	49.5	34.8	27.7
Insulation	3.35	3.87	3.19	3.21	3.19
Conductor width	1.46	0.975	2.07	3.72	4.80
radial thickness	6.07	9.29	6.04	6.12	5.96
fraction of stabilizer	0.947	0.924	0.658	0.648	0.638
Plate thickness (10^{-2} m)	3.76	3.68	3.07	1.84	1.28
Radial dimension of turn	0.078	0.110	0.077	0.078	0.077

Table III
Poloidal Field Magnet Constraints

$V_{terminal}$	20	(kV)
I_{cond}	45	(kA)
B_{max}	13.6	(T)
$\sigma_{Tresca\ membrane}$	1000	(MPa)
$f_{critical}$	0.6	
$T_{max,dump}$	150	(K)
T_{margin}	0.5	(K)
Suggested		
E_{margin}	500	(mJ/cm^3)
$f_{well-cooled\ recovery}$	0.8	

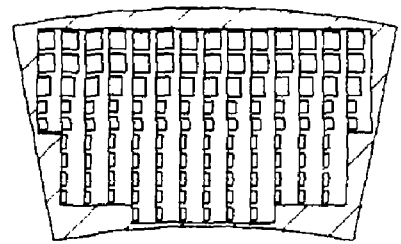

Fig 4 Cross section of the coil in the midplane.

Figure 6 shows the resulting thickness of the cap for the loads shown in Figure 5. Two ports have been assumed, one for removing the divertor targets and another on the midplane. The thickness of the superstructure is increased in these areas in order to reinforce it. Elsewhere, the cap thickness varies between 0.05 and 0.2 m away from the bucking cylinder. In order to fabricate such a cap, the thickness variation should be smoothed out.

The resulting shear stresses are shown in Figure 7. The shears in the bucking cylinder due to the out-of-plane loads are about 75 MPa. (the thickness of the bucking cylinder is determined mainly by the radial loads and it is fixed at 0.95 m). Note that there is a reversal of the shear stresses in the inner top of the superstructure, occuring at about a height of 3 m. At this location, the shears that react the out-of-plane loads are small, and as a consequence, the out-of-plane structure can be discontinuous. The fact that the superctructure be discontinuous at a point is very important in order to be albe to take the system apart (if the superstructure were in one piece, the chosen modular maintenace and assembly methods would not work).

We have analyzed several scenarios to determine the height of the region with zero shear. These include different OH bias, different plasma pressure (to simulate startup and shut-down), and simple disruption scenarios (for all the cases described above) We have found that the location of the zero shear varies by only a few cm for these cases. Furthermore, some shear capability can be provided across the gap by keying the caps and the bucking cylinder together.

6.1 PF System Design

The PF coils in ARIES are external to the TF system. They are superconducting, using internally-cooled, cable-in-conduit conductor. The conductors are internally-cooled composites of copper and binary Nb_3Sn. The design of the poloidal field (PF) magnet system does not share the feasibility and development issues of the TF system. ARIES has a steady-state plasma and a modest plasma current of 11.1 MA. The peak field in the PF system is only 12 T and pulsed losses in the PF system are modest in comparison with those of the toroidal field (TF) system, because of the much smaller volume of superconductor required.

In 1988, the ITER Magnet groups held a workshop that established design allowables for the superconducting magnets[28]. These are listed in Table III, along with suggested additional constraints on energy and power balance criteria for recovery from disturbances. The ARIES PF design follows the ITER recommendations, with the exception that the Tresca membrane stress allowable is 800 MPa for ITER and 1000 MPa for ARIES. All PF magnets are self-supporting against tensile loads and the central solenoid is self-supporting against vertical loads. The ARIES coils are more conservative than those of ITER in

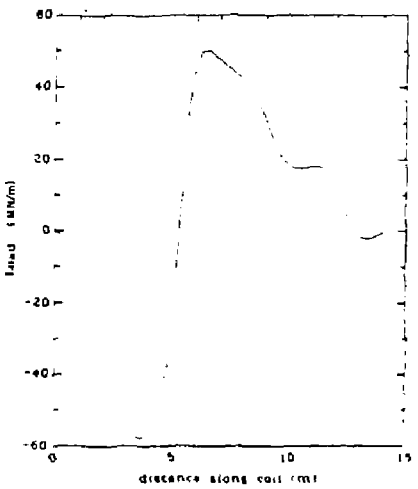

Fig 5 Out-of-plane load distribution for the worse case analyzed as a function of the distance along the coil (starting at the inner midplane)

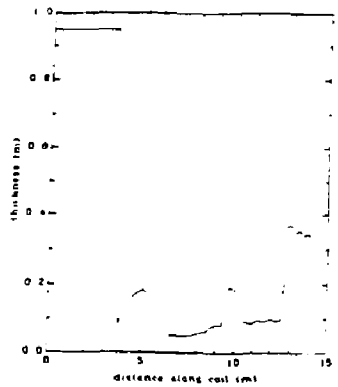

Fig 6 Thickness of the superstructure. The location of the two sets of ports (for removing the divertor target and at the midplane) can be readily identified.

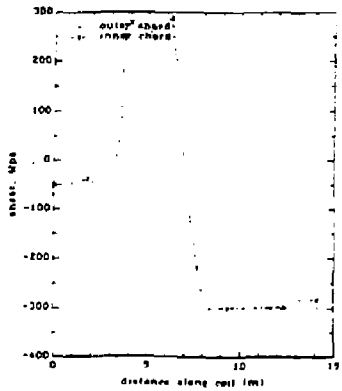

Fig 7 Shear stress distribution

that they are also designed for energy margins greater than 500 mJ/cm^3 and fractions of critical current in the well-cooled recovery regime. Trade studies indicate that when these constraints are included, Nb_3Sn is preferable to $NbTi$, even at low fields.

MHD equilibria were generated over a range of flux linkages at high and low beta, in order to evaluate the capabilities of the PF system [25]. PF trade studies showed that the design of ARIES was qualitatively different from that of other PF systems, such as those for ITER and CIT. Since there is no ohmic startup, the design doesn't require maximization of volt-second capability. However, conventional methods for minimizing stored energy lead to designs with unrealistically small fractions of metal in the coil winding packs. Furthermore, because of the flatness of the cost and energy minima, a significant amount of flattop and startup volt-second capability can be included for a small additional increase in coil costs. Given the probable need to handle off-normal conditions, a modest flattop capacity of 35 V-s was selected. Additional constraints on overall metal fraction and copper-noncopper ratio were added to ensure coil fabricability.

The peak PF energy of 12 GJ is smaller than that of ITER. Because of the slow charging of the coils, the peak power and power supply requirements are modest. A SAVAR power-factor correction control circuit is used in order to prevent large circulating reactive power in the utility line feeding the PF circuits[27]

Conclusion

There are many difficulties in the development of commercial tokamak with very high field magnets. These difficulties have been identified and the issues analyzed. Using present day materials that exist in the laboratory (both structure and superconductor), it is possible to design 24 T field superconducting tokamak reactors.

References

(1) F. Najmabadi, R. W. Conn, and the ARIES Team, elsewhere in this conference.

(2) D.R. Cohn et al., *High Field Compact Tokamak Reactor Conceptual Design*, MIT, PFC RR-79-2 Jan. (1979).

(3) J. Schwartz, L. Bromberg, D. R. Cohn, and J. E. C. Williams, *Fusion Technology*, Vol. 15. 957. March (1983).

(4) S. Pourrahimi, C.L.H. Thieme and S. F[illegible]er, *Proceedings of the Applied Superconductivity Conference*, Baltimore. Md., October, 1986.

(5) K. Togano and K. Tachikawa, *Adv. Cryo. Engr (Materials) 34*, A.F. Clarke and R.P Reed, eds., p. 451, 1988.

(6) H. Morita, K. Watanabe, K. Noto and H. Fujimori, *Adv. Cryo. Engr (Materials) 34*, A.F. Clarke and R.P Reed, eds., p. 829, 1988.

(7) J.W. Ekin, in *Adv. Cryo. Eng. (Materials)*, Vol 30, p 823 , 1984

(8) J. Martin, R.G. Ballinger, M.M. Morra, M.O. Hoenig and M.M. Steeves, *Adv. Cryo. Engr. 34*, A.F. Clarke and R.P Reed, eds., p. 149, 1988.

(9) W.S. Neef, Memorandum, Structural Material Properties Relevant to Superconducting Magnet Applications, February, 1988.

(10) H. Nakajima et. al., *Adv. Cryo. Engr. 34*, A.F. Clarke and R.P Reed, eds., p.173, 1988.

(11) D.L. Corn, *Adv. Cryo. Engr. 12*, p. 532, 1966.

(12) P. Raboin, Sc.D. Thesis, Mechanical Engineering , MIT, expected May, 1989.

(13) K. Suemune and T. Sakamoto and T. Ogawa and T. Okazaki and S. Maehara", *Adv. Cryo. Engr. 34*, A.F. Clarke and R.P Reed, eds., p 123, 1988

(14) K. Nagai, T. Yuri, O. Umezawa and K. Ishikawa, *Cryogenic Materials '88*, Volume 2: Structural Materials, p.727, 1988.

(15) S.R. Allen, R.J. Farris and E.L. Thomas, *J. Mat. Sci.*, 20, p. 4583, 1985.

(16) T. Hamada, T. Nishida, Y. Sajiki and M. Matsumoto, *J. Mat. Res.*, 2(6), p. 850, 1987.

(17) M.E. Buck, *Mat. Engr. and Des.*, VIII(5), p. 272, 1987.

(18) Torayca Technical Reference Manual, available from Toray Industries, Inc. 1988

(19) K.K. Chawla, *Composite Materials*, Materials Research and Engineering Series, Springer–Verlag, 1987

(20) P.W. Jackson and J.R. Marjoramm, *Journal of Materials Science*, Vol 5, p. 9, 1970

(21) N.S. Wheeler and D.S. Lashmore, American Cyanamid and Institute for Materials Science and Engineering, National Bureau of Standards, Annual Report, Jan. 1989

(23) S.P. Grotz, F. Najmabadi, L. Bromberg, R.L. Creedon, C.P.C. Wong, R.A. Krakowski, D.K. Sze, and the ARIES Team, elsewhere in this conference

(24) E.S. Bobrov, *Nucl. Eng. and Design/Fusion*, Vol 1, p 34-50, 1984

(25) Y-K M. Peng, J.T.Hogan, D.J. Strickler, J.C.Whitson, M.Klasky, K. Evans, S.C. Jardin, C.G. Batkhe, J.A. Leurer and the ARIES Team, elsewhere in this conference.

(26) J. Miller et al, ITER-EL-MG-1-9-U-1, LLNL-ITER-89-020, February-March 1989

(27) H. Boenig and F. Cibulka, *IEEE Trans on Power Apparatus and Systems* PAS-101, No 10, Oct 1982

BLANKET DESIGN FOR THE ARIES–I TOKAMAK REACTOR

C.P.C. Wong, E.T. Cheng, R.L. Creedon,*
J.A. Leuer, K.R. Schultz
General Atomics, P.O. Box 85608
San Diego, California 92138-5608

S.P. Grotz, N.M. Ghoniem, M.Z. Hasan, R.C. Martin,
F. Najmabadi, S. Sharafat, T. Kunugi†
Institute of Plasma and Fusion Research
University of California
Los Angeles, California 90024

D.K. Sze
Argonne National Laboratory
Argonne, Illinois 60439

J.S. Herring
Idaho National Engineering Laboratory
Idaho Falls, Idaho 83415-3523

R.L. Miller
Los Alamos National Laboratory
Los Alamos, New Mexico 87545

E. Greenspan
University of California, Berkeley
Berkeley, California 94720

And The ARIES Team

Abstract: For the ARIES–I tokamak power reactor design, we evaluated two gas-cooled, low-activation ceramic blanket designs, a 5 MPa helium-cooled design, and a 0.5 MPa CO_2 gas-carried Li_4SiO_4 particulate design. The more extensive data base available for the helium-cooled option has led to the selection of this option as our reference design. The selected ARIES–I blanket design uses SiC composite as the structural material, 5 MPa helium as the coolant, Li_4SiO_4 as the solid tritium breeder, and Be metal pellets as the neutron multiplier. This combination of materials provides the design of a high nuclear performance blanket with high outlet temperature, good neutron multiplication, and adequate tritium breeding. It is a low-activation design that satisfies the criteria for 10CFR61 Class–C shallow land waste disposal and achieves inherent safety since it produces negligible afterheat, thus virtually eliminating the possibility of radioactivity release to the public.

Introduction

The ARIES research program is a multi-institutional effort to develop several versions of the tokamak as an attractive fusion reactor with enhanced economic, safety, and environmental features [1]. The ARIES–I design is a DT-burning, 1000 MW(e) (net) reactor based on modest extrapolation from the present physics database and featuring advanced technology such as utilization of very high-field superconducting magnets and a low-activation blanket [1]. The ARIES–I blanket uses low-activation SiC composites as the structural material. To enhance the blanket energy multiplication, Be metal is used as the neutron multiplier. We evaluated two blanket designs for ARIES–I. The first one uses Li_4SiO_4 as the solid tritium breeding material, in the form of a dilute suspension of fine particles (5 to 10 μm in diameter) in a 0.5 MPa pressure CO_2 carrier gas as the blanket coolant. The second one uses Li_4SiO_4 in stationary form and 5 MPa pressure helium gas as the coolant. Since the performance of the two designs is similar, and due to the relative availability of design data, we have selected the helium-cooled option as the reference blanket for the ARIES–I reactor design. This paper summarizes the choice of reference blanket design, the results of material selection, mechanical design, neutronics analysis, thermal-hydraulic analysis, power conversion system design, tritium extraction, and safety evaluation.

Coolant Selection

We investigated two coolants for the ARIES–I blanket design: a 5 MPa helium coolant design and an innovative, gas-carried solid lithium particulate design. The 5 MPa helium gas, due to its chemical inertness and transparency to neutrons, is a natural coolant for fusion reactors [2]. Being a gas, helium has to operate at relatively high pressure to provide good heat transfer and acceptable pumping power. When solid particles are mixed into the gas stream, the mixture will have a much higher volumetric heat capacity than the pure gas. In comparison, for the same heat transfer coefficient, the mixture of particulate and gas will have lower volume flow rate and pumping power, than a gas-only design [3,4]. For fusion application, an additional advantage for using a Li particulate and gas mixture is that the blanket coolant is also the carrier of the breeder material. This facilitates tritium extraction outside of the blanket and greatly reduces tritium inventory when compared to stationary solid breeder designs. This concept also eliminates the uncertainties of the helium purge flow tritium extraction design and solid breeder behavior under neutron irradiation for stationary breeder designs and may, thus, lead to much lower blanket

*Present address: Advanced Cryomagnetics, P.O. Box 210132, San Diego, California 92121.

†Permanent address: Japan Atomic Energy Research Institute, Naka, Ibaraki, Japan.

development cost. At the same time, the mechanical design complexity related to the tritium purge flow system is eliminated. When a higher density gas like CO_2 is used as the carrier gas, lower coolant pressure can be used while maintaining similar heat removal capability with that of a high-pressure helium design. The use of a ceramic composite as the structural material then becomes more attractive since the primary pressure stress will be lower by a factor of ten from that of the helium coolant pressure of 5 MPa. As the solid breeder is being circulated, we can adjust the blanket tritium breeding performance during operation by adjusting the ^{6}Li enrichment of the breeder particles. When these potential advantages were identified, it became obvious that we had to seriously consider this CO_2-particulate coolant concept for the ARIES-I blanket design.

There are two key design uncertainties associated with this innovative concept. They are the potential problems of particle and wall erosion and the circulation of particles both inside and outside of the blanket module. The use of gas-particulate mixtures as a coolant in fission reactors was investigated extensively in the 1960's [4]. It was shown that erosion problem could be solved by using graphite as the circulating particle material. There were limited erosion experiments performed with Al_2O_3 on aluminum alloys [5] which indicated an erosion threshold effect exists. That is, when the particle size is reduced, and the kinetic energy of a single particle reaches a certain minimum level, erosion cannot be measured. On the other hand, it is also true that the erosion effect is very sensitive to the properties and configuration of the impinging particles and surface material. Due to the lack of experimental erosion data of Li_4SiO_4 on SiC composite material, we remained skeptical on evaluating the erosion lifetime of this particulate blanket design. In order to enhance the credibility of the ARIES-I blanket design, we have selected to base our blanket design on the more conventional high-pressure helium as the blanket coolant and have left the innovative low-pressure CO_2 Li_4SiO_4 particulate design for the future when relevant erosion data are available.

Materials Selection

Structural Material

SiC composite ceramic is the structural material of the ARIES-I blanket. Ceramics have many desirable characteristics when compared with metals. The characteristics of high strength at high temperature and low-induced radioactivity are used in our design. The selection of SiC composite material avoids the brittle failure modes of monolithic ceramic materials [6]. The main method used to improve the strength and fracture toughness is through fiber reinforcement. Different methods can be used to infiltrate the SiC into a fibrous SiC preform [7]. Recent advances in SiC composite manufacturing processes have greatly improved the failure mode behavior, strain tolerance, and fracture toughness of these ceramics. For the ARIES-I design, we have selected a simple blanket configuration, as shown in Fig. 1, to tailor to the manufacturing process and to minimize the required number of joints. Micromechanical design equations were used to estimate material properties for typical SiC composite materials. These calculations reflect the degradation of fiber and matrix material properties due to imperfect manufacturing techniques and neutron irradiation effect at high temperatures. The maximum allowable design stress of the SiC composite was estimated to be 180 MPa a' the maximum allowable temperature of 1000°C. Detailed first-wall structural analysis shows that the th ermal, pressure, and bending stresses can be designed to be within these estimated design limits.

Breeding Material

Li_4SiO_4 has been selected as the tritium breeding material for the ARIES-I blanket design because of its chemical stability compared to Li_2O, and its low-induced radioactivity compared to $LiAlO_2$ which can generate ^{28}Al, which has a half-life of 0.73 million years. Even though Li_4SiO_4 has a lower lithium atomic density than Li_2O, adequate tritium breeding can be obtained when Be is used as the neutron multiplier [8].

Neutron Multiplier

Be metal is the best choice of low-activation neutron multiplier, since it does not have any other elements like oxygen to compete for the available neutrons. The key drawback for the use of Be is the limited resource of this material. Based on the ARIES-I geometry, we found that 400 to 500, 1000 MW(e) reactors could be supported by using the present United States' beryllium reserve. When recycling of Be is applied, still more reactors could be supported [8]. In the design of the ARIES-I blanket, the Be metal is also used for increasing the energy multiplication. Neutron multiplication by $(n, 2n)$ reactions give excess neutrons which are captured in Si to produce energy. The blanket energy multiplication is 1.36 when Be is used, as compared to 1.05 when Be is not used [8].

Blanket Configuration Design

The reference ARIES-I blanket is a 5 MPa helium-cooled, stationary sphere-pac Be multiplier and Li_4SiO_4 breeder design. The SiC composite blanket module is illustrated in Fig. 1. It consists of the radial zones of the first wall, neutron multiplier, breeder, and reflector. The blanket module is designed to

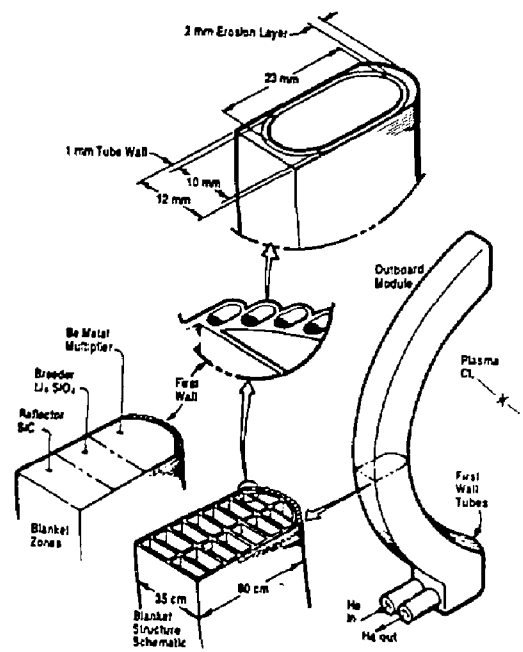

Fig. 1. ARIES-I SiC composite blanket module.

withstand the gas pressure of 5 MPa. The blanket module can be fabricated by first forming the complete poloidal segments of the module, with the inclusion of flow channels and structural supports before the high-temperature SiC infiltration and brazing process. The module can then be filled with the sphere-pac Be metal and Li_4SiO_4 pellets into their respective radial zones [7]. These multiplier and breeder zones are cooled by helium coolant channels. The ARIES–I blanket design parameters are summarized in Table 1.

Table 1
ARIES–I Blanket Design Input Parameters

Power:	
Fusion power, MW	1931.0
Alpha power, MW	398.0
Blanket Multiplier	1.36
Net electrical power, MW	1000.0
Materials:	
Structural, SiC–composite	
Breeder, Li_4SiO_4 sphere-pac	
Multiplier, Be metal sphere-pac	
Coolant, 5 MPa helium	
Wall Loadings:	
Average neutron wall loading, MW/m^2	2.74
Maximum neutron wall loading at mid-plane, MW/m^2	4.0
Average surface loading, MW/m^2	0.48
Maximum surface loading at mid-plane, MW/m^2	0.85
Geometry:	
Tokamak first-wall area, m^2	580.0
Module toroidal width, m	0.35
Outboard module height, m	6.5
Inboard module height, m	8.0
First-Wall Race Track Shaped Channel:	
Width, mm	10.0
Length, mm	23.0
First-wall minimum structural thickness, mm	1.0
First-wall CVD erosion layer thickness, mm	2.0
Thermal Power Fractions:	
First wall	0.16
Be zone	0.47
Breeder plus multiplier zone	0.33
SiC reflector	0.04
Calculational Assumptions and Models Used:	
First-wall SiC volumetric power generation, MW/m^3*	7.6
SiC thermal conductivity, W/mK	10.0
Maximum Li_4SiO_4 volumetric power generation, MW/m^3*	30.0
Breeder packed-bed effective thermal conductivity, W/mK	1.2
Packed-bed and surface contact heat transfer coefficient, W/m^{2}K	400.0

Twenty-percent reduction in first-wall heat transfer coefficient assumed due to nonisotropic heat flux

*Per 1 MW/m^2 neutron wall loading.

Neutronics and Waste Disposal

Based on the above configuration and design details of the ARIES–I blanket design, neutronics calculations were performed [9]. With the physical separation of the neutron multiplier and tritium breeder zones, we are able to optimize the design for adequate tritium breeding and maximum blanket energy multiplication. At a ^{6}Li enrichment of 20%, the tritium breeding ratio for this design is 1.12 and the blanket energy multiplication is 1.36 [8]. Decay heating of the SiC blanket structure is very low [8], and coupled with the high melting point of SiC at 2560°C, no safety concern of radioactivity released from the blanket material is warranted. Investigating the generation of long-lived induced radioactivities from the blanket materials, it was found that the entire blanket can satisfy criteria of 10CFR61 Class–C shallow land waste disposal [8].

First-Wall Design

In order to reduce the local bending loads of the first wall, a tube bank design approach is used with the rounded surface of the tube facing the plasma. Using a finite element calculation, the detailed structural design of the first wall was analyzed. It was shown that the maximum local stress can be designed to below the 180 MPa design limit of the SiC composite material [7].

Thermal Hydraulics

As shown in Fig. 1, the coolant helium enters the blanket module at the bottom, flows in parallel streams in the poloidal direction through the first wall, the breeder zone, and the reflector zone; it then turns around at the top of the module and flows down in the poloidal direction through the neutron multiplier zone. This flow configuration allows the coolant to exit from the Be neutron multiplier zone at a relatively high temperature of 650°C. Results of the thermal-hydraulic design of the ARIES–I blanket are presented in Table 2. As shown, the first-wall maximum temperature is less than the SiC design limit of 1000°C. The Li_4SiO_4 breeder can be designed to within the recommended operational window of 320° to 950°C [9]. The swelling tolerant Be pellet bed design can be designed to less than or equal to 820°C. At a coolant outlet temperature of 650°C, the selected supercritical steam Rankine cycle has a thermal efficiency is 48% [10,11].

Tritium Extraction

The bred tritium is to be extracted by a purge flow design through the Li_4SiO_4 breeder zone. At equilibrium, the expected tritium inventory in the blanket system is less than 1.0 kg. This will be further quantified pending the understanding of tritium behavior in Li_4SiO_4 under high lithium burnup [12]. Alternate solid breeders are $LiAlO_2$ and Li_2O.

Safety

With the selection of SiC as the structural material, helium as the blanket coolant, Li_4SiO_4 as the solid breeder, and beryllium as the neutron multiplier we have utilized all low-activation materials. They all have very low-induced afterheat and induced radioactivities. Because of these properties, no major release of radioactivities to the public is possible [13]. Therefore, the ARIES–I blanket design can be rated as an "inherently safe" design, achieving a Level 1 safety assurance rating [14].

Conclusions

We have selected the 5 MPa helium-cooled, stationary breeder low-activation blanket design for ARIES–I. A simple

Table 2
ARIES–I Outboard Blanket
Heat Transfer Results

First Wall, °C:	
Inlet temperature	350
First wall and breeder zones exit temperature	510
Maximum SiC Structure Temperature, °C:	
Inlet	620
Midplane	881
Outlet	772
Maximum Li_4SiO_4 Temperatures for a 3–mm Thick Zone, °C:	
Inlet	
T–surface	719
T–centerline	796
Midplane	
T–surface	795
T–centerline	873
Outlet	
T–surface	877
T–centerline	950
Maximum Be Packed-Bed Temperature for 5–mm Thick Zone, °C:	
Inlet	
T–surface	654
T–centerline	680
Midplane	
T–surface	791
T–centerline	800
Outlet	
T–surface	793
T–centerline	820
Blanket Outlet Temperature, °C	650
Total First Wall, Blanket Pressure Drop, MPa	0.32
Total First Wall, Blanket Pumping Power, MW	154

SiC-composite poloidal blanket module design is proposed. Separate Be multiplier and Li_4SiO_4 breeder zones allow a high-coolant outlet temperature of 650°C. Credible first-wall and blanket internal designs are also identified. Good neutronics performance can be obtained with a tritium breeding ratio of 1.12 and a blanket energy multiplication of 1.36. By coupling the helium coolant to a supercritical Rankine cycle power conversion system, the expected thermal efficiency is 48%. With the selected blanket materials, we have achieved our low-activation blanket design goals of producing minimum-induced afterheat and radioactivity and meeting the 10CFR61 Class–C waste disposal. The ARIES–I blanket design can be classified as a Level–1, inherently safe blanket design. This blanket offers a combination of good nuclear and thermal performance with excellent safety and environmental features for the ARIES–I reactor design.

Acknowledgment

The work at General Atomics was sponsored by the U.S. Department of Energy under Contract No. DE-AC03-89ER52153.

References

[1] F. Najmabadi, *et al.*, "The ARIES Tokamak Reactor Study," Proceedings of the 13th Symposium on Fusion Engineering, October 2–6, 1989, Knoxville, Tennessee.

[2] C.P-C. Wong, *et al.*, "Helium-Cooled Blanket Designs," Fusion Technology, vol. 8, July 1985.

[3] D.C. Schluderberg, *et al.*, "Gaseous Suspensions — A New Reactor Coolant," Nucleonics, vol. 19, No. 8, August 1961.

[4] D. Krucoff, "Armor Dust-Fueled Reactor," Nucleonics, June 1959.

[5] S.E. Smeltzer, *et al.*, "Mechanisms of Metal Removal by Impacting Dust Particles," J. Basic Eng., September 1970.

[6] G.R. Hopkins and J. Chin, "SiC/SiC Composite," General Atomics Report GA–A18295, also Proceedings of the Radar Absorbing and Armor Composite Workshop, October 29–31, 1985, Redstone Arsenal, Alabama.

[7] S. Sharafat, *et al.*, "SiC-Composites as Structural Material for the ARIES–I Reactor," Proceedings of the 13th Symposium on Fusion Engineering, October 2–6, 1989, Knoxville, Tennessee.

[8] E.T. Cheng, "Neutronics Studies for the ARIES–I Reactor," Proceedings of the 13th Symposium on Fusion Engineering, October 2–6, 1989, Knoxville, Tennessee.

[9] C.E. Johnson, *et al.*, "Solid Breeder Blanket Data Assessment," INTOR, Phase 2A, Part II, IAEA, Vienna, 1986.

[10] R.L. Bannister, *et al.*, "High-Temperature Supercritical Steam Turbines," Mechanical Engineering, February 1987, p. 60.

[11] M.Z. Hasan, "Thermal Cycle Power Conversion for the ARIES–I Tokamak Reactor," Proceedings of the 13th Symposium on Fusion Engineering, October 2–6, 1989, Knoxville, Tennessee.

[12] D.K. Sze, *et al.*, "Tritium System for the ARIES–I Tokamak Reactor," Proceedings of the 13th Symposium on Fusion Engineering, October 2–6, 1989, Knoxville, Tennessee.

[13] J.S. Herring, *et al.*, "Safety Engineering for the ARIES–I Tokamak Reactor," Proceedings of the 13th Symposium on Fusion Engineering, October 2–6, 1989, Knoxville, Tennessee.

[14] S.J. Piet, "Inherent/Passive Safety for Fusion," The 7th Topical Meeting on the Technology of Fusion Energy, Reno, Nevada, June 1986.

SILICON-CARBIDE COMPOSITE MATERIALS FOR THE ARIES-I REACTOR STUDY†

S. Sharafat, N.M. Ghoniem, L.Y.Yee, and the ARIES Team
Institute of Plasma and Fusion Research
University of California, Los Angeles
Los Angeles, CA 90024-1597

Abstract The ARIES-I tokamak is a conceptual reactor design based on advanced technology and modest extrapolation from the present day physics database. The ARIES-I blanket utilizes SiC/SiC composite materials as structural material with helium gas as the coolant. Until recently the brittle failure behavior of monolithic ceramic materials has posed a problem for using ceramics as structural materials. Recent developments in manufacturing and processing of fiber-reinforced ceramics make SiC/SiC composites a promising candidate for future power plants. Silicon carbide composites are advantageous from a safety and waste disposal stand point because of the low activation and their very low decay after-heat respectively. The thermomechanical properties and neutron irradiation response of SiC/SiC composite materials are reviewed. Composite design equations are used to approximate a window of allowable design stresses for the first wall and blanket structure of the ARIES-I tokamak reactor. The ANSYS finite element structural analysis code is used to analyse the thermal and mechanical behavior of the first wall under normal operating conditions. It is concluded that with minor extrapolations from todays manufacturing experience, SiC/SiC composites offer a viable structural material choice thus improving the safety and environmental aspects of future fusion power plants compared with coal or nuclear.

1. INTRODUCTION

The ARIES project is a multi-institutional effort exploring the potential of tokamaks as an attractive and competitive commercial power reactors Three visions of the tokamak are being considered with varying degrees of extrapolation in plasma physics and technology. The ARIES-I design assumes minimum extrapolation in physics and advanced extrapolation in engineering [1]. A summary of the ARIES-I fusion power core (FPC) is reported in Reference [2].

The ARIES-I design features a low activation ceramic composite as the structural material for the FPC. Ceramics have many desirable characteristics when compared to metals. One of the most attractive characteristics of ceramics is their high-strength at high temperatures. Typical operating temperatures of non-refractory metals do not exceed 600°C, while ceramics can potentially be operated between 1000 and 1500°C. Because of the very low level of neutron induced radioactivity, ceramics have been considered for structural materials for fusion reactors in the past [3]. However, despite advantages of ceramics over metals, the brittle fracture response of bulk ceramic materials causes the fracture tensile strength of monolithic ceramics to have wide statistical distributions making the failure points unpredictable. Furthermore, failure of monolithic ceramic materials is generally catastrophic, i.e., cracks propagate rapidly through the entire stressed region. To alleviate these two concerns, worldwide R & D programs [4] have been intensified using two different approaches: (1) development of high-performance monolithic ceramics; and (2) development of reinforced ceramic composites.

Properties of high-performance ceramics are enhanced by improving ceramic manufacturing processes aimed at reducing fabrication-induced flaws, minimizing volume changes during manufacturing, developing near-net shape processing techniques, improving sintering aids, and developing transformation-toughened and particle-toughened ceramics [5]. However, generally high-performance ceramics are limited to small component sizes.

The second approach to develop ceramic materials with predictable performance characteristics is through the use of fibers dispersed in the ceramic matrix. High strength can be achieved by transferring the load from the matrix to the fibers, taking advantage of the superior tensile strength of the fibers. Fracture-toughness values for ceramic matrix composites (CMC) are very high because energy is absorbed as fibers are pulled out of the matrix causing crack deflection, crack arrest, or crack blunting. Figure 1 compares the typical stress-strain curves for monolithic silicon carbide (SiC) and unidirectionally reinforced SiC composite materials. The SiC composite material referred to in this work consists of SiC-matrix material reinforced with SiC-fibers. The fracture toughness of a material is directly proportional to the area under the stress-strain curve (Fig. 1) and represents the energy required to fracture a material. Figure 1 clearly shows the large improvement in the fracture toughness of composites over monolithic SiC. The strain tolerances of SiC composite materials greatly exceed those of monolithic ceramics. Strain values above 2.5% are routinely measured for such composites [6], whereas monolithic SiC exhibits a strain values of less than 0.1% at initiation of fracture (Fig. 1).

The higher strain tolerance and larger fracture toughness of CMCs reduce the probability of catastrophic failure. The SiC composite material continues to carry a significant amount of the load after the ultimate stress is reached, while monolithic

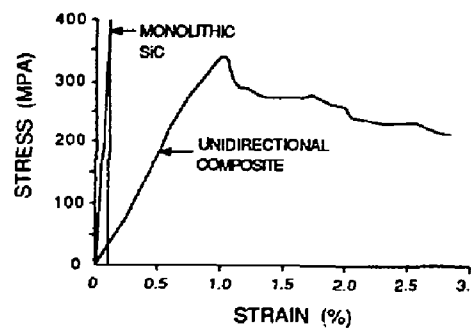

Figure 1. Stress-strain curve of unidirectional SiC-fiber-reinforced SiC composite [6].

ceramics fail catastrophically at their ultimate stress loads. Based on the significant advances in CMC materials achieved during the infancy phase of the industry, it is not premature to extrapolate from todays laboratory-scale material sample properties to large-scale CMC components.

† This work is supported by the U.S. Department of Energy.

The following section summarizes SiC composite properties. In section 3 micromechanical equations are used to estimate the design window of maximum allowable design stresses for SiC composite components. Section 3 also lists preliminary thermal stress results of the ARIES-I first wall using the ANSYS finite element analysis code [7]. In conclusion, major findings are summarized.

II. SiC COMPOSITE PROPERTIES

The most effective method used to improve the properties of ceramic material is through fiber reinforcement. For high temperature applications ceramic fibers are preferred over metallic fibers. Metallic fibers impose lower operating temperature because of the chemical interaction rates between metals and ceramics at elevated temperatures. Among the many methods for SiC composite fabrication, chemical-vapor infiltration (CVI) is most widely used, where a fibrous SiC preform is infiltrated with silane gases in a furnace. Silicon carbide is deposited from the decomposition of methyltrichlorosilane (CH_3SiCl_3) gas at temperatures less than 1200°C. Typical infiltration times of the order of weeks were necessary to produce millimeter thick SiC composite materials. Recently, however, new processes have been developed by the Oak Ridge National Laboratory that reduce infiltration times from weeks to about 24 hours [6]. Chemical-vapor infiltrated SiC composites typically have a porosity in the range of 10 to 15 %. Efforts are underway aimed at reducing the porosity.

Mechanical and physical properties of two commercially available SiC fibers are listed in Table 1.

Table 1: PROPERTIES OF SiC FIBERS [8]

Property	PCS-SiC*	CVD-SiC†
Diameter (μm)	9 -15	100 - 140
Length	Endless	Endless
Tensile Strength (GPa)	1.9 - 3.0	2.5 - 3.7
Young's Modulus (GPa)	180 - 200	380 - 420
Density (g/cm^3)	2.55 - 2.58	3.4 - 3.5
Thermal Expansion Coefficient (10^{-6}/K)	3.1	4.2 - 4.5

* PCS=polycarbosilane-derived fibers;

† CVD=chemical vapor deposited fibers

The strength of the SiC fibers is usually degraded during weaving or braiding processes and the effects of length. This degradation is caused by an increase in surface flaws on the fibers and also by fiber breakage during preform fabrications. To account for this effect, the Weibull distribution of tensile strength of SiC yarns is used. Yarns or tows contain between 500 to 1000 monofilament fibers. The strength of SiC yarns is about 2 to 4 times less than that of individual fibers. The average tensile strength of SiC yarn made from PCS-SiC (NICALON) was measured to be 1388 MPa and 1063 MPa for 5 and 25 cm gage length, respectively, while individual SiC fibers have average strengths of above 2400 MPa [9]. Using yarn properties instead of the superior fiber properties, a tensile strength of 750 MPa could result. This value was taken for a near-zero probability of failure data accumulated by Fang after testing over 2000 samples [9].

The effects of the length of the fibers were investigated by Fukada [10]. A conservative correction coefficient has been formulated to account for a fraction of fibers which would break during manufacturing of the composite material. Assuming 1 out of about every 7 fibers (17 %) to break during fabrication, a numerical value of 0.5 is estimated for the correction factor of the tensile strength of SiC fibers. This factor reduces the effective strength of the SiC fibers to a highly conservative value of 375 MPa.

The superior, high-temperature strength of SiC fibers is well documented. In particular, the effects of various environments were studied [11]. SiC fibers in vacuum retain their full strength up to about 1200°C. Strength degradation is measured when the fibers are heated in air and is caused by surface-oxidation processes. Therefore, care must be taken during the manufacturing of SiC composites to minimize the amount of trapped oxygen before the CVI process begins.

The effects of neutron irradiation on PCS-SiC fibers were investigated in Japan as part of a new national R&D program aimed at developing SiC composite materials [12]. Both 14 MeV neutrons form the RTNS-II facility in the U.S. and fission reactor neutrons were used [13]. Samples were irradiated to fluences of 5×10^{20} n/m^2 (14 MeV) and 1×10^{25} n/m^2 (fission spectrum). No significant change in the average tensile strength (2.7 MPa) and the average flexural strength (1.3 GPa) was measured for irradiation up to about 1×10^{24} of fast neutrons. At 1×10^{25} n/m^2, the tensile strength rises to about 3.2 GPa and the flexural strength increases to about 1.5 GPa. However, the average Young's Modulus rises steadily from an unirradiated-fiber value of 160 GPa to about 215 GPa at 1×10^{25} n/m^2 with a corresponding drop in elongation from 1.8 % to 1.6 %. These preliminary results show that SiC fibers have excellent stability under neutron irradiation. Therefore, in estimating SiC fiber properties for the ARIES-I design, neutron irradiation effects are neglected until a more extensive data base becomes available.

The lack of data on the thermo-mechanical properties of SiC composites necessitates the use of the micromechanical design equations [14]. Such design equations are used to estimate the longitudinal and transverse properties based on the composite constituent properties. For fusion applications neutron irradiation effects on SiC fiber and SiC matrix properties have to be incorporated. For the SiC matrix material, the truncated and irradiated Weibull distribution function for the tensile strength of CVD SiC with a near-zero probability of failure was used [15]. Samples of CVD SiC were first proof-tested and consequently irradiated up to 10^{26} n/m^2 with fast neutrons (E_n >0.1 MeV). Some samples showed close to 700 MPa flexural strength with a high failure probability, however, an average flexural strength of about 435 MPa was shown to have a near 100% survival probability. Assuming that the tensile strength of ceramics is about 0.75 of the flexural strength, 350 MPa was taken as the tensile strength of the CVD matrix material. The effect of temperature on the strength of SiC bulk material depends on the manufacturing process and environment. Up to 1300°C, silicon-based carbides and nitrides show insignificant levels of loss of strength [16]. Thus, 350 MPa is taken as a conservative estimate for the high temperature (1000°C) tensile strength of irradiated CVD SiC matrix materials.

In summary, the conservatively estimated silicon carbide fiber strength value of 375 MPa reflects the degradation effects of weaving a fibrous SiC preform, fiber breakage during manufacturing, and the high-temperature (1000°C) operation capability in an intense neutron-irradiation environment while a 350 MPa is a conservative estimate for the high temperature strength of SiC bulk matrix material.

III. COMPOSITE DESIGN STRESS LIMITS

To estimate the tensile strength of the SiC composite, *the rule of mixtures* is used to formulate micromechanical design equations. For example, the CMC tensile strength in the direction parallel to the fiber orientation (longitudinal) is estimated as:

$$\sigma_c = V_f \sigma_{uf} f(b) + V_m \sigma_{um} f(v)$$

where: σ_c is the failure strength of the composite, σ_{uf} is the tensile strength of fibers, σ_{um} is the tensile strength of matrix, V_f is the volume fraction of fibers, V_m is the volume fraction of matrix, $f(b)$ is the coefficient that accounts for fiber breakage (0.5), and $f(v)$ is the matrix void fraction.

Figure 2 shows the estimated longitudinal strengths of the SiC composite as a function of fiber volume fraction with various matrix void fractions. By defining 2/3 of the composite *tensile strength as the maximum design stress limit*, SiC composites with a 10% porosity and a fiber volume fraction of 0.6 would have an allowable design stress limit window between 180 and 200 MPa at 1000°C. Future experience with CMCs and better understanding of the failure modes of CMCs will eventually produce firm guidelines for determining allowable design stresses instead of using 2/3 of the ultimate tensile strength.

To estimate other longitudinal and transverse properties such as Young's Modulus, compressive strengths, shear strength, Poisson's ratio, and thermal conductivity, the CLASS code [17] is used. Properties are calculated based on the rule of mixtures. For a SiC composite material with a 0.6 fiber volume fraction and a fiber orientation pattern of 0°/45°/90°/-45° the following properties are determined (x-longitudinal, y-transverse):

Elastic Modulus:	E_{xx} = 364 GPa E_{yy} = 357 GPa
Shear Modulus:	G_{xy} = 160 GPa
Poisson's Ratio:	ν_x = 0.17 ν_y = 0.157
Thermal Conductivity:	k_{xx} = 22.5 W/mK k_{yy} = 19.6 W/mK
Expansion Coefficient:	$\alpha_x = 3.751 \times 10^{-6}$/K $\alpha_y = 3.779 \times 10^{-6}$/K

The first wall of the ARIES-I tokamak reactor consists of SiC composite oval tubes with inner diameter of 1 × 2.3 cm. The plasma facing side of the tubes is 3 mm thick to allow a 2 mm erosion layer while the blanket facing side is 1 mm thick. The average heat load on the first wall is 0.48 MW/m^3 with a maximum of 0.85 MW/m^3 at the midplane. Volumetric heating loads are 23 MW/m^3 average with a maximum of 33 MW/m^3 at the first wall midplane. The coolant pressure is 5 MPa with a heat-transfer coefficient of 2500 W/m^{2}K inside the first wall tubes. The first-wall coolant inlet temperature is 350 °C and the outlet temperature is 510 °C. Preliminary normal operating thermal and pressure stress analysis using the ANSYS code shows that the maximum stress in the ARIES-I first wall SiC structure are less than 100 MPa (tensile), with a maximum wall temperature of 849°C occurring at the midplane

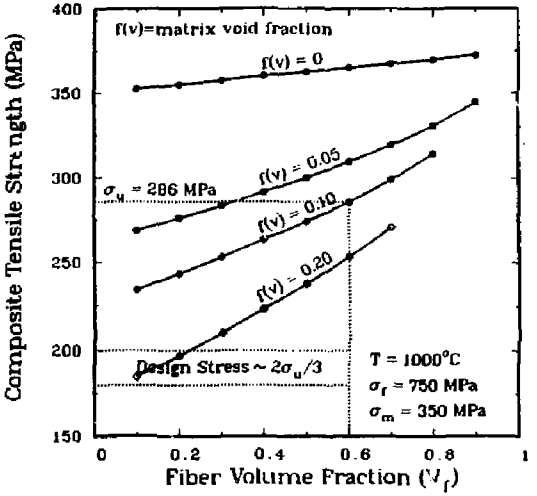

Figure 2. Longitudinal SiC-composite tensile strength estimated from micromechanical design equations (σ_f is the SiC fiber tensile strength; σ_m is the SiC matrix tensile strength).

of the first wall. A more detailed thermal and pressure stress modeling effort is currently underway to include the effects of the overall first wall and blanket structure on the behavior of the SiC composite.

IV. SUMMARY

The advantages of ceramics over metallic alloys for fusion applications have been well know for some time, however, *the brittle failure mode and the unpredictability of failure* of ceramics kept this material from being a viable choice for fusion reactors. Because of recent advances in developing high-performance ceramic materials for heat engines, these materials can be reconsidered for future fusion reactor applications. In particular the development of SiC fiber reinforced SiC matrix composites has shown great improvements in failure mode behavior, strain tolerances, and fracture toughness.

Micromechanic design equations were used to estimate material properties for typical SiC composite materials. These calculations reflect the degradation of fiber and matrix material properties in anticipation of imperfect manufacturing techniques. Furthermore, the effect of neutron irradiation on the SiC fibers and the SiC matrix material were reviewed and incorporated in estimating the composite strength. A maximum allowable design stress for a irradiated SiC composite material containing a 0.6 fiber volume fraction and 10% porosity, operating at 1000°C was estimated using conservative matrix and fiber properties to be around 180 MPa. Preliminary thermal and pressure stress calculations using the ANSYS code indicate that maximum stresses are well below the estimated design stress limit. In conclusion, recent improvements in ceramic composite material properties has made SiC composites a viable material choice for future fusion reactors.

REFERENCES

[1] F. Najmabadi, *et al.*, "The ARIES-I Tokamak Reactor Study," these proceedings.

[2] C.P.C. Wong, *et al.*, "Blanket Design for the ARIES-I Tokamak Reactor," these proceedings.

[3] Hopkins, G. R. and Price, R. J., "Fusion Reactor Design with Ceramics" Nuclear Engineering and Design/Fusion 2(1985)111-143

[4] Cassidy, D. J. and McLean, A. F., "Advances and Trends in Processing Complex Ceramic Components for Heat Engines", High Tech. Ceramics, edited by P. Vincenzini, Elsevier Science Publishers B. V., Amsterdam, 1987, pp. 2503-2517. Cassidy, *et al.*, 1987, HITEMP)

[5] Kamo, R., "Ceramics for Advanced Heat Engines", High Tech. Ceramics, edited by P. Vincenzini, Elsevier Science Publishers B. V., Amsterdam, 1987, pp 2473-2487.

[6] Stinton, D., Caputo, A. J. and Lowden, R. A., "Synthesis of Fiber- Reinforced SiC Composites by Chemical Vapor Infiltration", Am. Ceram. Bull., 65 [2] 347-350 (1986).

[7] Desalvo, G. J., and Swanson, J. A. ANSYS-Engineering Analysis System, version 4.1. Swanson Analysis Systems Inc., Houston, Pennsylvania, 15342.

[8] Fitzer, E. and Gadow, R. Fiber-Reinforced Silicon Carbide. Am. Ceram. Bull., 65 [2] 326-335 (1986).

[9] Fang, P., Ko, C., and Koczak, M., "Stress-Strain-Time Relationship of SiC Yarns", Proceedings of the International Symposium on Composite Materials and Structures, Bejing, China, June 10-13, 1986.

[10] Fukada, H., *et al.*, "Probabilistic Approach on the Strength of Fibrous Composites", in Composite Materials, eds., K. Kawata and T. Akasaka, Japan-U.S. Conference, Tokyo, Japan, 1981.

[11] Fukunaga, H. and Goda. K., "The Tensile Characteristics of Coreless and Carbon-Core Silicon Carbide Fibers Exposes to Some Environments", Proceedings of the International Symposium on Composite Materials and Structures, Bejing, China, June 10-13, 1986.

[12] Hayashi, T., Proceedings of the 5th International Conference on Composite Materials, TMS-AIME, (1985)1641-1656

[13] Okamura, K., Matsuzawa ,T. Sato, M., Higashiguchi, Y, and Morozumi, S., "Effects of Neutron Irradiation on SiC Fiber", J. Nucl. Mater. 133&134 (1985) 705-708.

[14] Chamis, C. C., "Simplified Composite Micromechanics Equations for Mechanical, Thermal, and Moisture-Related Properties", in Engineer's Guide to Composite Materials, American Society for Metals, 1987, pp. 3-8 to 3-24.

[15] Price, R. J. and Hopkins, G. R., "Flexural Strength of Proof-Tested and Neutron Irradiated Silicon Carbide", J. Nucl. Mater. 108&109(1982)732.

[16] Davidge, R. W., "Mechanical Properties and Engineering Design with Ceramics", Ceramics in Advanced Energy Technologies. Editors H. Krockel, M. Merz, O. Van Der Biest. D. Reidel Publishing Company, Boston, 1984.

[17] Kibler, J., CLASS, Composite Laminate Analysis Systems, Release 3.5, 1987. Materials Sciences Corporation. ASM International, Metals Park, Ohio 44073.

NEUTRONICS STUDIES FOR THE ARIES-I REACTOR

E.T. Cheng and the ARIES Team
General Atomics, P.O. Box 85608
San Diego, California 92138-5608

Abstract: A high-performance helium-cooled, solid breeder fusion blanket was designed for the innovative ARIES-I reactor. The Li_4SiO_4 breeder material is placed behind a beryllium zone to maximize the beryllium neutron multiplication. A modest beryllium inventory of about 40 metric tons is needed to achieve a blanket energy multiplication of 1.35 or more, while breeding adequate tritium in the blanket. The decay heat values and radiological hazard potentials of ARIES-I blanket and shield (SiC + B_4C) materials are found to be at least two to three orders of magnitude lower than those from metallic alloys such as ferritic steel and vanadium alloy. Inherent safety will be achieved for the ARIES-I blanket because the minimum radioactive inventory precludes meltdown of the first wall and structural SiC material. However, the safety design of the divertor which uses tungsten alloy particle-collector plates and vanadium alloy structure will need to be carefully done because of higher levels of afterheat. All ARIES-I components will qualify for disposal as 10 CFR 61 Class C waste if averaging over the first wall and blanket component is allowed, and if some exotic impurity elements (Ag, Nb, Mo) are controlled below 1 ppm.

Introduction

ARIES-I is a DT-burning, 1000 MW(e) (net) tokamak reactor design based on advanced technology and modest extrapolation from the present physics data base [1,2]. A comparative neutronics study of blanket concepts was performed for the ARIES-I reactor. Three blanket concepts were selected for further study after a preliminary investigation of many possible blanket concepts: (1) a FLiBe molten salt-cooled, low pressure blanket concept with vanadium alloy structure; (2) a high pressure, helium-cooled ceramic composite structured blanket concept; and (3) a gas-carried particulate-cooled, low pressure, ceramic composite-structured blanket concept. The tritium breeders considered in the gas-cooled systems include Li_2O, $LiAlO_2$, Li_4SiO_4, and Li_2C_2. Neutron-multiplier materials Be and BeO were also employed in this comparison.

SiC composite material was selected as the structural material for ARIES-I blanket and shield due to its low activation features. Beryllium metal was determined to be the neutron multiplier because of the high (n, 2n) performance capability. Li_4SiO_4 was chosen as the breeder material for a number of reasons, including favorable thermophysical properties, good tritium recovery, and low activation. Finally, the high-pressure, helium-cooling blanket concept was selected for the ARIES-I design rather than the low-pressure, gas-carried particulate-cooled blanket concept because of its relatively known operation database.

Low Activation Motivations [3,4,5]

The 14 MeV neutrons produced as a result of deuterium-tritium fusion reactions in the ARIES-I reactor provide the major source of nuclear energy for conversion into thermal heat in the blanket component. However, these neutrons are also capable of producing radioactive materials when reacting with first wall and blanket materials. These radioactive materials will raise concerns over safety and environmental issues during the operation of fusion reactors. Nevertheless, the level of activation and specific radioactive isotopes in the first wall and blanket depend entirely on selected component materials that may cause the activation level to differ by many orders of magnitude. The goals of the ARIES-I reactor design study are to maximize the possibility of designing an inherently safe reactor and to minimize its environmental impacts.

The safety and environmental concerns due to radioactivity and the considerations specifically embodied in the ARIES-I design are discussed below.

1. Safety. Safety is the most important concern regarding the development of a reactor concept. It is generally related to the radioactive inventories and the potential for release of these radioactive inventories. The design approaches of the ARIES-I blanket are to minimize the production of radiologically hazardous materials, and to minimize the decay heat that is the main energy source to heat up the first wall and blanket components above their melting temperatures during accidents.
2. Maintenance and Decommissioning. During normal operation and under accident conditions, the radiation exposure of working personnel is of major concern as far as the selection of an energy source is considered. The minimization of radioactive inventory in the ARIES-I design will help achieving the goal of "as low as reasonably achievable" exposure for maintenance and decommissioning.
3. Nuclear Waste Disposal and Reuse of Materials. Shallow-land burial (10 CFR 61 Class C) waste disposal or better is a desirable method of handling nuclear waste for fusion reactors. In some cases, the recycling of resource-limited materials should also be made possible. These goals could be achieved only if the long-lived radioactive inventory is minimized.

By comparing the candidate structural, neutron multiplying and tritium breeding materials, we found that a combination of SiC, Be, and Li_4SiO_4 form a set of radioactively benign materials to achieve the low activation goals of the ARIES-I reactor design [6,7].

ARIES-I Blanket Concept and Performance

High blanket nuclear performance is one of the design requirements for the ARIES-I reactor. The major approach in meeting this design requirement is to employ beryllium, the only low activation neutron multiplying material, as the blanket material. Lead is the other possible non-fissionable neutron multiplier. However, the radiological hazard potential for lead in a fusion reactor is at least four orders of magnitude higher than SiC, and is nine orders of magnitude higher than beryllium. In the conceptual design of the ARIES-I blanket, we are also motivated to minimize the beryllium inventory due to resource limitation concerns [8].

The best approach to effectively utilize the beryllium neutron multiplication is to install the beryllium component immediately behind the first wall and to maximize the beryllium fraction in this zone. To enhance the nuclear energy multiplication in the ARIES-I blanket, we also allow the excess neutrons to be absorbed in silicon (Q = 8.5 MeV) which appears in the beryllium zone as the constituent element in the structural material, SiC. Tritium breeder materials are placed behind the beryllium neutron multiplying zone primarily due to concerns

Table 1
Helium-Cooled Beryllium-Multiplying SiC-Composite Blanket
(ARIES-I Blanket Concept)

Zone	Thickness (cm)	Compositions
First Wall	1.8	48.7% SiC + 51.3% He or Void
Beryllium multiplying Zone 1	5	26.4% SiC + 42.6% Be[a] + 31% He or Void
Beryllium multiplying Zone 2	5	21.1% SiC + 50.9% Be + 28% He or Void
Beryllium multiplying Zone 3	15	19.2% SiC + 53.6% Be + 27.2% He or Void
Tritium breeding zone	20	19.2% SiC + 53.6% breeder[a,b] + 27.2% He or Void
Reflector	33	95% SiC + 5% He
Shield	100[c]	SiC + B_4C + 5% He

[a] 90% dense.
[b] Li_4SiO_4 or Li_4SiO_4 and beryllium mixture.
[c] 50 cm is adequate to protect the S/C magnet; 100 cm is needed to provide hands-on access near the S/C magnet.

of tritium over-breeding and high lithium-6 burnup that would cause design difficulties if the breeder materials were allowed to exist in the beryllium zone. Table 1 shows the zoning and material compositions of such a design. The nuclear performance and characteristics of the ARIES-I blanket are displayed in Figs. 1 and 2, and tabulated in Table 2.

Figure 1 shows the relationship between blanket energy multiplication (M) and tritium breeding ratio (TBR) as a function of beryllium zone thickness. Two breeder materials are used in these calculations: a pure Li_4SiO_4 ceramic compound and a mixture of 80% Li_4SiO_4 and 20% beryllium by volume. Natural lithium with 7.4% Li-6 is employed for both breeder materials. As shown in Fig. 1, M and TBR are 1.05 and 0.82 (100% Li_4SiO_4 case), respectively, when no beryllium zone is introduced. They

Table 2
Neutronic Performance of the ARIES-I Blanket

Tritium Breeding (T/D-T Neutron)		
Li-6 (n,α) T	1.0916	
Li-7 $(n,n\alpha)$ T	0.0250	
Be (n,T)	0.0128	
Tritium breeding ratio	1.129	
Neutron Multiplication (Reactions/D-T Neutrons)		
Be $(n,2n)$	0.833	
Nuclear Heating (MeV/D-T Neutron)		
First wall	1.041	(5.4%)[a]
Beryllium zone	9.651	(50.2%)
Breeder zone	7.551	(39.3%)
Reflector	0.986	(5.1%)
Total blanket heating	19.23	(M = 1.36)[b]
Nuclear energy leakage	0.455	

[a] Fraction of blanket nuclear heating.
[b] Blanket energy multiplication, M.

will increase when a beryllium zone is employed and reach the peak of 1.2 for TBR when the beryllium zone is 15 cm thick. The blanket energy multiplication increases to 1.3 at this beryllium thickness and keeps increasing when the beryllium zone continues to thicken. However, the TBR drops when the beryllium zone thickness exceeds 15 cm. This is because SiC structure in the beryllium zone continues to absorb neutrons such that fewer neutrons will leak into the breeder zone and be absorbed by Li-6 to generate tritium. From Fig. 1, it appears that the optimum beryllium zone thickness is about 25 cm for obtaining a TBR of 1.1. Figure 1 also shows the corresponding Be $(n,2n)$ reaction rate which clearly indicates that the neutron multiplication from beryllium begins to saturate when the beryllium zone thickness exceeds 25 cm.

Table 2 displays the neutronic performance of the ARIES-I blanket at 25 cm beryllium zone thickness. As shown in Table 2, the tritium breeding ratio from the 1-D full coverage blanket model is 1.13 tritons per D-T neutron. With blanket

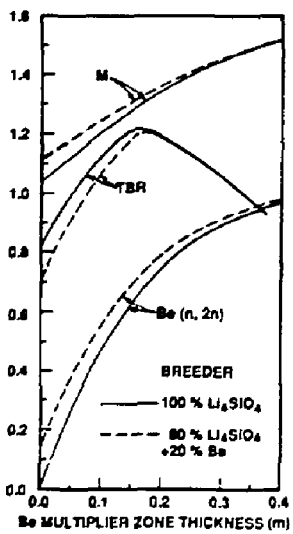

Fig. 1. Blanket energy multiplication (M), tritium breeding ratio (TBR), and Be $(n,2n)$ reaction rate as a function of beryllium zone thickness.

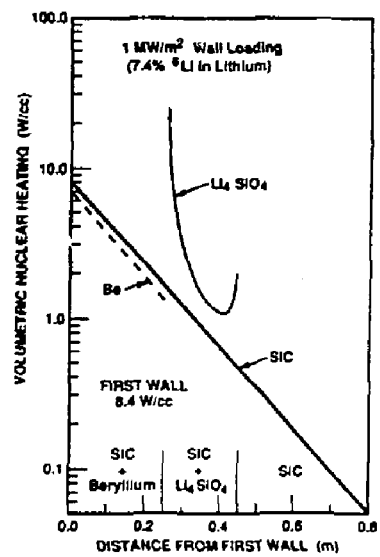

Fig. 2. Volumetric nuclear heating in ARIES-I blanket components normalized to 1 MW/m² neutron wall loading

material also located behind the divertor components, a multi-dimensional calculation shows that the overall tritium breeding ratio will be about 1.10, adequate to tolerate other losses in tritium breeding due to vacuum ducts, current drive waveguide windows, etc. The blanket energy multiplication is 1.35 (19.23 MeV/D-T neutron), as also shown in Table 2. About 50% of the blanket nuclear heating is deposited in the beryllium zone which helps greatly in lowering the temperature of the tritium breeder materials [2]. Note that 0.5 m of SiC + B_4C shield is adequate to protect the superconducting magnet where the lifetime (150 MW-y/m^2) limitation is the fast neutron fluence of 1×10^{19} n/cm^2 at the superconductor [9]. However, a 1-m shield will be needed to limit the neutron flux level at the support structure and magnet component such that the shutdown biological dose rate near those components (behind the shield) will not hinder the possibility of hands-on maintenance.

Figure 2 depicts the volumetric nuclear heating distribution in the blanket components of the ARIES-I blanket, normalized to 1 MW/m^2 neutron wall loading. It shows in Fig. 2 that the volumetric nuclear heating rates in beryllium and SiC have the same slope. They are about 7 and 8 W/cc, respectively, immediately behind the first wall. They drop to 1.3 and 1.8 W/cc, respectively, at the rear of the beryllium zone, as shown in Fig. 2. The volumetric nuclear heating rate in the Li_4SiO_4 breeder is significant, about 30 W/cc at 1 MW/m^2, at the interface between beryllium and tritium breeder zones. It then decreases substantially as the location moves into the breeder zone, and reaches about 1.2 W/cc at 15 cm from the beryllium zone. These are shown in Fig. 2 for the beginning of irradiation when the blanket is fresh. Significant Li-6 burnup occurs at the high nuclear heating location of the breeder material since the Li-6 consumption rate dominates the nuclear heating in the breeder material. Li-6 burnup will significantly affect the location of the peak nuclear heating in the breeder zone, which is an important consideration in the thermal design of the ARIES-I blanket. This will be discussed further in the next section.

Burnup Considerations

Beryllium and Li-6 are the most important isotopes in the ARIES-I blanket. The burnup and consumption rates of these two isotopes need to be explored.

Beryllium. The Be $(n,2n)$ reaction rate is about 0.833 reactions per D-T neutron. The annual consumption rate of beryllium in ARIES-I is about 380 kg assuming a fusion power of 2500 MW. The beryllium inventory in ARIES-I blanket is estimated to be about 40 metric tons. The overall burnup rate is about 1% per year. The maximum local burnup rate occurs at the location immediately behind the first wall, and results in the generation of helium at 72,400 ppm concentration when the blanket reaches the lifetime exposure of 20 MW-y/m^2. The helium concentration will cause significant swelling of the beryllium components that will need to be assessed and handled in the design.

Lithium-6. Li-6 burnup rate is significantly high at the front face of the breeder zone as described previously. At the beginning of blanket life, the maximum burnup rate is as high as 30% per year at 1 MW/m^2. Lithium-6 will be depleted at locations of high consumption rate during reactor operations. The peak consumption (heating) location will move from the interface between beryllium and breeder zones into the breeder interior region. At the end of blanket life, the peaking location is found to be at 8 cm from the interface. The variation of peak nuclear heating locations must be considered in the blanket thermal design. Figure 3 depicts the nuclear heating distribution in the breeder zone at several exposure stages: 0 (beginning of blanket life), 2, 4, 8, 16, and 20 (end of blanket life) MW-y/m^2.

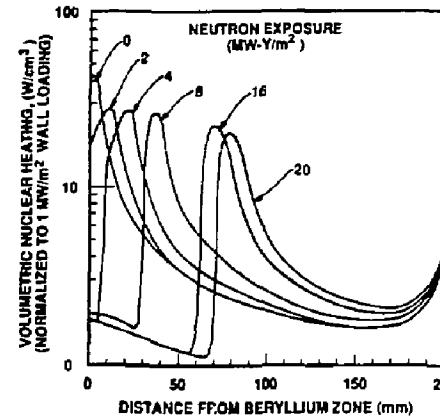

Fig. 3. Variation of volumetric nuclear heating rate distribution in Li_4SiO_4 breeder material at several blanket operation stages: 0 (beginning of blanket life), 2, 4, 8, 16, and 20 (end of blanket life) MW-y/m^2 neutron exposures at first wall.

Tritium breeding in the ARIES-I blanket will decrease as the effective breeder zone thickness is reduced during blanket exposures. This is already demonstrated in Fig. 1. The reduction of tritium breeding ratio at the end of 20 MW-y/m^2 exposure is about 15% when naturally enriched Li_4SiO_4 is employed. The increase of blanket energy multiplication, however, is modest, only about 2%. Lithium-6 enrichment in Li_4SiO_4 will reduce the burnup rate of Li-6 and hence inhibit the reduction rate of the effective breeder zone thickness. Less variation in tritium breeding ratio and a more stable nuclear heating performance can be expected when enriched Li_4SiO_4 is used.

Activation Considerations

The characteristics of radiological impacts due to the selection of blanket and reactor component materials are analyzed and discussed in this section. Selection of SiC, beryllium, Li_4SiO_4, and B_4C as first wall, blanket, and shield materials provides the optimum safety and environmental advantages of fusion. The integrated decay energy induced from these low activation materials is two to three orders of magnitude lower than that induced from vanadium alloy and ferritic steel structural materials. The maximum adiabatic temperature increase for the activated material is the integrated decay energy divided by the material's specific heat. It is a conservative measure of heatup during a loss of cooling accident. The maximum adiabatic temperature increase occurs at the SiC-composite first wall in ARIES-I. It is about 750 and 1120 K at 1 day and 10 days after shutdown, respectively. The SiC first wall will never reach the melting point even with an operating temperature of 1300 K. The shutdown biological dose rate from the ARIES-I blanket and shield is about three to four orders of magnitude lower than that from a metallic alloy structured blanket and shield.

The significance of accidental radiological hazard potential of activated materials was recently defined and quantified in a systematic manner [5]. The radiological hazard potential (defined as latent dose index, LDI) is quantified as the number of potential cancer deaths due to the latent dose effect when the activated material is assumed released during a reactor accident. Table 3 compares these hazards due to SiC, ferritic steel and vanadium alloy as first wall materials. The significance of a low activation fusion reactor is clearly seen in Table 3, since the accidental radiological hazard potential for SiC is several orders of magnitude lower than vanadium alloy and ferritic steel. It can

be further reduced to minimum because no meltdown will occur in the ARIES-I first wall and blanket and thus the hazard cannot be dispersed. The radiological hazard potentials from 17Li83Pb and lithium coolant, and tungsten (divertor material), are also shown and compared in Table 3.

Table 3
Comparison of Accidental Radiological Hazards in ARIES-I and BCSS First Wall and Blanket Components
(First Wall: 500 m^2 surface area, 5 mm thick; 108 m^3 Coolant Volume)

	LDI/cm^3	Max. LDI
SiC (ARIES-I/first wall)	4.2×10^{-4}	No meltdown[a]
W (ARIES-I/divertor)[b]	0.12	60,000
HT9 (BCSS/first wall)	0.91	2,275,000
V15Cr5Ti (BCSS/first wall)	0.021	52,500
17Li83Pb (BCSS/blanket)	0.40	72,000,000
Lithium (BCSS/blanket)[c]	1×10^{-5}	1,800

[a] The maximum LDI is 2,100 if 100% SiC first wall (1 cm) is released.
[b] Divertor plates occupy 20% of ARIES-I first wall surface area. Tungsten layer is assumed to be 5 mm thick.
[c] Due to impurity elements: Na, Ca, and K.

As far as waste disposal is concerned, the ARIES-I blanket will qualify as 10 CFR 61 Class C (shallow-land burial) waste since the maximum waste disposal rating for SiC at first wall is 0.5 after 20 MW-y/m^2 exposure. Of course, this is also subject to the control of some exotic impurity elements such as Ag, Nb, and Mo, below 1 ppm levels [10].

Use of tungsten/vanadium-alloy divertor collector plates in the divertor component of the ARIES-I reactor is a major concern from safety and maintenance viewpoints. The integrated decay energy from tungsten is about two orders of magnitude higher than that from SiC within one day after shutdown. The safety design of the divertor collector plates must be carefully performed since the radiological hazard potential for the divertor collector plates is about the same as for vanadium-alloy as shown in Table 3 and meltdown is possible.

Summary and Conclusions

In summary, the ARIES-I reactor is designed to employ a high performance blanket using Li_4SiO_4 breeder and beryllium multiplier, with a blanket energy multiplication of 1.35 or more. It possesses the advantage of low activation features by using SiC structure. The tritium breeding zone is located behind the beryllium zone to maximize the neutron multiplication in beryllium while still breeding adequate tritium. Such a blanket material management approach will result in the optimum utilization of beryllium in a fusion blanket. The annual beryllium consumption rate is about 380 kg for ARIES-I (2500 MW fusion power) and the needed beryllium inventory is about 40 metric tons.

The decay heat values and radiological hazard potential from SiC, beryllium, and Li_4SiO_4 are at least two to three orders of magnitude lower than that from metallic structural materials, ferritic steel and vanadium. Selection of helium as coolant also eliminates safety concerns that would occur when other coolants such as 17Li83Pb and liquid lithium are used. Because of the minimum radioactive inventory involved in the ARIES-I blanket, inherent safety can be achieved since the integrated decay energy is insufficient to cause the release of radioactivity due to first wall meltdown.

The only safety concern in the ARIES-I reactor from the radiological consideration is probably the divertor collector plates made of high-Z tungsten alloy. Safety design of this divertor component is essential.

The radiation shield is also made of low activation SiC and B_4C materials. The total blanket and shield thickness required to protect the superconducting magnet is 1.3 m; 1.8 m is provided to allow hands-on access behind the shield and near the magnet component.

All ARIES-I reactor components will be disposed of as 10 CFR 61 Class C waste provided that some impurity elements such as Ag, Nb, and Mo, are controlled below 1 ppm.

The lithium-6 burnup rate in the front face of the breeder zone will be significant. The peak nuclear heating will occur in this region and will move into the breeder zone interior with time due to depletion of Li-6. Tritium breeding and blanket energy multiplication will also be affected by the Li-6 depletion phenomenon. Detailed analysis of Li-6 depletion and the dynamic blanket performance during blanket exposure stages need to be fully understood and incorporated in the thermal and mechanical design of the ARIES-I blanket.

This work was sponsored by the U.S. Department of Energy under Contract No. DE-AC03-89ER52153.

References

[1] F. Najmabadi, *et al.*, "The ARIES Tokamak Reactor Study," in Proceedings of this symposium.

[2] C.P.C. Wong, E.T. Cheng, R.L. Creedon, J.A. Leuer, K.R. Schultz, S.P. Grotz, N.M. Ghoniem, M.Z. Hasan, R.C. Martin, F. Najmabadi, S. Sharafat, J.S. Herring, and the ARIES-I Team, "Blanket Design for the ARIES-I Tokamak Reactor," in Proceedings of this symposium.

[3] R. Conn, *et al.*, "Lower Activation Materials ar l Magnetic Fusion Reactors," Nuclear Technology/Fusion 5, (1984) 291.

[4] C. Ponti, "Recycling and Shallow Land Burial as Goals for Fusion Reactor Materials Development," Fusion Technology 13, (1988) 157.

[5] S. Piet, E.T. Cheng, and L. Porter, "Accident Safety Comparison of Elements to Define Low Activation Materials," EGG-FSP-8552, INEL Informal Report, July 1989; also submitted for publication in Fusion Technology.

[6] E.T. Cheng, "Radioactivity Aspects of Fusion Reactors," Fusion Engineering and Design 10, (1989) 231.

[7] E.T. Cheng, *et al.*, "Activation Evaluation of Fusion Solid Breeder Materials," in Proceedings of this symposium.

[8] D.H. Berward and S. Zenczak, "Assessment of Beryllium Resources for Fusion Applications," Fusion Technology 8, (1985) 1143.

[9] M.E. Sawan and P.L. Walstrom, "Superconducting Magnet Radiation Effects in Fusion Reactors," Fusion Technology 10, (1986) 741.

[10] S. Fetter, *et al.*, "Long-Term Radioactivity in Fusion Reactors," Fusion Engineering and Design 6, (1988) 123.

SAFETY IN THE ARIES TOKAMAK DESIGN STUDY

J. Stephen Herring
Fusion Safety Program, Idaho National Engineering Laboratory
Idaho Falls, ID 83415-3523

Clement P.-C. Wong and E. T. Cheng
General Atomics, San Diego, CA 92138-5608

Steven Grotz
University of California at Los Angeles,
Los Angeles, CA 90024-1597

and the ARIES Design Team

ABSTRACT

Safety is one of the primary goals of the ARIES Tokamak Design Study. Public safety goals are the achievement passive safety which is demonstrable in tests that could precede operation and the assurance that releases from accidents be passively limited such that no evacuation plan is necessary. Strategies for safety of the plant investment are factory fabrication, short construction times and a design such that no off-normal operational transient results in damage which could not be repaired in routine maintenance.

ARIES-I, the first of three 'visions' of potential tokamak reactors, will use He at 5 MPa as a blanket coolant and SiC/composite ceramic for the first wall and blanket materials. Both the coolant and the structural material were chosen for their low activation, both in the short term after accidents and for long term waste management. The breeder, Li_4SiO_4 (backup choice: $LiAlO_2$), was also chosen for low activation.

Contemporary plasma physics and aggressive technology are used in ARIES-I, which results in very high toroidal fields (24 T maximum at the coil). The stored TF energy will be about 130 GJ. A central concern is the safe discharge of this stored energy under electrical fault conditions and prevention of a failure in the magnet set from propagating into systems containing radioactive inventories. The TF coil system consists of 16 coils, each containing two separate windings powered by two independent power supplies. Arcs and shorts between the two power supply systems and across individual windings have been modeled. In addition, delay or failure in circuit breaker opening has been modeled. The safety impacts of LOCA, LOFA and disruptive events have also been evaluated.

INTRODUCTION

Safety, to the general public, to the operators and to the investors in a fusion power plant, is of paramount importance. The ARIES Tokamak Design Study has made low radioactive inventories and the avoidance of toxic materials central in the reactor design.

SAFETY GOALS IN THE ARIES DESIGN In order to protect the public from accidents at the reactor, the goal in the design is to achieve Level 1 or 2 safety, as adopted by Piet [1]. A reactor which has Level 1 safety is inherently safe, having an insufficient inventory of radioactive materials and stored energy to release hazardous materials to cause prompt fatalities among the general public. Level 2 is "large-scale passively safe." It requires no large-scale active safety systems to protect the general public as long as the large features of the plant are maintained. A second safety goal is to maintain inventories of radioactive and toxic materials in the plants low enough so that an off-site evacuation plan is unnecessary. A third goal for protecting the public in the long term is that all wastes produced by the plant be disposable as Class C waste in shallow land burial as regulated by 10CFR61.

Investor safety is being enhanced by using factory fabrication and testing whenever possible, by keeping the construction time short and by achieving a level of public safety such that the viability of the utility would not be threatened by any event within the plant.

SUPERCONDUCTING MAGNET TRANSIENTS

The ARIES-I design required very high magnetic fields in order to minimize the size of the machine and therefore minimize the cost of electricity (COE). The characteristics of the toroidal field coils are shown in Table 1.

Table 1. ARIES-I Toroidal Field Coils

Number of Coils	16
Turns per coil	174
Conductor current	126 kA
Max. Field at the conductor	24 T
Stored Energy	130 GJ
Dump Resistors	5 mOhm/winding
Coupling coefficient between adjacent coils	0.90
Internally cooled, conduit conductors	

Each of the coils have been divided into two windings of 87 turns. The schematic for the coils, power supplies, circuit breakers and dump resistors are shown in Figure 1. In the figure, the coil containing the fault and its immediately adjacent coils (and their associated resistors and breakers) are individually modeled, while the remaining thirteen coils have been lumped together into two sets of components. The two sets of windings, powered by independent power supplies and labeled a and b, are connected by resistor RGDab in order to minimize winding-to-winding voltages. The worst case for arc, shorts and winding-to-winding voltages occurs diametrically opposite RGDab.

A variety of magnet transients were simulated using the MSCAP code [2]. Those transients are summarized in Table 2. The turn-to-turn voltages for transient 3 are shown in Figure 2 and the power and deposited energy due to a 10 μOhm short are shown in Figure 3.

The most severe of the transients, in terms of energy deposited energy, are the arcs within one winding. A model of the quench propagation within the winding has been developed and used to account for the partitioning of energy between the arc and the resistive heating of the copper stabilizer. This model assumes that a quench is initiated by over-current in the arcing winding while the rest of the coil set is discharging normally. Quench fronts begin to propagate in both directions along each turn of

*This work is supported by U.S. DOE Contracts DE-AC07-76IDO1570 and DE-AC03-89ER52153

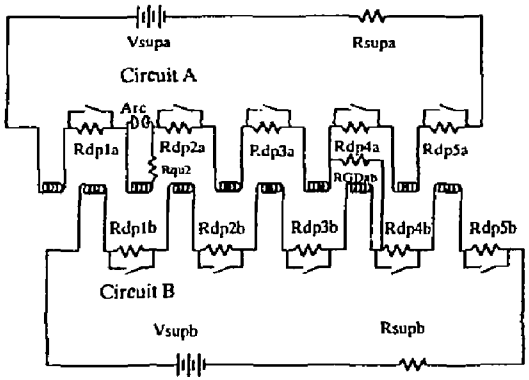

Figure 1. Schematic of ARIES-I Toroidal Magnet Circuit

the conductor from the location of maximum field. The temperature-dependent copper resistivity and specific heat were used to model the heat deposition in the copper stabilizer and thus the energy partitioning between the stabilizer and the arc. Plots of deposited power and energy in the arc and in the stabilizer are shown in Figure 4.

Table 2. Transients considered

1. Routine discharge to establish baseline
2. Turn-to-turn voltages in adjacent windings due to one circuit breaker delaying 10 s in opening
3. Turn-to-turn voltages due to failure of single circuit breaker
4. 10 μOhm short between adjacent windings, with 10 s delay in opening of one breaker.
5. 20 V and 35 V arcs between adjacent windings with 10 s delay in breaker opening
6. 20 V and 35 V arcs between adjacent windings with complete failure of one breaker
7. 20 V and 35 V arcs within one winding, normal breaker operation

ARIES BLANKET DESIGN

The ARIES-I blanket, described in other papers of this session, employs a SiC-composite as the structural material to attain low

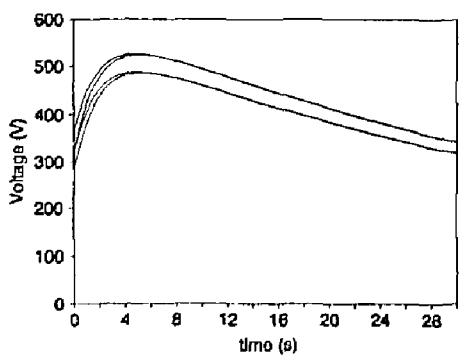

Figure 2. Turn-to-turn voltages due to failure of an circuit breaker.

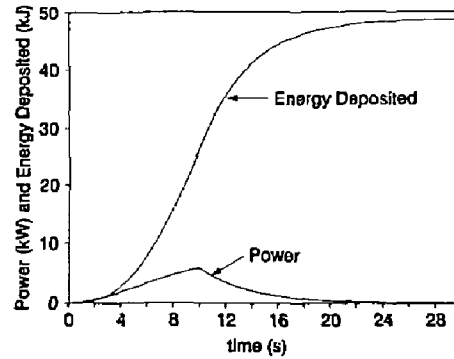

Figure 3. Power and Deposited Energy due to 10 μOhm winding-to-winding short

afterheat, thereby reducing accident concerns, and low activation to reduce concerns for ultimate waste disposal. The breeder

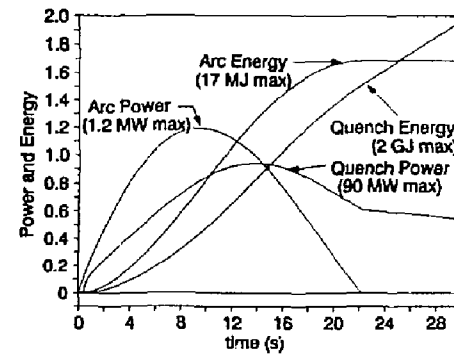

Figure 4. Power and Deposited Energy in Arc and Stabilizer due to Internal Arc in Winding

material is Li_4SiO_4, again for low afterheat and low activation. The first wall and blanket are cooled by helium at 5.0 MPa.

The multiplier is beryllium metal in a sphere-pac form. The sphere-pac form can be fabricated with a minimum of machining and grinding, thereby minimizing the occupational hazards from the inhalation of Be dust. Either the sphere-pac form or a compliant layer is necessary to accommodate swelling in the Be during irradiation due to the formation of He bubbles. A critical question is the point at which the swelling saturates due to the interconnection of gas bubbles, as has been seen in Integral Fast Reactor (IFR) fuel [3,4].

The manufacturing, handling and disposal of Be-metal presents a toxilogical hazard primarily in the formation of fine particles which cause an allergic reaction in the lung. Through well-established procedures in forming operations, occupational hazards can be effectively controlled [5]. The Be used in the multiplier zone of the ARIES-I blanket will be consumed at 38 kg/yr from a total inventory of 34 tonnes. Since Be is a relatively scarce material, the preferred disposal option would be to : (1) allow the (53 d) Be-7 isotope to decay, (2) remove the dissolved tritium through fracturing and heating in a vacuum and (3) refabricate

the Be-metal into either plates or sphere-pac for use in future reactors.

The first wall cooling tubes are woven composites with SiC fibers and a SiC matrix. The first wall surface is overlaid with a SiC coating, deposited by chemical vapor deposition (CVD).

The structure for the blanket and multiplier regions is composed of SiC plate, typically 10 mm thick, joined by silicon braze. Alternatively, the entire FW/blanket module could be woven, avoiding the need for brazing.

Piet, Cheng and Porter [6] assigned release categories to each of the elements based on the minimum boiling temperature of the element or an identifiable oxide. For the elements of interest to the ARIES-I blanket, the boiling temperatures and release classes are shown in Table 3.

Table 3: Release Classification

Element	Boiling Temp. (C) Element	Oxide	Assigned Release Fraction
Li	1342	2327 (Li_2O)	0.30
Be	2970	3900 (BeO)	0.10 (ignites)
C	3367	-192 (CO)	1.00
O	-183	-183 (O_2)	1.00
Si	2355	2230 (SiO_2)	0.01

Note that the compounds used in the ARIES-I blanket have characteristics that should allow a small release fraction to be assigned.

Table 4: Material Damage Temperatures

Compound	Melting Temp. (C)	Boiling Temp. (C)
SiC	2700	(sublimes and decomposes)
Li_4SiO_4	1256	
Be	1278	2970

Since the maximum temperature rise due to afterheat, using the generic adiabatic/radiative model, for any of the elements is 64°C, as shown in Table 5, the use of a low release fraction seems justified. Note that, in the purely adiabatic temperature rise shown in Table 6, the structural material, SiC, is still well below

Table 5. Figures of Merit for Elements Used

Element	TBD	MTR
Li	inf	12
Be	inf	0
C	inf	0
O	inf	0
Si	inf	64

TBD: Time Before Damage
Time before an adiabatic blanket model shows a temperature rise of 300 K

MTR: Maximum Temperature Rise
The maximum first wall temperature rise from complete loss-of-coolant in a simple generic blanket/shield model

a damaging temperature 10 days after the beginning of the accident.

As shown in Table 5 the accident ratings, as developed by Piet, Cheng and Porter [6], for the elements used are quite good. All the materials have an infinite Time Before Damage (TBD) due to afterheat and have a Maximum Temperature Rise (MTR) of 65 K or less.

The decay heating, integrated decay energy and adiabatic temperature rise for SiC, W and V15Cr5Ti as used on the ARIES-I blanket and divertor are shown in Table 6.

Table 6. Comparison of Decay Heating in SiC, V-alloy, and W at the First Wall of the ARIES-I Blanket

Time After Shutdown	600 s	1200 s	3600 s	1 d	10 d
Decay Heating (W/cm^3)					
SiC	0.29	0.095	0.052	0.012	5.5e-4
V15Cr5Ti	0.36	0.30	0.28	0.192	0.0161
W	3.73	3.69	3.69	3.60	3.10
Integrated Decay Heat (J/cm^3)					
SiC	718	810	960	2920	4340
V15Cr5Ti	285	478	1154	2.0e4	6.9e4
W	2540	4760	1.4e4	3.2e5	2.9e6
Adiabatic Temperature Rise (K)					
SiC	185	210	24	755	1120
V15Cr5Ti	78	131	315	5519	1.9e4
W	990	1850	5300	1.2e5	1.1e6

Melting of W/V divertor plates will occur within about 20 minutes at LOCA due to the lower melting temperature of the vanadium alloy

A comparison of the Latent Dose Index of the ARIES-I blanket with other recent blanket designs is shown in Table 7. Note again that this comparison assumes a release of 100 % of the component inventory, without regard to melting temperatures and rates of temperature rise for the compounds and alloys. We believe, that for the materials chosen for ARIES-I, that the temperature rise would be so small that no materials would be released from the blanket.

In addition to concerns about the radiological effects of accidents in a possible ARIES-I reactor, the chemical toxicity of various construction and coolant materials has also been investigated. Both nitrogen dioxide and mercury have been proposed as coolant materials, because of their higher potential operating temperatures and higher electrical conversion efficiencies. While it was felt that a sutiable reactor could be designed to successfully contain those Hg or NO_2 coolant inventories in the event of an accident, it was generally felt that the inclusion of large amounts of toxic materials was contrary to the spirit of the ARIES design.

ECONOMIC BENEFITS IN PASSIVELY SAFE DESIGNS

In reducing the radioactive inventories in the ARIES-I design through the use of SiC, Be and Li_4SiO_4, the reactor can demonstrate that major releases of activated material are not

Table 7. Blanket comparison

Blanket Design	*LDI/cm*^{3}	
SiC (ARIES-I/First Wall)	4.2 e-4	(no melting)
W (ARIES-I/Divertor)	0.12	
HT9 (BCSS/First Wall)	0.91	
V15Cr5Ti (BCSS/First Wall)	0.021	
17Li83Pb (BCSS Blanket)	0.40	
Lithium (BCSS/Blanket) a	1.e-5	

a. Due to impurity elements: Na, Ca, and K

LDI: Latent Dose Index
number of fatal cancers to population within 80 km radius, 50 year dose commitment

possible. Therefore, more of the plant can be constructed from standard industrial-grade components rather than the nuclear-safety-grade required currently. This change will allow major savings in the cost of components. Earlier studies [7,8] had shown cost reductions of up to 25 % due to the avoidance of nuclear-safety-grade equipment.

CONCLUSIONS

Through the selection of low afterheat, low activation materials, the accident and long-term risks in the operation of an ARIES-I reactor have been minimized. This may result in significant cost savings because of the reduced need for nuclear-safety-grade components.

REFERENCES

1. S. J. Piet, "Approaches to Achieving Inherently Safe Fusion Power Plants," Fusion Technology 10 July 1986, pp. 7-30.

2. H. G. Kraus and J. L. Jones, "Hybrid Finite Difference/ Finite Element Solution Method Development for Non-Linear Superconducting Magnet and Electrical Circuit Breakdown Transient Analysis," International Journal for Numerical Methods in Engineering, 23, 1003-1022 (1986).

3. Leon C. Walters, B. R. Seidel, and J. Howard Kittel, "Performance of Metallic Fuels and Blankets in Liquid-Metal Fast Breeder Reactors," Nuclear Technology, Vol 65, No. 2, May 1984.

4. C. E. Lahm, J. F. Koenig, P. R. Betten, J. H. Bottcher, W. K. Lehto and B. R. Seidel, "EBR-II driver fuel qualifications for loss-of-flow and loss-of-heat-sink tests without scram," Nuclear Engineering and Design, Vol. 101, No. 1, 1987.

5. Christopher Dorn, Brush-Wellman, Inc. Be-workshop, September 11, 1989.

6. S. J. Piet, E. T. Cheng and L. J. Porter, "Accident Safety Comparison of Elements to Define Low Activation Materials," INEL Informal Report, EGG-FSP-8552, July 1989. to be published in Fusion Technology.

7. "Nuclear Power in an Age of Uncertainty (Washington, D.C.: U. S. Congress, Office of Technology Assessment, OTA-E-216, February 1984).

8. J. P. Holdren, et.al., "Exploring the Competitive Potential of Magnetic Fusion Energy: The Interaction of Economics with Safety and Environmental Characteristics," Fusion Technology, 13, January, 1988, pp 7-55.

THERMAL CYCLE POWER CONVERSION FOR THE ARIES-I TOKAMAK REACTOR*

Mohammed Z. Hasan and the ARIES team
Department of Mechanical, Aerospace and Nuclear Engineering
and Institute of Plasma and Fusion Research
University of California, Los Angeles
Los Angeles, CA 90024-1597

Abstract

The selection and analysis of a suitable power conversion system for the ARIES-I tokamak fusion reactor are presented. Two main groups of thermal cycles have been investigated. One group comprises of the non-conventional Brayton and Rankine dissociating-gas cycles employing such reacting gases as nitrogen tetroxide (N_2O_4) and nitrosyl chloride ($NOCl$). The other group consists of the conventional inert-gas Brayton cycle and Rankine steam cycles. The dissociating-gas cycles has the potential to operate at higher temperatures and offer higher conversion efficiency and more compact design. However, because of the severe safety problems associated with the toxicity of N_2O_4 and $NOCl$, a dissociating-gas cycle was not selected. An inert-gas Brayton cycle, although more compact, offers much lower conversion efficiency compared with a Rankine steam cycle. The selected power conversion system for ARIES-I is, therefore, based on advanced supercritical Rankine steam cycle with double reheat. A gross conversion efficiency of about 48% is predicted.

Introduction

The ARIES is a multi-institutional research program aimed at developing various approaches of attractive tokamak fusion reactors for commercial application [1]. ARIES-I is a D-T reactor producing 1000 MWe net. The primary emphasis for ARIES-I has been on safety, minimum extrapolation in physics data-base, and the use of advanced magnet and blanket design. The magnitude of toroidal field at the coil axis is 24 T. The blanket uses low-activation SiC composite as the structural material to achieve a very safe design from activation and waste disposal points of view [2].

For a commercial reactor design, an objective would be to convert the thermal power into electricity at the highest possible conversion efficiency. Higher efficiency will lead to smaller thermal pollution and, in general, lower cost of electricity. The conversion efficiency of a thermal cycle is directly related to the temperature potential at which the thermal power is recovered from the reactor core. Hence the selection of a thermal cycle and the obtainable conversion efficiency are intimately related to the thermal-hydraulic design of the first wall, blanket and divertor. For ARIES-I helium at 50 atm pressure is used as the primary coolant.

Table 1 shows the main parameters of ARIES-I. For the first wall and blanket, the inlet and exit temperatures of He are 350°C and 650°C, respectively. The divertor thermal-hydraulic design is on-going. Since the heat flux on the divertor plates is much higher than that on the first wall, the exit temperature of He is expected to be about 400°C. Of the total thermal power, about 90% is removed by the first-wall/blanket circuit and the rest by the divertor circuit.

This paper presents the various thermal cycles that have been investigated, the selection of the reference cycle, and the results of analysis of the reference cycle.

*Work supported b 'US Dept. of Energy

Candidate thermal cycles

Several types of thermal power cycles, both conventional and non-conventional, have been considered in order to select a suitable power system for ARIES-I. Two main categories of thermal cycles were investigated. These are:

1. Dissociating-gas Brayton and Rankine cycles, and
2. Inert-gas Brayton and Rankine steam cycles.

Dissociating-gas cycles

Dissociating-gas cycles are non-conventional cycles under theoretical and experimental investigations[3-6]. They use chemically reacting gases as the working fluids which undergo endothermic dissociation reaction when heated (in the heat exchanger, regenerator, etc.) and exothermic recombination reaction when cooled (while expanding through the turbine). These gases have higher effective heat capacity, higher effective thermal conductivity, and smaller specific volume at low temperature compared with the commonly-used inert gases. A partial list of prospective dissociating gases is given in Table 2[3]. Table 3[3,4] provides the main physical properties of the two most prospective and most studied dissociating gases both as heat transfer media and working fluids for power cycles. These are nitrogen tetroxide (N_2O_4) and nitrosyl chloride ($NOCl$). These gases are, however, toxic and corrosive.

$NOCl$ is used in Brayton cycle and N_2O_4 can be used both in Brayton and Rankine cycles. Typical predicted efficiencies for given maximum cycle temperatures are shown in Table 4[3-5]. $NOCl$-N_2O_4 stands for a compound cycle with a topping Brayton cycle using $NOCl$ and a bottoming Rankine cycle using N_2O_4. Because of higher heat capacity and smaller specific volume at low temperature, dissociating-gas turbines are smaller than both inert-gas and steam turbines. A comparison of a N_2O_4 turbine and a steam turbine is shown in Table 5[6].

Table 1: Main Parameters of ARIES-I	
Major toridal radius, m	6.5
Circularized plasma radius, m	1.75
plasma ion temp. (den. ave), KeV	20.0
Plasma elec temp. (den. ave), KeV	19.9
On-axis toroidal field, T	12.9
Field at the coil axis, T	23.7
Plasma current, MA	10.9
Toroidal beta, %	1.9
Fusion power, MW	1991
Neutron wall loading, MW/m^2	2.8
Alpha power, MW	398
Current drive power, MW	157
Total useful thermal power, MW	2812
Helium (FW/BL) inlet temp.,°C	350
Helium (FW/BL) exit temp., °C	650

Table 2: A partial list of dissociating gases[3]			
Dissociating gas	C^1	ΔH_r^*	T-Range(^oC)
$N_2O_4 \rightleftharpoons 2NO_2$	2	13.7	25-170
$2NO_2 \rightleftharpoons 2NO + O_2$	1.5	27.0	140-850
$2NOCl \rightleftharpoons 2NO + Cl_2$	1.5	9.21	25-900
$Al_2Br_6 \rightleftharpoons 2AlBr_3$	2	30.0	300-1400
$Al_2Cl_6 \rightleftharpoons 2AlCl_3$	2	29.8	200-1100
$Al_2Br_6 + 4Al(liq) \rightleftharpoons 6AlBr$	6	282.4	670-1400
$Al_2Cl_6 + 4Al(liq) \rightleftharpoons 6AlCl$	6	263.8	670-1200

[1] Coeff. of increase of gas constant.

[*] Heat of reaction, $Kcal/g.mole$.

Table 3: Properties of N_2O_4 and $NOCl$[3,4]		
Property	N_2O_4	$NOCl$
Mol. wt. (g/mole)	92.02	65.46
Boiling pt.(^oC)	21.3	-5.8
Melting. pt. (^oC)	-11	-61.5
Crit. temp. (^oC)	158.3	167.5
Crit. pres. (atm)	103.3	90.0
ΔH_v ($Kcal/Kg$)	149/293	141.7
Reaction	$N_2O_4 \rightleftharpoons 2NO_2 \rightleftharpoons 2NO + O_2$	$2NOCl \rightleftharpoons 2NO + Cl_2$
Temp. Range(^oC):		
1 atm	25-850	25-900
100 atm	25-1200	—

Table 4: Typical cycle efficiency		
Cycle	$T_{max}(^oK)$	Eff.(%)
$NOCl - N_2O_4$	1000	55[4]
$N_2O_4 - N_2O_4$	1000	51[4]
$AlBr_3 - N_2O_4$	1000	48[4]
$Al_2Br_6 - N_2O_4$	1000	56[3]
$NOCl$	900	40[5]

Table 5: N_2O_4 and H_2O turbines[6]		
Item	N_2O_4	H_2O
Turbine output, MW	500	500
Pres. at turb. inlet (atm)	240	240
Temp. at turb. inlet (^oC)	565	580
Pres. at turb. exit (atm)	1.4	0.035
Number of stages	10	42
Length of turbine (m)	16.8	29.1
Weight of turbine ($tons$)	180	964
Cost, 1000 rubles	619	1600

Among the advantages of a dissociating-gas cycle are: (1) higher possible maximum cycle temperature and higher efficiency compared with Rankine steam cycle and (2) smaller turbine, regenerator, etc., leading to a more compact design compared with both inert-gas Brayton and Rankine steam cycles. The disadvantages are: (1) safety hazard from the toxicity of N_2O_4 and $NOCl$ and (2) materials need to be developed especially for high-temperature applications. Because of the safety concerns[7] dissociating-gas cycles were not selected for ARIES-I. In addition, suitable materials for these corrosive gases, especially at high temperatures, need to be developed.

Inert-gas Brayton cycle

A power plant based on inert-gas Brayton cycle is more compact than a Rankine steam plant and can have much higher maximum cycle temperature. Open-cycle gas turbines such those as used in aircraft engines have maximum cycle temperature of about 1200^oC. Closed-cycle gas turbines (CCGT) are, however, limited to lower maximum temperatures. Existing fossil-fuel CCGT plants have the maximum temperature of about 750^oC. The maximum temperature for advanced coal-fired CCGT plants is expected to be about 850^oC. Even at this high temperature, the efficiency of CCGT is about 40% [8]. This is much lower than the efficiency of an advanced Rankine steam cycle with the maximum temperature of about 600^oC. Therefore, Rankine steam cycle was selected for ARIES-I reactor.

Reference cycle for ARIES-I

Status of Rankine steam cycles

Both subcritical and supercritical steam plants are operational at present. The present-day standard supercritical Rankine cycle has the steam conditions of 3500psia/1050/1050/1050^oF, which means that the maximum throttle steam pressure is 3500psia, there are two reheats, and the steam temperatures after superheat and each reheat are equal to 1050^oF. The goal for the 1990's with advanced Rankine steam cycles is to obtain the steam conditions of 4000-5000psia/1100/1100/1100^oF. The Electric Power Development Co. of Japan is studying cycles with the steam conditions of 5000psia/1200/1100/1100^oF [9].

Advanced supercritical steam cycles are operational at present primarily for testing, data gathering, and studying technical issues and economic competitiveness. The Eddystone Station (unit-1) supercritical steam plant of the Philadelphia Electric Co. has the steam conditions of 5000psia/1200/1050/1050^oF [9]. It has been operating for over 20 years. Its capacity is 325 MWe and achieved an availability of 76%.

Results of a study by EPRI [9]

A study of advanced, coal-fired, supercritical steam plants was sponsored by EPRI. The main results/recommendations of this study are: (1) under the present/near-future conditions, the economically optimum cycle has the steam conditions of 4500psi/1100/1100/1100^oF, (2) the availability can be increased from the present 82.2% to 87.2-88.2%, (3) a unit with capacity more than 800MWe would require the expensive cross-compound arrangement of the turbines, (4) the 1100^oF temperature limit is due to the coal-ash corrosion on the gas side becoming serious for reheaters beyond this temperature, (5) 12%-Cr steel should be used to handle the ash corrosion of the superheater tubes, (6) for a 800MWe plant, the direct cost of producing electricity is about \$1.066/KWh, and (7) over the plant lifetime, the fuel cost saving is estimated to be between 59 and 97 million dollars when switched to the optimum advanced steam plant. The efficiency of the recommended cycle is 48.1%.

Advanced steam cycle for ARIES-I

The variation of gross cycle efficiency with maximum steam temperature is shown in Figure 1 and with maximum throttle steam pressure in Figure 2. These results were obtained using the code PRESTO [10]. The gross efficiency increases with both maximum pressure and temperature. A gross efficiency of about 49% can be obtained with an advanced steam cycle having the parameters close to those recommended by the EPRI study.

The selected steam cycle for ARIES-I has the following particulars:

1. steam conditions: 4500psia/1112/1112/1112^oF(600^oC),
2. two reheats,
3. nine regenerative feedwater heaters,
4. condenser back pressure of 2 inch of Hg.

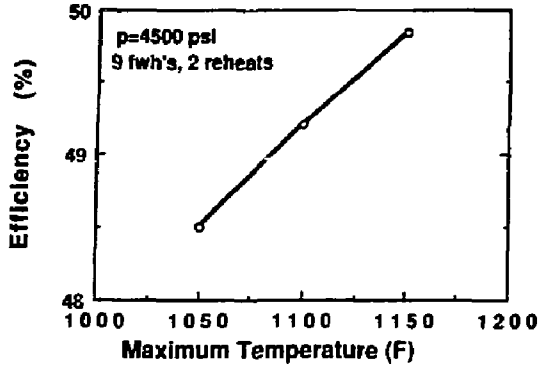

Figure 1: Gross efficiency versus maximum cycle temperature. $T_{SH}=T_{RH1}=T_{RH2}$ and p_{max}=4500psia. There are 9 regenerative feedwater heaters.

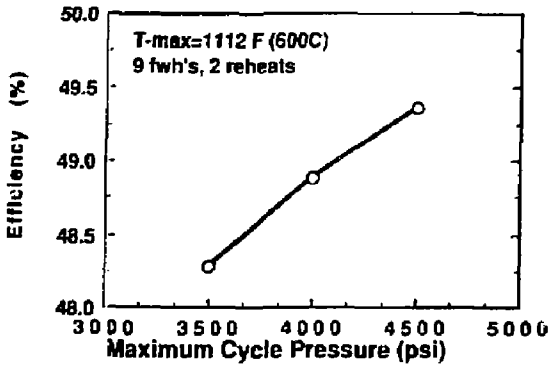

Figure 2: Gross efficiency versus maximum throttle pressure. $T_{SH}=T_{RH1}=T_{RH2}=1112°F(600°C)$. There are 9 regenerative feedwater heaters.

The objective has been to stay close to the recommended cycle in EPRI study. Since He is not corrosive, maximum cycle temperature higher than that recommended by EPRI study might be possible for ARIES-I.

Results of analysis of the reference cycle

The thermodynamic analysis of the cycle has been done using the code PRESTO [10]. The minimum temperature difference between the primary coolant (He) and H_2O is kept about $50°C$. Figure 3 is a schematic diagram of the power cycle where the superheater and the reheaters are in conventional series arrangement. Figure 4 is the corresponding temperature-energy diagram. In order to realize the maximum steam temperature of $600°C$ after superheat and each reheat, the maximum He temperature (first-wall/blanket exit temperature) needs to be $750°C$. Figures 5 and 6 are the corresponding figures for parallel arrangement of the superheater and reheaters. In such an arrangement the maximum He temperature of $650°C$ can be allowed. In order to ease the maximum blanket material temperature, the exit temperature of the primary coolant He has been limited to $650°C$. Therefore, the non-conventional parallel arrangement of the superheater and reheaters has been assumed for the reference power cycle for ARIES-I.

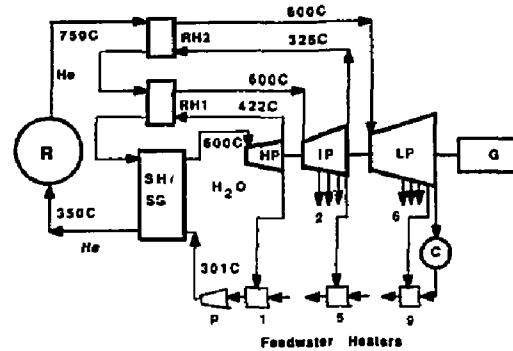

Figure 3: Schematic flow diagram of the power cycle. The reheaters and the superheater are in series. R=reactor core, SG=steam generator, SH=superheater, RH1=first reheater, RH2=second reheater, HP=high-pressure turbine, IP=intermediate-pressure turbine, LP=low-pressure turbine, G=electric generator, C=condenser, and P=feedwater pump.

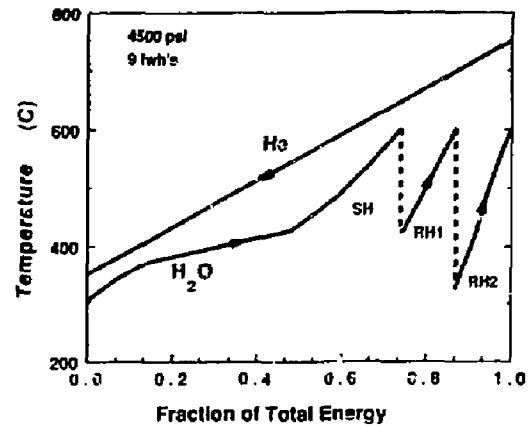

Figure 4: Temperature-Energy diagram for the cycle with the superheater and reheaters in series. $T_{SH}=T_{RH1}=T_{RH2}=1112°F(600°C)$. The maximum He temperature required is $750°C$.

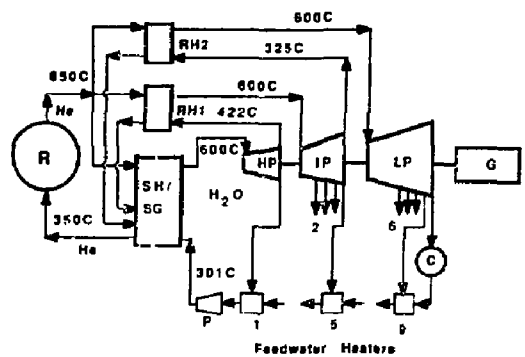

Figure 5: Schematic flow diagram for the power cycle with the reheaters and superheater in parallel. R=reactor core, SG=steam generator, SH=superheater, RH1=first reheater, RH2=second reheater, HP=high-pressure turbine, IP=intermediate-pressure turbine, LP=low-pressure turbine, G=electric generator, C=condenser, P=feedwater pump.

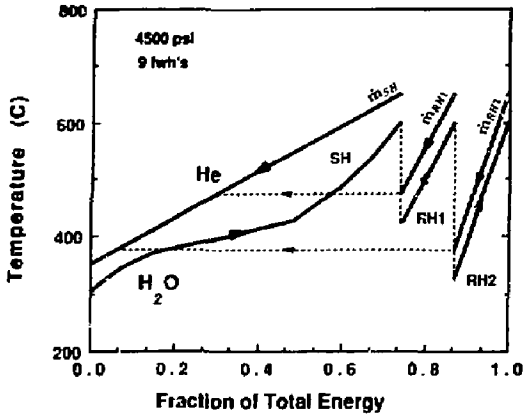

Figure 6: Temperature-Energy diagram for the power cycle with the reheaters and superheater in parallel. $\dot{m}_{SH}$=0.64, $\dot{m}_{RH1}$=0.22, $\dot{m}_{RH2}$=0.14. Maximum He temperature of 650°C can be allowed.

The fractions of parallel mass flow rates of He through the superheater and reheaters are: $\dot{m}_{SH}$=0.64, $\dot{m}_{RH1}$=0.22, and $\dot{m}_{RH2}$=0.14. To stay within the 800MWe limit for a unit, two turbine-generator sets each using one-half of the FW/BL thermal power have been used. The turbines are arranged in tandem-compound arrangement in each unit. The gross thermal efficiency is 49.37%.

The divertor thermal-hydraulic design has not been completed yet. Because of higher heat flux on the divertor plates than on the first wall, the exit temperature of He in the divertor circuit is expected to be about 400°C. A PWR type of power cycle with an expected efficiency of 35% could be selected for converting the divertor thermal power which is about 10% of the total thermal power. This would lead to an overall gross efficiency of about 48% for ARIES-I. These results are summarized in Table 6.

Summary and Conclusions

An advanced, double reheat, supercritical Rankine steam cycle has been selected for converting the thermal power in the first wall and blanket of ARIES-I tokamak fusion reactor. There are nine regenerative feedwater heaters and the condenser back pressure is 0.98 psia. The steam conditions are: 4500psia/1112/1112/1112°F(600°C). These are similar to those of the advanced cycle recommended by the EPRI study. The power cycle analysis has been done by the code PRESTO. The minimum temperature difference between He and H_2O is kept about 50°C. In view of the He exit temperature of 650°C, the unconventional parallel arrangement of the superheater and reheaters has been used. The gross efficiency of this advanced cycle is 49.37%. A PWR-type power cycle is expected to be selected for the divertor thermal power giving a gross efficiency of about 35%. The overall gross conversion efficiency for ARIES-I is about 47.9%. Although in reference to the standard steam plants the selected FW/BL power cycle is an advanced steam cycle, by the time fusion reactors become commercially available, this cycle or even more advanced cycles might become standard steam power cycles.

Table 6: Power conversion results for ARIES-I	
Total thermal power, MW_t	2812
FW/BL thermal power, MW_t	2532
Divertor thermal power, MW_t	280
FW/BL power cycle:	
Total He flow rate, Kg/s	1623.0
Total steam flow rate, Kg/s	887.4
No. of turbine-generator sets	2
Arrangement of the turbines	tandem
No. of reheats	2
No. of regenerative feedwater heaters	9
Steam conditions:	
Maximum throttle pressure, psia	4500
Temperature after superheat, °C	600
Temperature after 1st reheat, °C	600
Temperature after 2nd reheat, °C	600
Extraction pressures(psia):	
Heater 1	1304
Heater 2	550
Heater 3	350
Heater 4	250
Heater 5	165
Heater 6	68
Heater 7	38
Heater 8	20
Heater 9	6.9
Condenser back pressure, psia	0.98
Feedwater inlet temperature, °C	301
Gross thermal efficiency, %	49.37
Divertor power cycle:	
PWR-type power cycle	
Expected gross efficiency, %	35
Overall gross efficiency, %	47.9

Reference

[1] F. Najmabadi et al., "The ARIES Tokamak Reactor Study", this conference.

[2] C.P.C. Wong et al., "Blanket Design for the ARIES-I Tokamak Reactor", this conference.

[3] V.B. Nesterenko, "Thermodynamic Schemes and Cycles of APS Using the Dissociating Gases", published in Dissociating Gases as Heat-Transfer Media and Working Fluids in Power Installations. American Pub. Co., New Delhi, p-8, 1975.

[4] H. Huang and R. Govind, "Studies of Power Plants Using Dissociating Gases as Working Fluids", Chem. Eng. Comm., vol.72,No.1,p-95.

[5] K. Kesavan and J.F. Osterle, "Brayton Cycle Using Dissociating Nitrosyl Chloride ", Proc. 16th Intersoc. Energy Conv. eng. conf., p-2204, 1981.

[6] B.I. Lomashev and V.B. Nesterenko, "Gas Turbines with Dissociating Working Fluids", published in Dissociating Gases as Heat-Transfer Media and Working Fluids in Power Installations. American Pub. Co., New Delhi, p-74,1975.

[7] B.H. Nichols, "The Clinical Effects of the Inhalation of Nitrogen Dioxide", paper read at the Thirtieth Annual Meeting, American Roentgen Ray Society, New York City, Sept. 17-20, 1929, Am. J. Roentgentol. 1930; 23:516-520.

[8] C.F. McDonald and C.P.C. Wong, "Closed-Cycle Gas Turbine Applications for Fusion Reactors", GA-A16025, GA Technologies, Inc. (Aug. 1980).

[9] "Development Plan for Advanced Fossil-Fuel Power Plants", Final Report, EPRI CS-4029, May 1985.

[10] L.C. Fuller and T.K. Stovall, "User Manual for PRESTO: A Computer Code for the Performance of Regenerative Superheated Steam-Turbine Cycles", ORNL-5547, NASA CR-15940, June, 1979.

ENERGY CONVERSION OPTIONS FOR ARIES-III —A CONCEPTUAL D-^{3}He TOKAMAK REACTOR*

J. F. Santarius, J. P. Blanchard, G. A. Emmert, I. N. Sviatoslavsky, L. J. Wittenberg
University of Wisconsin, 1500 Johnson Dr., Madison, WI 53706

N. M. Ghoniem, M. Z. Hasan, T. K. Mau, University of California, Los Angeles

E. Greenspan, UC-Berkeley and Israel Atomic Energy Commission

J. S. Herring, Idaho National Engineering Laboratory

W. Kernbichler, University of Illinois and Technische Universität Graz, Austria

A. C. Klein, Oregon State University

G. H. Miley, University of Illinois

R. L. Miller, Los Alamos National Laboratory

Y-K.M. Peng, Fusion Engineering Design Center, Oak Ridge National Laboratory

M.J. Schaffer, C.P.C. Wong, General Atomics

D. Steiner, Rensselaer Polytechnic Institute

D-K. Sze, Argonne National Laboratory

and the ARIES Team**

Abstract

The potential for highly efficient conversion of fusion power to electricity provides one motivation for investigating D-^{3}He fusion reactors. This stems from: (1) the large fraction of D-^{3}He power produced in the forms of charged particles and synchrotron radiation, which are amenable to direct conversion, and (2) the low neutron fluence and lack of tritium breeding constraints, which increase design flexibility. The design team for a conceptual D-^{3}He tokamak reactor, ARIES-III, has investigated numerous energy conversion options at a scoping level in attempting to realize high efficiency. The energy conversion systems have been studied in the context of their use on one or more of three versions of a D-^{3}He tokamak: a first stability regime device, a second stability regime device, and a spherical torus. The set of energy conversion options investigated includes bootstrap current conversion, compression-expansion cycles, direct electrodynamic conversion, electrostatic direct conversion, internal electric generator, liquid metal heat engine blanket, liquid metal MHD, plasma MHD, radiation boiler, scrape-off layer thermoelectric, synchrotron radiation conversion by rectennas, synchrotron radiation conversion by thermal cycles, thermionic/AMTEC/thermal systems, and traveling wave conversion. The original set of options is briefly discussed, and those selected for further study are described in more detail. The four selected are liquid metal MHD, plasma MHD, rectenna conversion, and direct electrodynamic conversion. Thermionic energy conversion is being considered, and some options may require a thermal cycle in parallel or series.

Overview

This study aims to identify attractive, high-efficiency energy conversion schemes for a D-^{3}He tokamak reactor. The loss channels for a D-^{3}He plasma are through charged particles, neutrons, and radiation (synchrotron and bremsstrahlung), with only a few percent of the energy loss in neutrons. In contrast to D-T fusion reactors, this gives high leverage to energy conversion methods which apply to charged particles or radiation. The ideas investigated here focus on efficiently converting such energy to electricity or on converting thermal energy in ways which make effective use of fusion reactor characteristics, such as high magnetic fields.

The energy conversion methods investigated are given in Table I, which also indicates whether the concept was chosen for further study and the applicability of the concept to the three tokamak versions under consideration for ARIES-III: a high-field reactor (HFR), a second stability reactor (SSR, and a spherical torus (ST). Options not selected for further pursuit within the ARIES project will be described briefly, and those selected will be discussed more extensively. Selection criteria included cost, efficiency, technical feasibility, and how well a concept made use of fusion-specific features. An option not being selected for further pursuit within the ARIES-III study does not necessarily imply that it is unsuitable for alternate fusion reactor configurations; a D-^{3}He tokamak has some unique characteristics and constraints which had a strong impact on the winnowing process.

Options Studied Only in the Initial Phase

Some early ideas were revisited, including conversion of the bootstrap current[1] or travelling waves[2] using an external antenna system to damp out either part of the bootstrap current, a naturally growing instability, or an artificially stimulated instability. The key difficulty is effectively coupling to the antennas, and no efficient solution was found. Similarly, the projected scrape-off layer thermoelectric efficiency was low.

Two ideas attempted to take advantage of the high in situ tokamak magnetic fields. The internal electric generator (IEG) would put a generator within a toroidal field coil. The difficulties in effectively

Table 1. Energy conversion options investigated for the ARIES-III, D-^{3}He tokamak reactor.

Option	Further Study?	Applicability
Bootstrap current conversion	no	HFR, SSR, ST
Compression-expansion cycles	no	ST
Direct electrodynamic conversion (DEC)	yes	ST
Electrostatic direct conversion	no	HFR, SSR, ST
Internal electric generator (IEG)	no	HFR, SSR, ST
Liquid metal heat engine blanket	no	HFR, SSR, ST
Liquid metal MHD (LMMHD)	yes	HFR, SSR, ST
Plasma MHD (PMHD)	yes	HFR, SSR(?)
Radiation boiler	no	HFR, SSR, ST
Scrape-off layer thermoelectric	no	HFR, SSR, ST
Synchrotron conversion by rectennas	yes	HFR, SSR(?)
Synchrotron conversion by thermal cycles	no	HFR, SSR(?)
Thermionic-AMTEC -thermal cycle	no	HFR, SSR, ST
Traveling wave conversion	no	HFR, SSR, ST

driving such a generator with a hot working fluid and the low leverage to be gained in replacing the already efficient generator caused this option to be abandoned. The liquid metal heat engine blanket, based on ideas developed primarily at LANL[4], uses a set of closely spaced radial plates inside a liquid metal blanket. The radial temperature gradient drives oscillations, whose energy would be extracted by MHD conversion. The predicted efficiency was low, ~30%.

A large fraction of the fusion power in a D-^{3}He tokamak will appear as bremsstrahlung radiation. Therefore, the early idea[5] of achieving a high working-fluid temperature by using a low-Z first wall, relatively transparent to bremsstrahlung, and absorbing the radiation on a high-Z material behind that wall was revisited. The difficulty in finding a material suitable from both transparency and structural considerations led to this option being abandoned.

In a tokamak, the experimentally demonstrated technique of electrostatic direct conversion[3] requires a bundle divertor, with a consequent negative impact on stability and difficulty in bucking the very high fields at the toroidal field coils (except in an ST). Because it converts the Maxwellian, scrape-off layer plasma, a multi-stage direct converter is needed for high efficiency.

Two concepts, thermal conversion of synchrotron radiation and thermionic conversion, were retained in partial form by investigating their features in the context of other options. Absorbing synchrotron radiation in a molecular gas, in order to achieve a high working-fluid temperature, showed some merit. However, the various features of the method overlapped the rectenna and MHD conversion options, so this method was not separately pursued. The concept of using thermionic, AMTEC (thermoelectric), and thermal conversion systems in series was examined, but the high cost of the AMTEC system led to the retention of thermionic conversion as a topping cycle for the MHD options and the abandonment of AMTEC.

For the ST, where the external magnetic field is low, compression-expansion cycles appear attractive. These are analogous to the standard Otto thermal cycle, but gains in efficiency because of the high temperature of plasmas[1]. Preliminary analysis was favorable, including operational questions such as the effect on magnets and transport. However, lacking resources to continue investigating two options for an ST, work on this option was halted in favor of DEC.

Options Selected for Further Study

Liquid Metal MHD Conversion (LMMHD)

The source energy in LMMHD is converted to DC electricity by: (1) Thermal energy to kinetic energy of a liquid metal (LM), and (2) LM kinetic energy to electricity as the LM traverses a perpendicular magnetic field. In (1), the LM is mixed with a thermodynamic working fluid(TWF)—a volatile liquid or a gas. As the TWF expands, it accelerates the LM. Approaches to LMMHD design differ in the combination of TWF and LM they use and in the way these fluids are coupled and separated [6-8]. A unique feature is that the expansion of the TWF is nearly isothermal.

The Ericsson LMMHD cycle, shown in Figure 1, appears most promising for ARIES-III[7,8,9]. It is the LMMHD counterpart of a gas turbine cycle, with multiple reheating and intercooling stages. The LMMHD cycle is free of rotating machinery, can be hermetically sealed and, hence, directly coupled with the reactor coolant, and is free of reheating and intercooling heat exchangers. The upper cycle temperature strongly depends on the first wall and blanket design details, as well as on the design of a topping cycle, if used. It appears likely that the LMMHD cycle can be designed to have a high temperature of at least T_h=1200 C. Three design approaches are under consideration: (1) Cool the first wall and blanket with He at inlet temperature T_i=900 C and outlet temperature T_o=1500 C, heating the LM TWF by direct He contact; (2) Divert the synchrotron radiation out of the fusion core and dump it into the LM using a simple heat exchanger. Use He TWF to remove the remaining fusion power. Here, T_o=1200 C could suffice; and (3) Mist cooling. Add LM droplets to the He, thus significantly reducing T_o-T_i and T_h-T_o, while avoiding adverse MHD effects[9].

The LMMHD technology potentially offers 50% to 61% efficiency using a single system featuring direct cycle, relatively low operating pressures, as well as simple and robust stationary components. The relatively large efficiency range reflects the uncertainty in the expected performance of system components. The TWF and LM are assumed to be He and Li, and the expansion ratio is 2.5.

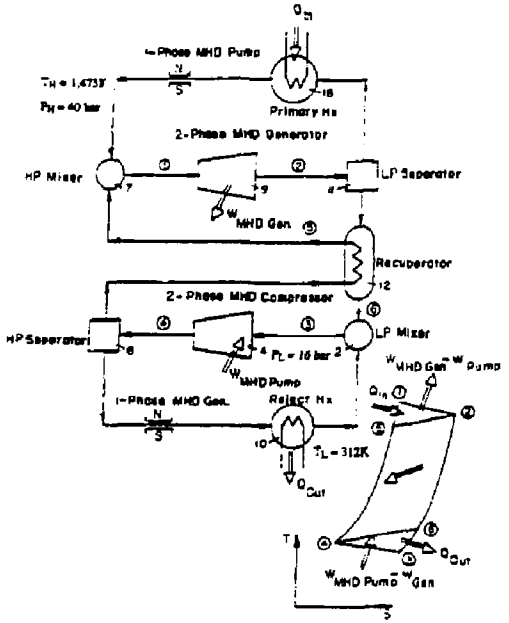

Figure 1. Schematic of an all LMMHD Ericsson Cycle

Plasma MHD Conversion (PMHD)

In PMHD, the electrical conductivity of the working fluid is obtained by thermal ionization. Since appreciable ionization of common gases requires temperatures of ~5000 K, a small amount of seed material (~0.1 atom percent) such as cesium or potasium is added, giving sufficient electrical conductivity at about 3000 K. Fairly extensive theoretical and experimental work in PMHD exists[10,11,12], and ARIES-III would use closed-cycle MHD (CC-MHD).

For ARIES-III, He working fluid seeded with Cs or K has been chosen. The CFAR[12] concept for a DT reactor uses Hg, however Hg vapor toxicity poses unacceptable safety concerns in a D-^{3}He fusion reactor—where safety and environmental advantages are a key reason for investigating the fuel cycle. The bottoming cycle is a supercritical Rankine steam cycle with multiple reheat. The power conversion flow diagram is shown in Figure 2. The stagnation temperature of the working fluid is ~2000 K. The use of synchrotron radiation to further heat the working fluid while keeping the chamber wall at much lower temperature makes this option fusion-specific.

The predicted thermodynamic efficiency of the combined PMHD/Rankine steam cycle is ~64%. The component cycle efficiencies are ~30% for the topping PMHD and ~49%[13] for the bottoming Rankine steam cycle. The MHD duct is simple and reliable, without any moving parts, and the high conversion efficiency leads to a smaller reactor thermal output, compact balance of plant, and an expected decrease in cost of electricity. Issues include the high temperature blanket, transport of synchrotron radiation, efficiency of heating the working fluid by synchrotron radiation, the synchrotron radiation window, and the possibility of activation of the seed materials by fusion neutrons.

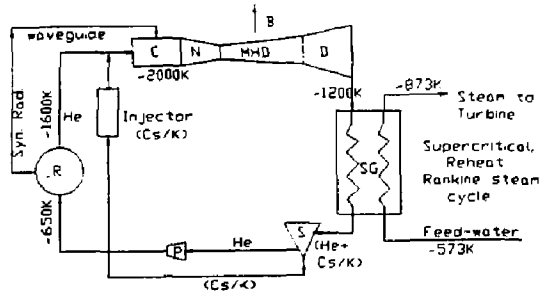

Figure 2. Schematic of PMHD System. R=reactor core, C=chamber, N=nozzle, D=diffuser, SG=steam generator, S=separator, P=pump/compressor, B=magnetic field

Thermionic Conversion

Thermionic energy conversion is a well-advanced technology utilizing thermally stimulated electron emission (thermionic emission). The cathode (emitter) and anode (collector) are separated by a small interelectrode space. To obtain good efficiency and heat flux capability, the emitter should operate at ~2000 K, while the collector should operate at ~1000 K. Typical emitter/collector materials are tungsten/molybdenum. Operating systems have achieved efficiencies (η) of ~10% and heat fluxes of ~0.1 MW/m^2, and projections give η ~20% and heat fluxes of ~0.25 MW/m^2.

The conversion would occur out of pile and, therefore, the thermionic converters would not be subject to radiation and magnetic fields. The thermionic converters would be configured as two concentric tubes of ~1 m in length. One module would consist of a close-packed array of ~900 converters, handling ~80 MW of thermal energy. The key technical issue for ARIES-III is the high emitter temperature. One possible combination of blanket structure and coolant would be titanium carbide and helium, which would exhibit attractive activation characteristics.

Direct Electrodynamic Conversion (DEC)

A direct electrodynamic converter (DEC) would consist of a chamber above the core plasma into which the scrape-off layer plasma would be diverted. It could also function as a divertor. As shown in Figure 3, the DEC plates would be biased so that particle drifts would separate ions from electrons. Ions would be collected on the top plate, while electrons would be collected on the end plate[14].

A DEC would operate in a low-recycle divertor regime, and the scrape-off layer plasma temperature would be 2-5 keV. The mode of operation would be similar to that of an in situ MHD disk generator. Details of the particle drifts and distribution functions within the DEC are being pursued, but a preliminary estimate of the efficiency is 50%.

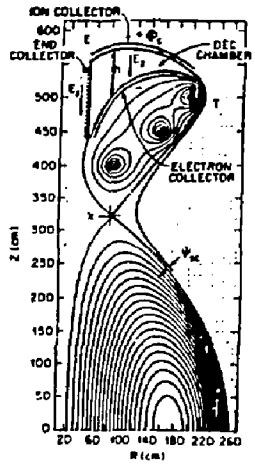

Figure 3. Schematic of a Spherical Torus with DEC

Synchrotron Radiation Conversion by Rectennas

The concept of directly converting synchrotron radiation to electricity at ~80% efficiency using rectennas (rectifying antennas) was originated by Grant Logan[15]. This method appears attractive for D-^{3}He fusion reactors[16]. Overmoded waveguides would channel synchrotron radiation out of the tokamak and convert it in a separate chamber. Rectennas, not yet developed at frequencies of interest, require integrated circuit technology within the state of the art. Big production runs of large-scale integrated circuits indicate rectenna costs are reasonable. A high fraction of the fusion power must be generated as synchrotron radiation, placing more stringent requirements on energy confinement, as reaching high synchrotron radiation fractions requires higher magnetic fields and higher plasma temperatures. It may be necessary to enhance transport of the ash above that of fuel ions to avoid choking the fusion burn.

The spectrum of synchrotron radiation will be approximately 1.5 to 30 THz. The chamber walls must be highly reflective, so that most of the synchrotron radiation is lost out the waveguide. Proper waveguide positioning causes preferential absorption of synchrotron radiation, calculated to drive a large fraction of the total plasma current. Internal waveguide losses are calculated to be less than 5%. The key circuit components not presently available at the high frequencies of interest are diodes. However, Schottky diodes have been progressing rapidly in frequency as have vacuum microelectronics. Experimental programs exist in two regimes that bracket the range of interest for ARIES-III: 90-240 GHz and 1-28 THz[17].

Synchrotron radiation conversion by rectennas is intrinsically a D-^{3}He mode of operation because of the leverage gained by a high synchrotron radiation to fusion power ratio. The expected benefits in power plant simplicity, reliability, and cost must balance the more difficult physics requirements and the need to demonstrate rectenna technology at THz frequencies.

Conclusions

A wide slate of energy conversion candidates for the D-^{3}He tokamak reactor design ARIES-III has been narrowed down to four: liquid metal MHD, plasma MHD, rectenna conversion of synchrotron radiation, and direct electrodynamic conversion. The rectenna and DEC options are specific to fusion, but apply only to the high-field reactor and the spherical torus, respectively. LMMHD would apply to any ARIES-III version and is the only option not necessarily coupled to another energy conversion system. The PMHD option considered here requires synchrotron radiation superheat, and thus is best suited to a high-field reactor. If a second stability reactor can be operated in a high synchrotron radiation fraction regime, it might be suitable for PMHD or rectenna conversion.

References

[1] G.H. Miley, *Fusion Energy Conversion* (ANS, 1976).

[2] D.G. Samaras, *Applications of Ion Flow Dynamics* (Prentice-Hall, NJ, 1962).

[3] W.L. Barr and R.W. Moir, Nucl. Technol./Fusion 3, 98 (1983).

[4] G.W. Swift et al., J. Acoust. Soc. Am. 78, 767 (1985).

[5] R.T. Taussig and A. Hertzberg, in C.K. Choi, ed., *Proceedings of the Review Meeting on Advanced-Fuel Fusion*, EPRI Report ER-536-SR, p. 179 (1977).

[6] M. Petrick and H. Branover, *Progress in Astronautics and Aeronautics, Vol. 100*, p. 371 (1985).

[7] L. Blumenau et al., Fusion Technology 10 914. (1986).

[8] E. Greenspan et al., *Progress in Astronautics and Aeronautics, Vol. 111*, p. 129 (1988).

[9] E. Greenspan, IEEE 13th Symposium on Fusion *Engineering (Knoxville, 1989).*

[10] W.D. Jackson, in V. A. Kirilin and A. E. Sheyndlin, ed., *MHD Energy Conversion—Physicotechnical Problems* (VAAP, 1983) (English trans., AIAA, 1986).

[11] R.F. Grundy, ed., *Magnetohydrodynamic Energy for Electric Power Generation* (Noyes Data Corp, 1978).

[12] K. Yoshikawa et al., IEEE 13th Symposium on Fusion Engineering (Knoxville, 1989).

[13] M.Z. Hasan, IEEE 13th Symposium on Fusion Engineering (Knoxville, 1989).

[14] Y-K.M. Peng, Bull. APS 33, 2044 (1988).

[14] B.G. Logan, Fusion Power Associates Annual Meeting, (Wash., DC, 1986).

[15] G.A. Emmert et al., IEEE 13th Symposium on Fusion Engineering, (Knoxville, 1989).

[16] J.L. Christian, Jr. and R.J. Acosta "Candidate Technologies for Beamed Space Power Application," NASA Lewis Report draft (1989).

* Work supported by US Dept. of Energy

** ANL, CFFTP, Culham Lab., FEDC/ORNL, General Atomics, Georgia Tech, INEL, LANL, LLNL, MIT, Oregon State U., PPPL, RPI, UC-Berkeley, UCLA, U. Ill., U. Wis.

NUMERICAL SIMULATION OF TURBULENT GAS-PARTICLE FLUID FLOW AND HEAT TRANSFER

Tomoaki Kunugi*, Mohammad Z. Hasan** and the ARIES Team

Department of Mechanical,Aerospace and Nuclear Engineering
6288 Boelter Hall, University of California
Los Angeles, CA 90024

**Institute of Plasma and Fusion Research
6291 Boelter Hall, University of California
Los Angeles, CA 90024

Abstract

The ARIES-I blanket utilizes SiC-composites as the structural material and pure 5MPa He gas. A previous choice was to use 0.5MPa CO_2 gas with particulates as the primary coolant. In this option with CO_2 gas, these small particles mixed with the coolant gas act as a circulating-bed heat transfer medium resulting in a reduced system pressure, a reduced pumping power for coolant circulation, and a higher heat transfer coefficient. Although the addition of solid particles increases the heat transfer coefficient, the physical mechanism is not fully understood. In this study, a computer code using an algebraic second order closure model(ASM) for the continuous phase and a stochastic separation flow model(SSF) for the particulate phase is employed to investigate the microscopic and macroscopic fluid dynamic and heat transfer behaviors of the gas-particulate mixture flow. First, we confirm the validity of this code for a single phase impinging wall jet flow, and then we apply it to a gas-particulate flow though a circular pipe. The variables in this study are the particle size, loading ratio, Reynolds number and the pipe diameter. This paper describes some preliminary results concerned with the particle size and Reynolds number. The velocity profiles, turbulence quantities and temperature distributions are obtained and are compared with the experimental ones. It is found that this code can be applied to the gas-particle flow simulation in a pipe. However, one need to carry out further calculations and investigate the physical mechanism and the modeling of this gas-particle flow and heat transfer phenomena in order to obtain a fully understanding.

Introduction

The ARIES research program is a multi-institutional effort to develop several visions of tokamak as an attractive fusion reactor. The ARIES-I design is a DT-burning, 1000MWe(net) reactor based on advanced technology and modest extrapolation from the present data [1]. The ARIES-I blanket utilizes SiC-composites as the structural material and pure 5MPa He gas. The option of CO_2-particulate was not selected because of the lack of understanding of the erosion rate and the limited data-base for the heat transfer [2]. The addition of particulates increases the heat transfer coefficient in general and hence allows one to reduce the system pressure. But the physical mechanisms leading to the increase in heat transfer coefficient is not fully understood.

Many experimental investigations were carried out for this gas-particle flow and heat transfer. Boothroyd [3] and Soo [4] summarized and collected together these investigations in their books respectively. For numerical investigations, the models are generally classified into two groups, that is a locally homogeneous flow model (LHF) and a separation flow model (SF).

In this study, a computer code [5,6] using an algebraic second order closure model (ASM) [7] for the continuous phase and a stochastic separation flow model (SSF) [8] for the particulate phase is employed to investigate the microscopic and macroscopic fluid dynamic and heat transfer behaviors of the gas-particulate mixture flow. The previous numerical investigations using SF model were successful for the free jet flow cases, but no application of SSF model to the internal flow and heat transfer exists to the best of our knowledge. First, we carried out some calculations for a single phase turbulent impinging wall jet in order to confirm the validity of this code, and then we apply this code to a gas-particulate flow though a circular pipe. The variables in this study are the particle size, loading ratio, Reynolds number and the pipe diameter. This paper describes some preliminary results with the particle size and Reynolds number as parameters. The velocity profiles, turbulence quantities and temperature distributions are obtained and are compared with the experimental ones.

Governing equations

In this study, assuming the incompressible fluid flow, we apply the Reynolds decomposition and the ensemble averaging technique to the Navier-Stokes and the energy equations. The continuity equation, Reynolds equation and energy equation can be written for the general unsteady turbulent flows as follows:

For the continuous phase:

Continuity equation

$$\frac{\partial \overline{\rho u_i}}{\partial x_i} = 0 \qquad \text{..... (1)}$$

Reynolds equation

$$\frac{D\overline{\rho u_i u_j}}{Dt} = -\frac{\partial}{\partial x_k}\{\overline{\rho u_i u_j u_k} - \mu\frac{\partial \overline{\rho u_i u_j}}{\partial x_k} + \overline{p(\delta_{ik}u_j + \delta_{jk}u_i)}\} - \overline{u_i u_k}\frac{\partial \rho U_j}{\partial x_k} - \overline{u_j u_k}\frac{\partial \rho U_i}{\partial x_k} + \overline{p\left(\frac{\partial u_i}{\partial x_j} + \frac{\partial u_j}{\partial x_i}\right)} - 2\mu\overline{\frac{\partial u_i}{\partial x_k}\frac{\partial u_j}{\partial x_k}} + Sr \qquad \text{..... (2)}$$

Energy equation

$$\frac{\partial(\rho c_p T)}{\partial t} + \frac{\partial(\rho c_p U_j T)}{\partial x_j} + St = \frac{\partial(\lambda T)}{\partial x_j \partial x_j} - \frac{\partial(\overline{\rho c_p u_j T})}{\partial x_j} \qquad \text{..... (3)}$$

where U is the mean velocity, u is the fluctuating velocity component, p is the fluctuating pressure, T is the temperature, ρ

---

*Visiting research scientist from Japan Atomic Energy Research Institute
Permanent address: Tokai-mura, Naka-gun, Ibaraki-ken, 319-11, Japan

is the density of gas, μ is the viscosity, c_p is the specific heat, λ is the thermal conductivity, δ is Kronecker delta and x denotes the coordinate. T' denotes the fluctuating component of temperature. The time averaging is denoted a over-bar. Sr is a source term of the momentum exchange between phases and St is a source term of the heat transfer effect due to the particles.

We use the algebraic second order closure [7] for the Reynolds stresses. A triple correlation of the velocity fluctuations is modeled by Daly & Harlow [9], and the turbulence field(k) is assumed almost isotropic in case of the high local Reynolds number. Therefore, turbulence dissipation rate(ε) is assumed isotropic. The redistribution terms of the pressure-strain correlation are modeled by using Gibson-Launder model [10]. Finally, we get the k-ε model and ASM equations.

k-ε model

$$\frac{D(\rho k)}{Dt} = c_k \frac{\partial}{\partial x_k}\left(\frac{\partial \rho k}{\varepsilon}\overline{u_k u_l}\frac{\partial k}{\partial x_l}\right) + P_k - \rho\varepsilon + Sk \qquad \text{..... (4)}$$

$$\frac{D(\rho\varepsilon)}{Dt} = c_\varepsilon \frac{\partial}{\partial x_k}\left(\frac{\partial \rho k}{\varepsilon}\overline{u_k u_l}\frac{\partial \varepsilon}{\partial x_l}\right) + \frac{\varepsilon}{k}(c_1 P_k - c_2\rho\varepsilon) + S\varepsilon \qquad \text{..... (5)}$$

ASM

$$\frac{\overline{u_k u_l}}{k}(P_k - \rho\varepsilon) = P_{ij} - \frac{2}{3}\delta_{ij}\rho\varepsilon + \phi_{ij,1} + \phi_{ij,2} + \phi_{ij,w1} + \phi_{ij,w2} \qquad \text{..... (6)}$$

where P_k is a diagonal part of the turbulence production term P_{ij}. ϕ-terms represent the redistribution of the pressure-strain terms(see Ref.[10]). Sk and Sε are the source terms to represent the turbulence modulation effects. These contributions of the particles to the continuous phase are considered by Crow's PSI-Cell method [11]. The turbulence modulation effect is considered through the Chen's model [12]. We use the standard values for the model constants (see Ref.[10]).

The turbulent heat flux term in the energy equation can be written by the ASM as:

$$\frac{\overline{u_i T'}}{2k}(P_k - \rho\varepsilon) = -\overline{u_i u_k}\frac{\partial \rho T}{\partial x_k} + P_{it} + \phi_{it,1} + \phi_{it,2} + \phi_{it,w1} + \phi_{it,w2} \qquad \text{..... (7)}$$

where $P_{it} = -\overline{u_k T'}\frac{\partial \rho U_i}{\partial x_k}$ and ϕ-terms represent the redistribution of the pressure-temperature terms (see Ref.[10]). The effect of the particle heat transfer is considered in the energy balance equation as the source term, but not including the thermal radiation effect. The source term of the equation(3) is expressed as follows:

$$St = h_p A_p(T - T_p)n_p \qquad \text{..... (8)}$$

where h_p is a heat transfer coefficient of the particle, A_p is the surface area of particle, n_p is the dispersion density of the particulate phase and T_p is the particulate phase temperature.

For the particulate phase: we assume the following for the particulate phase.

(1)Particles are sufficiently dispersed so that the particle-particle interaction is negligible.

(2)Mean flow is steady and the material properties of two phases are constant.

The contribution of the particles is accomplished by integrating the following particle equation of motion, the so-called Basset-Boussinesq-Ossen(BBO) equation.

$$\frac{1}{6}\pi d_p^3 \rho_p \frac{du_p}{dt} = 3\pi d_p \mu(u-u_p) - \frac{1}{6}\pi d_p^3 \frac{\partial P}{\partial x} + \frac{1}{2}\frac{1}{6}\pi d_p^3 \rho\xi + \frac{2}{3}d_p^2\sqrt{\pi\rho\mu}\int_{t_0}^{t}\frac{\xi}{\sqrt{t-t'}}dt' + \text{External force (gravity etc.) .... (9)}$$

where d_p is the particle diameter, u_p is the particle velocity, ρ_p is the density of the particle and ξ is the deviation of the mean flow motion. In this study, the density ratio of the gas and particle ρ/ρ_p is of order of 10^{-3}. In this case, an acceleration(3rd term of the right hand side of equation(9) and the pressure gradient(2nd term) are negligible. Basset force(4th term) is also smaller than the Stokes drag(1st term). Therefore, the main term of this equation(9) is the first term, that is Stokes drag. Finally, we get the equation of particle motion as follows:

$$\frac{du_p}{dt} = \frac{3\rho C_D}{4 d_p \rho_p}|u-u_p|(u-u_p) + g \qquad \text{..... (10)}$$

where C_D is the standard drag coefficient and g is the gravity. The particle trajectories are obtained by solving this equation. In SSF model, the stochastic model is used in order to consider the turbulent diffusion due to the interaction between the particle and eddies. We assume the probability density function of the gas velocity fluctuation to be Gaussian profile. In this study, the new technique of the random sampling of the instantaneous fluctuating velocity [6] is used. We determine the interaction time between the particle and the eddy by comparing the eddy life time with the time required for one particle to pass through one eddy.

The energy equation for the particulate phase is assumed to be the continuum approximation of the dispersion density of the particles(ρ_m), and assumed that there is no thermal diffusion and thermal radiation. The heat exchange between phases is only due to the heat conduction. Therefore, the energy equation of the particulate phase is expressed as follows:

$$\frac{\partial(\rho_m c_p U_i T)}{\partial x_j} + h_p A_p(T_p - T)n_p = 0 \qquad \text{..... (11)}$$

Numerical procedure

This code uses a finite difference method. A QUICK scheme[13] is applied to the convective terms of the momentum equation in order to suppress the numerical oscillation and to get a more accurate numerical solution. Other convective terms of the scalar transport equations use PLD-Scheme[14]. The pressure correction equation is solved by PISO method[15].

A typical grid number in the numerical simulation is 40x80 for the jet case and 40x40 for the gas-particle flow case. For the gas-particle simulation case, we need four computational steps: (1) Calculation of the single flow field, (2) calculation of the particle trajectory, (3) calculation of two phase flow field and (4) calculation of the energy equation after converging the entire flow field. The CPU time is about 30 minutes for the jet case and about 200 minutes for the gas-particle flow case on CRAY-2.

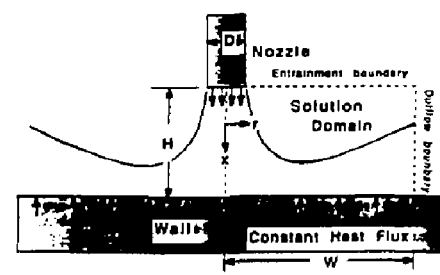

Fig.1 Solution Domain and Boundary Conditions for the Turbulent Impinging Jet

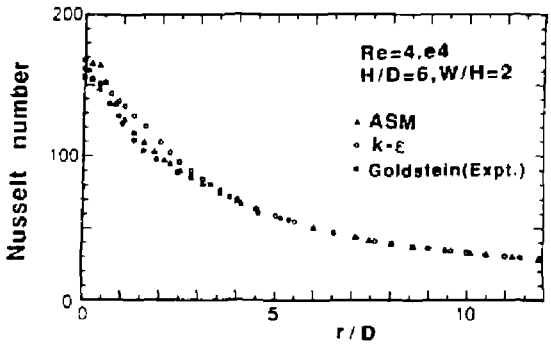

Fig.2 The variation of the Nusselt number along the Wall

Results and discussion

A. Turbulent impinging jet In order to confirm the validity of this code, we carry out the single phase turbulent impinging jet simulation. One of the authors already reported the results of this flow simulation results using the k-ε model of turbulence[5]. Figure 1 shows the solution domain and the boundary conditions of the impinging jet. At the impinging wall, the velocity parallel to the wall is calculated from the law of the wall, the so-called 'Wall-function' method. The wall is heated with a constant heat flux. For the energy equation, we apply the equivalent diffusivity [5] to the nearest computational cell. Figure 2 shows the variation of the Nusselt number along the radial direction (r/D : D is a nozzle diameter) of the wall. The ASM results are in much better agreement with the experimental results by Goldstein[16] than the k-ε results[5]. We have thus confirmed the validity of this code for the complex recirculating flow problem.

B. Gas-particle flow in the pipe We apply this code to the gas-particle flow and heat transfer problem. In this preliminary simulation, we are chiefly interested in the upward flow in a vertical circular pipe. Figure 3 shows the solution domain and the boundary condition. The velocity and temperature at the inlet are set to constant values. At the outlet, the streamwise gradient of all the variables are set to zero. For the continuous phase, the wall-function method is applied to the closest computational cell along the wall. For the particulate phase, the elastic collision of the particle with the wall is assumed. The pipe wall is heated with a constant heat flux. We assume that there is no heat conduction and radiation between the particle and wall. In this problem, the velocity and temperature field are developing simultaneously. The physical and thermal properties of the 0.5MPa CO_2 gas and SiC particle are used in this study. The average diameters of the SiC particles are assumed d_p=0.01 and 0.03 mm. The loading ratio of the particulate phase to the gas phase is set to Γ=0.1,1 and 10. Reynolds number based on the pipe diameter is set to 5.e4 and 5.e5. Figures 4 and 5 show the axial and radial velocity profiles respectively. It is found that the velocity field is developing after acceleration at the entry region. Figure 6 shows the dispersion density ratio (ρ_m/ρ). The majority of the particulate phase transfers to the pipe center region. We feel that this phenomena is a consequence of the acceleration of the fluid at the entry region and the tracking method of the particles. We need to carry out further calculations for this mechanism. Figures 7 to 9 show the ratio of the turbulence energies: k_p is the turbulence energy of the particulate phase and k_s is that of the single phase. Figure 7 shows the experimental results by Maeda [17] and Tuji [18,19]. Their experiments were carried out using the more heavy (ρ/ρ_p=1.3e-4 Maeda, d_p=0.0136mm) and light (ρ/ρ_p=1.2e-3: Tuji, d_p=0.02 and 0.05mm) particles than our simulations

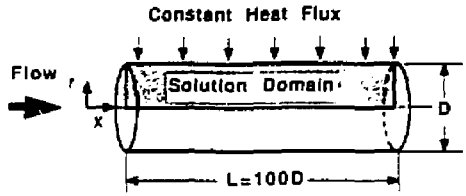

Fig.3 *Solution Domain for the Gas-Particle Flow in a Vertical Pipe*

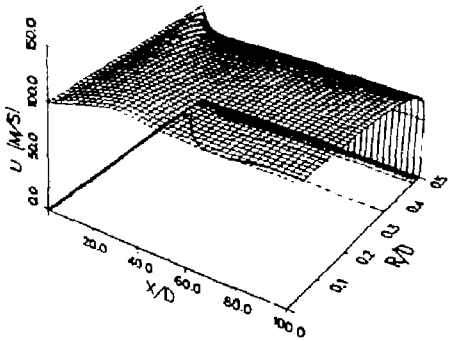

Fig.4 Streamwise velocity (U) Profile
(d_p=0.03mm,Γ=1.0,Re=5.e5)

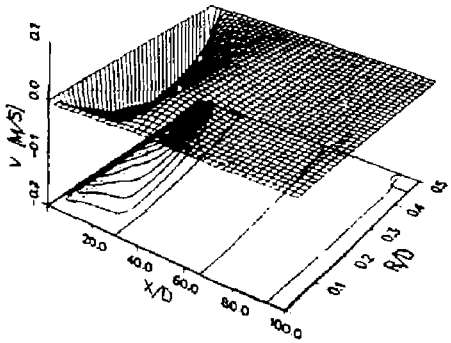

Fig.5 Radial Direction Velocity (V) Profile
(d_p=0.03mm,Γ=1.0,Re=5.e5)

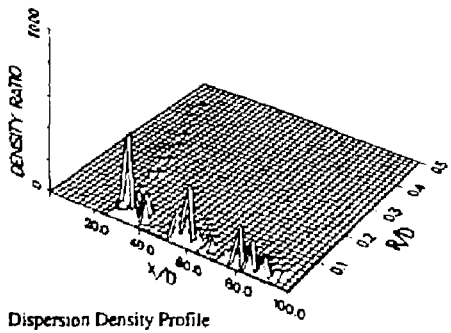

Fig.6 Dispersion Density Profile
(d_p=0.03mm,Γ=1.0,Re=5.e5)

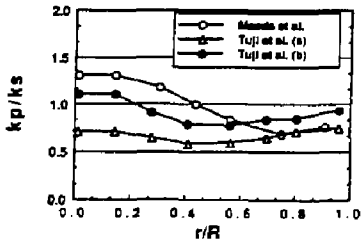

Fig.7 Comparison of the Turbulence Intensities
Maeda: d_p=0.0136mm,Γ=0.54
Tuji: (a)d_p=0.02mm,(b)d_p=0.05mm, Γ=1.3

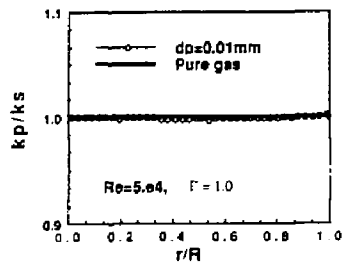

Fig.8
Comparison of the Turbulence Energies
(d_p=0.01mm,Γ=1.0,Re=5.e4)

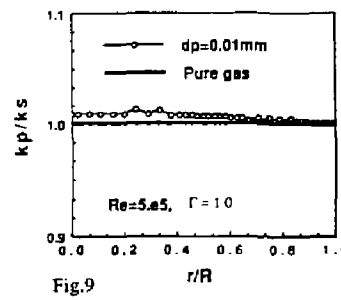

Fig.9
Comparison of the Turbulence Energies
(d_p=0.01mm,Γ=1.0,Re=5.e5)

(ρ/ρ_p=3.3e-4, d_p=0.01mm). Therefore, we can not compare our results with their ones directly. But, the tendency of the variation of the ratio shown in Fig.7 is similar to our results shown in Figs.8 and 9. Figure 10 shows the temperature distribution of the gas-particulate flow. The temperature contours are slightly waved near the center region of the pipe. This is caused by the existence of the particles. Figure 11 shows the variation of the Nusselt number along the axial direction of the pipe. The heat transfer in the case of the smaller particles is better than that of the larger particles and single flow at the entry region. This is caused by the heat transfer characteristics of the particles depending on the particle size. But, at the developed region, the heat transfer of the smaller particles is lower than that of the larger particles and single flow. We consider that this is caused by the dispersion density of the particulate phase which is concentrated near the center region of the pipe by the acceleration of the mixed phase at the entry region.

It is found that this code used SSF model can be applied to the gas-particle flow simulation in a pipe. However, one need to carry out further calculations and investigate the physical mechanism and the modeling of this gas-particle flow and heat transfer phenomena in order to obtain a fully understanding.

Acknowledgements

We would like to acknowledge helpful discussions with Dr.C.P-C.Wong of GA San Diego and Prof.Z.R.Gorbis of UCLA. We also would like to thank Dr.Y.Seki of JAERI for his encouragement. This work was supported by JAERI and USDOE.

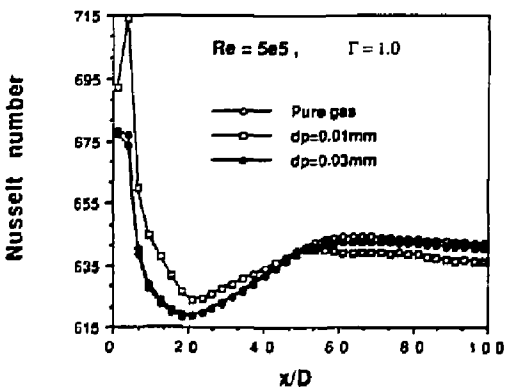

Fig.11 The Variation of the Nusselt Number along the Axial Direction of the Pipe.

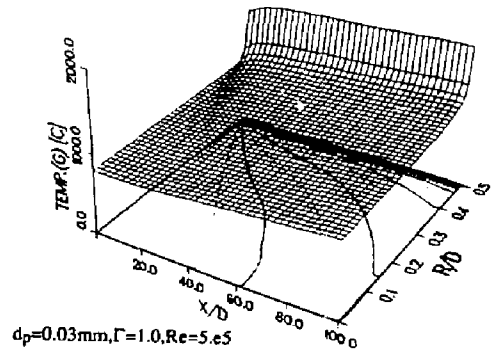

d_p=0.03mm,Γ=1.0,Re=5.e5

Fig.10 Temperature Distribution of the Gas-Particle Flow

References

[1] F.Najmabadi, et al.,"The ARIES Tokamak Reactor Study", this conference, 21-I-01,Oct. 1989.
[2] C.P.C.Wong, et al.,"Blanket Design for the ARIES-I Tokamak Reactor", this conference, 21-O-04,Oct. 1989.
[3]R.G.Boothroyd, Flowing Gas-Solids Suspensions. London: Chapman and Hall, 1971.
[4]S.L.Soo, Fluid Dynamics of Multiphase Systems. Waltham: Blaisdell, 1967.
[5] T.Kunugi, et al.,"Transport Phenomena in Turbulent Flows Theory, Experiment and Numerical Simulation", edited by M.Hirata and N.Kasagi, pp.593 - 604, Hemisphere,1988.
[6] T.Kawamura,"Numerical analysis of Two-dimensional Gas/Solid Two-Phase Impinging Jet Using a Stochastic Modeling", Master Thesis in Kyushyu University,1989 [in Japanese].
[7]W.Rodi, ZAMM, vol.56, pp.219,1976.
[8]A.D.Gosman et al., AIAA paper, no.81-0323, 1981.
[9]B.J.Daly et al., Phys. Fluid,vol.13,no.11,pp.2634, 1970.
[10]M.M.Gibson et al., J. Fluid Mech., vol.86,pp.491,1978.
[11]C.T.Crowe et al.,ASME J.Fluid Eng.,vol.99,pp.325,1977.
[12]C.P.Chen et al., J.Chem.Eng.Comm.,vol.63,pp.349,1984.
[13]B.P.Leonard, Comp. Meths. Appl. Mech. Eng., vol.9, pp.59, 1979
[14]S.V.Patankar, Numerical Heat Transfer and Fluid Flow, Hemisphere, McGraw-Hill, 1980.
[15]R.W.Benodekar, AIAA J.,vol.23,no.3,pp.359,1985.
[16]R.J.Goldstein,Int.J.Heat Mass Transfer,vol.25,pp.1857, 1982.
[17]M.Maeda et al.,Trans.JSME, ser.B,vol.46,pp.2313,1980.
[18]Y.Tuji et al.,J. Fluid Mech.,vol.120,pp.358,1982.
[19]Y.Tuji et al.,J Fluid Mech.,vol.139,pp.417,1984.
[20]R.A.Gore et al.,Int.J.Multiphase Flow,vol.15,no.2, pp.279,1989.